Aus dem Institut/der Klinik für Kardiologie

der Medizinischen Fakultät Charité – Universitätsmedizin Berlin

DISSERTATION

Impact of CD362+-selected mesenchymal stromal cells on left ventricular function in type 2 diabetic db/db mice

zur Erlangung des akademischen Grades

Doctor medicinae (Dr. med.)

vorgelegt der Medizinischen Fakultät

Charité – Universitätsmedizin Berlin

von

Fengquan Dong

aus Wenzhou, China

Datum der Promotion: 23.06.2019

CONTENTS

ABSTRAKT（Deutsch）

Angesichts ihrer immunmodulatorischen, anti-fibrotischen und endothel-protektiven Eigenschaften, stellen mesenchymale stromale Zellen (MSZ) einen vielversprechenden Zelltyp für zell-therapeutische Interventionen dar. Das EU Komitee für zukunftsweisende Therapien unterstrich die Notwendigkeit von Strategien zur Selektion und Aufreinigung von MSZ, woraufhin das sulfatierte Proteoglykan CD362, welches auf der Zelloberfläche der MSZ zu finden ist, als neuer Kandidat identifiziert wurde.

Ziel der vorliegenden Studie war es, den Einfluss von intravenös (i.v.) applizierten Wildtyp (WT), $CD362^-$- und $CD362^+$-selektieren MSZ auf die linksventrikuläre (LV) Funktion in Typ-2 diabetischen Mäusen zu vergleichen und die zugrunde liegenden Mechanismen zu untersuchen. Hierfür wurden 10^6 WT-MSZ, $CD362^-$- bzw. $CD362^+$-Zellen oder PBS i.v. in 20 Wochen alte diabetische BKS.Cg-m+/+Leprdb/BomTac db/db-Mäuse injiziert. Nicht diabetische db+/db-Mäuse, welchen PBS appliziert wurde, dienten als Kontrolle. Vier Wochen nach Applikation erfolgte die hämodynamische Charakterisierung und anschließende Euthanasie der Tiere. Für durchflusszytometrische Analysen wurde die Milz entnommen, sowie der LV für Immunhistologie, Molekularbiologie und bildgebende Massenspektrometrie.

Die i.v. Injektion von WT-MSZ und $CD362^-$-Zellen, aber nicht von $CD362^+$-Zellen, verbesserte die LV Funktion in den db/db-Mäuse, was sich in einer Verbesserung der Kontraktilitätsparameter dP/dt_{max}, dP/dt_{min} und/oder Tau zeigte ($p < 0.05$). Bezüglich der Immunmodulation, erhöhte nur die Gabe der $CD362^+$-Zellen den prozentualen Anteil an regulatorischen T Zellen (Tregs) in der Milz um das 1.3-fache ($p<0.001$), wohingegen WT-MSZ, $CD362^-$- und $CD362^+$-Zellen den Anteil an apoptotischen Tregs in der Milz verringerten ($p<0.001$ jeder Zelltyp gegenüber db/db-Mäuse). Verglichen mit den PBS-behandelten db/db-Mäusen war zusätzlich die Zahl an kardialen $CD3^+$-Zellen um das 1.5-fache ($p<0.05$), 1.8-fache ($p<0.01$) und 1.7-fache

($p<0.01$) nach Injektion von WT-MSZ, $CD362^-$- bzw. $CD362^+$-Zellen reduziert. Interessanterweise führte die Applikation von WT-MSZ, $CD362^-$- bzw. $CD362^+$-Zellen auch zu einer 1.6-fach ($p<0.05$), 1.8-fach ($p<0.01$) bzw. 1.6-fach ($p<0.05$) verringerten Zahl an kardialen $CD68^+$-Zellen. Die hypothesenfreie Proteomanalyse mittels bildgebender Massenspektrometrie zeigte darüber hinaus eine verringerte Expression der Titin-Isoform N2B in den db/db-Mäusen gegenüber den db+/db-Mäusen, welche durch i.v. Anwendung aller untersuchten Zellen verbessert werden konnte.

In Übereinstimmung mit der LV Funktion war die totale Titin-Phosphylierung in den db/db-Mäusen, im Vergleich zu den db+/db-Mäusen, um das 1.8-fache ($p<0.01$) herunterreguliert, welche nur durch die Applikation von WT-MSZ (1.6-fach; $p<0.05$) und $CD362^-$-Zellen (1.5-fach; $p<0.05$) induziert wurde. Parallel dazu, fiel die Proteinkinase G-Aktivität um das 1.5-fache ($p<0.05$) in den db/db-Mäusen gegenüber den nicht-diabetische db+/db-Mäusen und war in WT-MSZ und $CD362^-$ db/db-Mäusen wieder normalisiert.

Abschließend kann gesagt werden, dass WT-MSZ und $CD362^-$-Zellen, aber nicht die $CD362^+$-Zellen, die LV Funktion durch eine Regulation von Titin verbessern.

ABSTRACT（English）

Mesenchymal stromal cells (MSCs) are an attractive cell-type for cell therapy, given their immunomodulatory, anti-fibrotic, and endothelial-protective features. The EU Committee for Advanced Therapies highlighted the need for strategies of selecting and purifying MSCs, whereupon the cell-surface sulfated proteoglycan CD362 has been identified as a new candidate.

The aim of the present study was to compare the impact of intravenous (i.v.) application of wildtype (WT), $CD362^-$- and $CD362^+$-selected MSCs on left ventricular (LV) function in type 2 diabetic mice and to investigate the underlying mechanisms. For this purpose, 10^6 WT-MSC, $CD362^-$, or $CD362^+$ cells or PBS were i.v. injected into 20-week-old diabetic BKS. Cg-m+/+Leprdb/BomTac db/db mice. Non-diabetic db+/db mice injected with PBS served as controls. Mice were hemodynamically characterized and sacrificed four weeks after cell or PBS application. Spleens were collected for flow cytometry and LVs for immunohistochemistry, molecular biology, and imaging mass spectrometry.

I.v. injection of WT-MSC and $CD362^-$ cells, but not of $CD362^+$ cells improved LV function in db/db mice as indicated by an improvement of the contractility parameters dP/dt_{max}, dP/dt_{min} and/or Tau ($p<0.05$). With respect to immune modulation, only $CD362^+$ cells raised the percentage of splenic regulatory T cells (Tregs) by 1.3-fold ($p<0.001$), whereas WT-MSC, $CD362^-$, and $CD362^+$ cells all decreased the percentage of splenic apoptotic Tregs in db/db mice ($p<0.001$ each versus db/db mice). Additionally, the number of cardiac $CD3^+$ cells was 1.5-fold ($p<0.05$), 1.8-fold ($p<0.01$), and 1.7-fold ($p<0.01$) reduced in db/db mice injected with WT-MSC, $CD362^-$, and $CD362^+$, respectively, compared to db/db mice. Interestingly, application of WT-MSC, $CD362^-$, and $CD362^+$ cells led to a 1.6-fold ($p<0.05$), 1.8-fold ($p<0.01$), and 1.6-fold ($p<0.05$) decreased number of cardiac $CD68^+$ cells. A hypothesis-free proteome analysis via imaging mass spectrometry further indicated a

lower expression of the titin isoform N2B in db/db versus db+/db mice, which could be overcome after i.v. application of all investigated cells. In agreement with the LV function, total titin phosphorylation was 1.8-fold ($p<0.01$) downregulated in db/db versus db+/db mice, which was only induced after application of WT-MSC (1.6-fold; $p<0.05$) and $CD362^-$ (1.5-fold; $p<0.05$). In parallel, protein kinase G activity dropped by 1.5-fold ($p<0.05$) in db/db versus non-diabetic db+/db mice and was normalized to control levels in WT-MSC db/db and $CD362^-$ db/db mice.

In conclusion, WT-MSC and $CD362^-$ cells, but not $CD362^+$ cells improve LV function in diabetic db/db mice via titin regulation.

ABBREVIATIONS

ABC	avidin-biotin complex
AGE	advanced glycated endproducts
ANOVA	analysis of variance
AP	alkaline phosphatase
ASC	apoptosis-associated speck-like protein-containing protein
α-SMA	alpha-smooth muscle actin
ATMP	Advanced Therapy Medicinal Products
BM	bone marrow
BW	body weight
Ca^{2+}	calcium
CD	cluster of differentiation
cDNA	complementary DNA
CI	cardiac index
DAMP	damage-associated molecular pattern
db	diabetes
DCM	dilated cardiomyopathy
DM	diabetes mellitus
DNA	deoxyribonucleic acid
dP/dt_{max}	maximum left ventricular pressure rise rate
dP/dt_{min}	maximum left ventricular pressure drop rate
ECM	extracellular matrix
EDTA	ethylenediaminetetraacetate
EF	ejection fraction
ELISA	enzyme-linked immunosorbant assay
EU	European Union
FOXP3	transcription factor forkhead box protein P3
HbA_{1c}	glycated hemoglobin A1c
HF	heart failure

HLA	human leukocyte antigen
HR	heart rate
HRP	horseradish peroxidase
HSPG	heparan sulfate proteoglycan
IHC	immunohistochemistry
IL	interleukin
i.p.	intraperitoneal
i.v.	intravenous
LOX	lysyl oxidase
LV	left ventricular / left ventricle
LVP_{max}	maximum left ventricular pressure
mRNA	messenger RNA
MNC	mononuclear cell
MSC	mesenchymal stromal cell
NLRP3	domain-like receptor protein 3
NOD	nucleotide-binding oligomerization domain
OCT	optimum cutting temperature
PAMP	pattern-associated molecular pattern
PBS	phosphate-buffered saline
PCR	polymerase chain reaction
REDDSTAR	Repair of Diabetic Damage by Stromal Cell Administration
ROS	reactive oxygen species
RNA	ribonucleic acid
RT	room temperature
SEM	standard error of the mean
STZ	streptozotocin
Tau	time of the LV pressure decrease
TGF-β	transforming growth factor-beta
TLR	toll-like receptor

TNF-α	tumor necrosis factor-alpha
Tregs	regulatory T cells
UNG	uracil-DNA N-Glycosylase

1. Introduction

1.1. Diabetic cardiomyopathy

1.1.1. Definition - Diabetes mellitus

Diabetes mellitus (DM) is a significant global health problem currently affecting over 300 million people currently worldwide and an estimated about 450 million people by 2030 [1]. DM is a multifactorial and metabolic disease, characterized by impaired metabolism of carbohydrate, fat, and proteins, as a result of the deficiency of insulin secretion, insulin action, or both. There are two major forms of DM. Type 1 is defined as insulin-dependent DM and type 2 is defined as non-insulin-dependent DM. Insulin is a hormone produced by the pancreas, which is primarily responsible for controlling blood glucose levels. Autoimmune destruction of ß cells, which produce insulin in the pancreas leads to type 1 DM, whereas insulin resistance with or without insulin deficiency leads to type 2 DM. Hyperglycemia is the key mark of DM. It increases the total number of free fatty acids, which leads to abnormalities in calcium homeostasis and lipid metabolism, and also promotes the production of reactive oxygen species, which promotes among others apoptosis in cardiomyocytes.

DM can lead to serious diseases affecting the heart and blood vessels, nerves, eyes, kidneys, and limbs. In addition, people with diabetes also have a high risk of recurrent infections. Cardiovascular disease, particularly coronary artery disease, represents a leading cause of morbidity and mortality in patients with DM [1]. Because of these complications, especially coronary artery disease, DM is one of the top ten causes of death [2].

1.1.2. Diabetic cardiomyopathy

Diabetic cardiomyopathy is one of the most common causes of heart failure, contributing to the main mortality and morbidity rate of cardiomyopathy [3]. It was first discovered in 1972 by Rubler *et al.* [4] as a new type of specific cardiomyopathy,

described in an autopsy report from four diabetic patients who had congestive heart failure and normal coronary arteries. Then, in 1974, the definition of diabetic cardiomyopathy was given by Hamby *et al.* [5]. Diabetic cardiomyopathy can be described as a cardiac disorder with myocardial structural and functional changes, in the absence of coronary artery disease, chronic hypertension and significant valvular disease [6][7]. Epidemiological, clinical, and experimental studies during the past three decades subsequently confirmed the existence of diabetic cardiomyopathy. Still at present, diabetic cardiomyopathy is a poorly understood "entity" [8] and there is no widely accepted way for diagnosing diabetic cardiomyopathy.

1.1.3. Epidemiology

Although several epidemiological studies demonstrate an increased risk of heart failure in diabetic patients [9][10], the prevalence and natural history of diabetic cardiomyopathy remains rarely defined. In the year 2014, Sanjay selected 2042 residents randomly, aged 45 years or older over a 3 years period [11]. All patients underwent echocardiographic assessment of systolic and diastolic function. The diagnosis of diabetic cardiomyopathy was made in 23 people, corresponding to a community population prevalence rate of 1.1%. Among diabetic patients, 16.9% met the standard of diabetic cardiomyopathy and 54.4% had diastolic dysfunction. DM was associated with an average 1.9-fold increase in the risk of any left ventricular dysfunction, which can be separately described as a 1.7-fold increase in the risk of diastolic dysfunction, and a 2.2-fold increase in the risk of systolic dysfunction. Among patients with diabetic cardiomyopathy, the morbidity and mortality of patients with diabetic cardiomyopathy are high, approaching 31% over a period of 9 years.

1.1.4. Pathogenesis of diabetic cardiomyopathy

Diabetic cardiomyopathy is associated with impaired cardiac function due to cardiomyocyte hypertrophy [12], interstitial and perivascular fibrosis [13][14][15], intramyocardial microangiopathy [16], interstitial inflammation [17], abnormal

intracellular calcium (Ca^{2+})-handling [18], endothelial dysfunction [19], cardiomyocyte stiffness [20][21], and/or a defect in substrate metabolism [22]. The pathogenesis of diabetic cardiomyopathy is multifactorial. Hyperglycemia, hyperinsulinemia, and dyslipidemia, each trigger cellular signaling leading to specific alterations in cardiac structure [23][24] (**Figure 1**). These processes are not mutually exclusive and are likely to occur synergistically. The pathological relevance of each of the different metabolic perturbations that accompany diabetes, including hyperglycemia, hyperinsulinemia, and dyslipidemia, and the cellular consequences leading to altered myocardial structure and function still remains not fully understood [25].

The relevance of the duration and severity of hyperglycemia is reflected in the incidence of diabetic cardiomyopathy in patients with DM [24]. Several studies have demonstrated that hyperglycemia directly causes cardiac damage, contributing to the development of diabetic cardiomyopathy. Hyperglycemia induces oxidative stress by triggering the generation of reactive oxygen species (ROS) via increasing glucose oxidation, leading to the generation of advanced glycated end-products (AGE) and mitochondrial generation of superoxide on the one hand and by decreasing the production of antioxidant enzymes on the other hand [26]. This has a negative influence on Ca^{2+} homeostasis and leads to the production of irreversible crosslinks between extracellular matrix (ECM) proteins [27] and impairs contractile function (**Figure 1**).

Animal models with hyperinsulinemia without hyperglycemia have increased left ventricular mass and diastolic dysfunction, in the absence of systolic dysfunction. Hypertrophy is thought to be mediated via the insulin growth factor/phosphatidyl-inositol-3-kinase-Akt signaling axis [28] (**Figure 1**).

Hyperlipidemia, including increased triglycerides and non-esterified fatty acids, plays not only a central role as a trigger in cellular insulin resistance but also in the development of myocardial contractile dysfunction. The increased uptake of free fatty acids in the diabetic heart may lead to cell apoptosis/death [29]. These unoxidized free fatty acids can cause lipotoxicity, via conversion of FFA to harmful ceramide,

which can induce cellular apoptosis through the induction of NF-κB, caspase 3 activity, and cytochrome c release [25][30] (**Figure 1**).

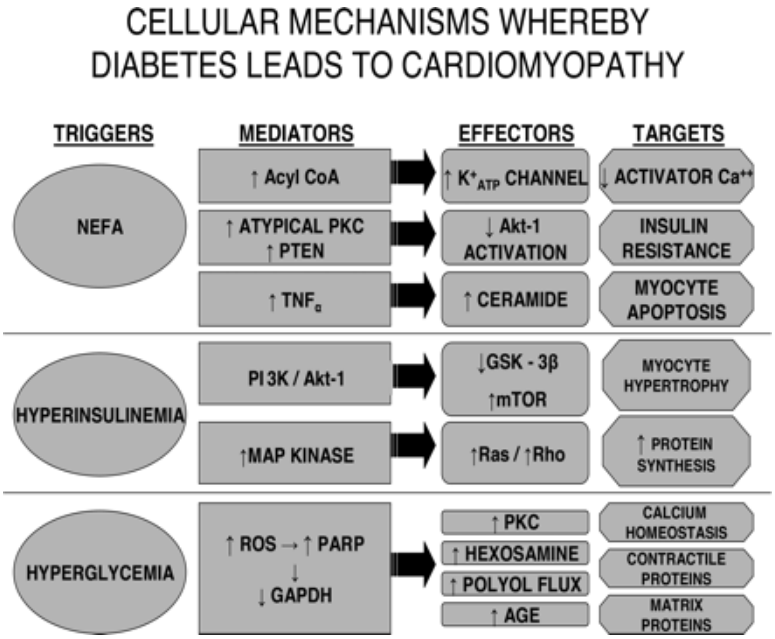

Figure 1. Scheme representing how diabetes mellitus-associated triggers can induce cardiomyopathy. The relationship between the metabolic triggers (non-esterified fatty acids (NEFA), hyperinsulinemia, and hyperglycemia) and the mediators, effectors, and targets is outlined [24].

1.1.5. Diabetic mouse models

In order to perform research on DM, several animal models have been developed in rodents (rats and mice) [31][32], dogs [33], horses [34], and other mammals.

Both models of type 1 and type 2 DM are available in rodents. To create Type 1 DM, mice are injected 1 or 5 days with streptozotocin (STZ), depending on the different dose used. STZ induces DM via its cytotoxic effect on the ß cells of the pancreas through DNA damage [35]. As a result of its action, ß cells undergo destruction by necrosis.

Obesity can be the result of natural mutations or genetic manipulation. Alternatively, obesity can occur by a high-fat feeding experiment. Monogenic models of obesity commonly used in type 2 diabetes research are the Lep ob/ob mouse, which is

deficient in leptin, and the Lepr db/db mouse and Zucker Diabetic Fatty (ZDF) rat, which are deficient in the leptin receptor. Polygenic models include the KK mouse and the OLETF rat. These models are widely used to test new therapies for type 2 DM [36][37][38].

1.2. Mesenchymal stromal cells

1.2.1. Definition

Mesenchymal stromal cells (MSCs) are self-renewable multipotent stromal cells that have the potential to differentiate into various lineages, including bone, cartilage, and adipose tissue [39][40]. In 2006, the minimal criteria for multipotent MSCs were defined in a position statement of the International Society for Cellular Therapy [41]. These minimal criteria include 1) the ability to adhere to plastic in standard culture conditions; 2) the expression of cluster of differentiation (CD)73, CD90, and CD105 and the lack of expression of the hematopoietic surface molecules CD14, CD34, CD45, CD11b, CD79 α, CD19 and HLA-DR [41] (**Figure 2**) and 3) the capacity to differentiate under specific cell culture conditions into osteoblasts, adipocytes, and chondrocytes.

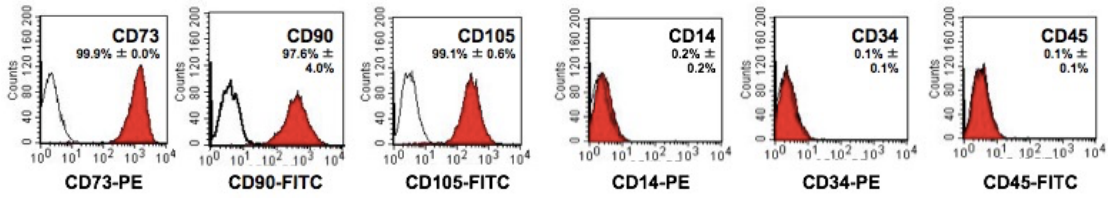

Figure 2. Specific surface antigen expression of mesenchymal stromal cells. MSCs are positive for the surface markers CD73, CD90, CD105, and negative for CD14, CD34, and CD45.

1.2.2. Bone marrow-derived mesenchymal stromal cells

In the bone marrow (BM) where MSCs were originally identified by Friedenstein *et al.* [42] in 1987, MSCs represent a rare population of ~1 in 10,000 nucleated cells and

they are 10-fold less abundant than hematopoietic stem cells [43]. They can be easily grown and expanded in culture [44]. For several decades, separation methods have been improved, and BM-derived MSCs have been used in numerous studies [45][46]. Meanwhile MSCs have been retrieved in virtually all post-natal organs and tissues [27], including the heart [32], fetal thymus [47], fetal pancreas [48], fetal liver [49], placenta [50][51], endometrium [52], umbilical cord blood [53], scalp tissue, and vermiform appendix [54].

1.2.3. Mesenchymal stromal cells for (cardiac) cell therapy

Besides their ease of culture, MSCs are especially attractive for cell therapy, given their immunomodulatory properties [55][56], their capacity to home to damaged tissues [57][56], and their low immunogenic nature, allowing allogeneic use [58].

With respect to cardiac repair, MSCs have been demonstrated to be able to differentiate into cardiomyocytes, endothelial cells, and smooth muscle cells [59]. However, the cardioprotective effects of MSCs are mainly attributed to facilitating endogenous repair via the release of paracrine factors including vascular endothelial growth factor, hepatocyte growth factor, stromal-derived factor 1, stem cell factor, and others, via which they exert their immunomodulatory [60][61], anti-oxidative [61], anti-fibrotic [62][56], anti-apoptotic [61], and pro-angiogenic effects [63][64] (**Figure 3**).

MSCs have also been demonstrated to have an anti-diabetic therapeutic potential in spontaneous autoimmune NOD- and STZ-induced diabetic mice [65][66]. Despite the ability of MSCs to differentiate into insulin-producing cells, the percentage of pancreatic islets derived from MSCs after *in vivo* administration is small. Therefore, the anti-diabetic effect of MSCs after *in vivo* administration is again mainly thought to be due to their ability to repair pancreatic ß cells, increase islet capillary density and reduce ß-cell apoptosis in a paracrine manner [67] (**Figure 3**).

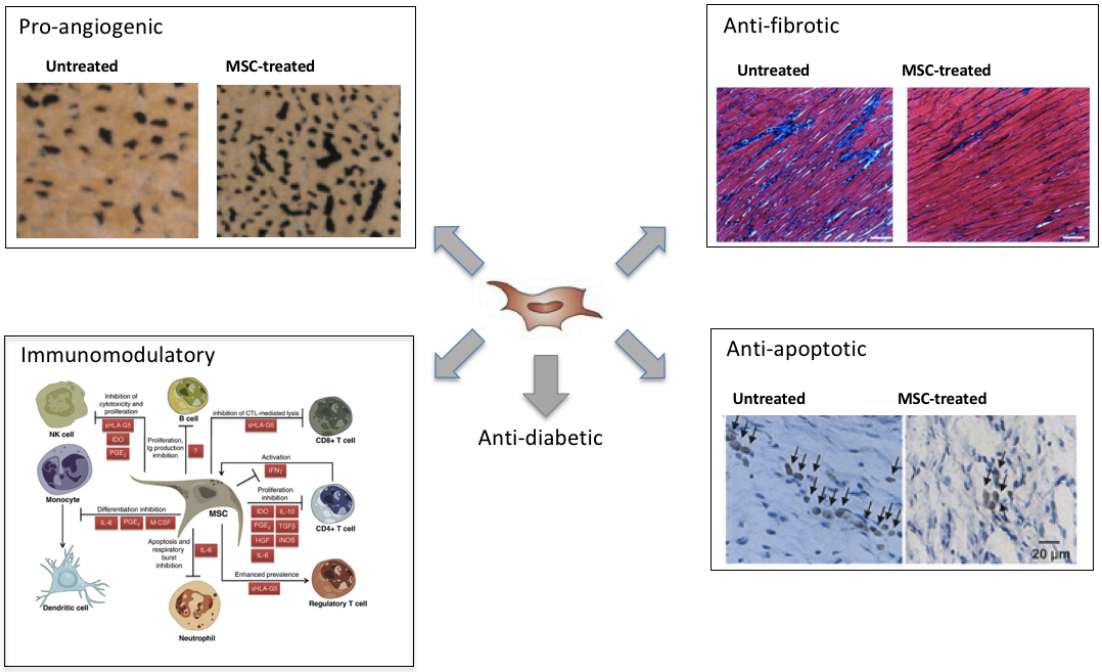

Figure 3. Therapeutic capacity of MSCs.

Importantly, MSCs are "clever" cells since they adapt to the environment/danger signals they are exposed to. For example, MSCs have pro-angiogenic features. However, in the context of tumorigenesis, anti-angiogenic properties of MSCs have been identified [68]. Furthermore, MSCs suppress T cell proliferation [69] and differentiation [70], but in the absence of exogenous inflammatory cytokines or T cell activation, MSCs actually prolong the survival of lymphocyte proliferation [71][67].

1.2.4. Clinical applications

After the discovery that BM-derived MSCs have the biological property of differentiating into mesenchymal lineages, BM-derived MSCs were thought to play a leading role in the normal turnover and maintenance of adult mesenchymal tissues [72]. As a result, MSCs became an attractive cell source for therapeutic applications in multiple fields of regenerative medicine. The most obvious application was to apply MSCs in mesenchymal tissue, e.g. for bone and cartilage regeneration. Actually, the first studies tried to use MSCs for repairing bone defects and for the treatment of

various bone diseases [73], including osteogenesis imperfecta, which defines a heterogeneous group of genetic disorders characterized by bone fragility and bone deformities such as osteoporosis. Clinical trials with MSCs have been started to treat children with osteogenesis imperfecta, which achieved good results [74][75].

There are currently several clinical trials evaluating the safety and efficacy of MSCs for treating diverse diseases, including idiopathic pulmonary fibrosis, chronic obstructive pulmonary disease [76], liver disease [77], heart disease [78][79] and DM [80]. With respect to heart disease, intracoronary MSCs application has been demonstrated to be save and to improve left ventricular (LV) ejection fraction (EF) and/or reduce scar tissue and improve myocardial perfusion in patients with ST-elevation after acute myocardial infarction [78][81][82]. Transendocardial MSCs injection has also been shown to improve LV function and/or ventricular remodeling and quality of life in patients with chronic ischemic cardiomyopathy [83][84]. Hare *et al*. [85] further showed for the first time that also intravenous (i.v.) application is safe and improves EF in myocardial infarction patients. Recently, Butler *et al.* [86] confirmed the safety and efficacy of the i.v. administration route in patients with non-ischemic cardiomyopathy. I.v. MSCs injection caused immunomodulatory effects and was associated with improvements in health status and functional capacity.

With respect to diabetes, nine clinical safety trials are currently ongoing and one has been finalized [80].

1.2.5. CD362 and CD362-selection of bone marrow-derived mesenchymal stromal cells

CD362, also called syndecan-2, is a heparan sulfate proteoglycan (HSPG). HSPGs are found at the cell surface and in the ECM and interact with a plethora of ligands, leading to a series of activations. HSPGs influence among others cell migration in the ECM, like cell-ECM attachment, cell movement, and cell-interaction. Furthermore, they bind cytokines, chemokines, and growth factors to protect them from proteolysis. HSPGs also affect angiogenesis [87]. Syndecan-1 is involved in inflammation and

fibrosis after myocardial injury and remodeling [88][89], and it plays a role in heart failure [90]. While syndecan-4 expression has been found in the infarcted region after myocardial infarction [91], the role of syndecan-2 (CD362) in heart disease has not been demonstrated before.

CD362 is expressed in cells of mesenchymal origin and in the main syndecan expressed during embryonic development [92]. CD362 expression can be detected in adult human BM and umbilical cord, and in mouse-digested/flushed marrow, adipose muscle tissue and lymphoid stromal cell populations [93][94].

The firm Orbsen Therapeutics Ltd (Galway, Ireland) defined CD362 as a marker to select MSCs from the mixture of BM cells, enabling the collection of a clearly defined population of MSCs from the BM of human donors. With the aim to use MSCs as a clinical product, this ability is expected to become a prerequisite for cell therapy products. In fact, the current standards of the European Union for defining a MSC-based Advanced Therapy Medicinal Products (ATMP) are very basic and focus on MSCs sterility and toxicology. However, both the European Union and the British Standard Institute highlight the BM-plating method of purifying MSCs as inadequate for defining or purifying MSCs for clinical use, as only 1:100,000 BM-derived MNCs plated are MSCs. The use of an anti-CD362 antibody, which allows MSCs to be selected from the BM beyond the MSCs/MNCs purity ratio of 1:13, a ratio obtained with a mixture of other antibodies directed against MSCs (*communications form Orbsen Therapeutics Ltd*). This superior ability of selecting a clearly defined population of MSCs formed the base of the "Repair of Diabetic Damage by Stromal Cell Administration" (REDDSTAR) Consortium of the European Commission 7th Framework, by which the efficacy of novel CD362^{+} versus CD362^{-} and unselected MSCs in alleviating diabetic nephropathy, diabetic neuropathy, diabetic retinopathy, diabetic cardiomyopathy and wound ulceration was evaluated.

2. Rationale

Despite advances in anti-diabetic therapies and patient self-management, DM represents a growing medical and economic problem. Glycemic control remains sub-optimal in many patients who develop significant secondary complications. One of the common complications of DM is diabetic cardiomyopathy, a specific cardiac disorder associated with cardiac dysfunction and cardiac structural alterations.

BM-derived MSCs are a mixed population of plastic-adherent cells with cardioprotective properties known to improve experimental diabetic cardiomyopathy. However, with the aim to have a clinical therapeutic cell product, a clearly defined population of MSCs is required, which has been shown to be possible via CD362 selection. Within the REDDSTAR consortium, this study was focused on investigating the efficacy of $CD362^{+}$- versus $CD362^{-}$- and unselected MSCs in alleviating diabetic cardiomyopathy in an experimental model of type 2 DM, the db/db mouse.

3. Materials and methods

3.1. Materials

Table 1. Consumption materials

Article	Description	Company
96-well Multiply®-PCR plate		Sarstedt, Nümbrecht, Germany
Cell Strainer	70 µm	BD Biosciences, New Jersey, USA
Coverslips	21 x 26 mm	R. Langenbrinck, Emmendingen, Germany
Cryotubes	1.5 ml	Carl Roth, Karlsruhe, Germany
Falcon tubes	15 ml, 50 ml	Corning, New York , USA
Folded filter	MN615 1/4·¢240 mm	Macherey-Nagel, Duren, Germany
Gloves		Sempercare, Northamptoshire, Germany
Masks		Charite, Berlin, Germany
MicroAmp®Optial 384-well plate	Reaction plate with Barcode	Thermo Fisher Scientific, Waltham, Massachusetts, USA
Microtome blades Feather®	A35 type	Pfm medical ag, Köln, Germany
PCR-tubes	0.2 ml, conical lid	Biozym, Hess. Oldendorf, Germany
Pellet pestle and tubes	Dstry-SR-15 and 1.5 ml tubes	Biozym, Hess. Oldendorf, Germany
Pipette tips	10 µl, 100 µl, 1000 µl	Biozym, Hess. Oldendorf, Germany
Pipettes		Corning, New York , USA

Plastic cannulas	18G und 20G	B.Braun, Melsungen, Germany
Plunger	2.5 ml syringe	TERUMO, Tokyo, Japan
Reaction Tubes	Safe-Lock or RNAse free	Sarstedt, Nümbrecht, Germany
Scalpels Feather®		Pfm medical ag, Köln, Germany
Slides	Super Frost Plus	R.Langenbrinck, Emmendingen, Germany

Table 2. Laboratory equipments

Equipment	**Description/Type**	**Company**
Conductance catheter	1.2 French	Scisense Inc., Ontario, Canada
Cryostat		Microm, Minnesota, USA
Freezer -20 °C	Economic super	Bosch AG, Stuttgart, Germany
Freezer -80 °C	Nuaire Ultralow Freezer	Zapf Instrumente, Sarstedt, Germany
Homogenizer	Pellet Pestle Motor	Sigma, Taufkirchen, Germany
Horizontal shaker	SM-25	Edmund Bühler, Tübingen, Germany
Ice maker	AF-10	Scotsman, Vernon Hills, USA
Incubator	Function Line	Heraeus, Osterode, Germany
Microscope	DMRBE	Leica, Bensheim, Germany
MACSQuant Tyto		Miltenyi Biotec, Bergisch Gladbach, Germany
pH meter	Knick Digital 646	Beyer, Düsseldorf, Germany
Pipettes		Eppendorf, Wesseling-Berzdorf, Germany
P-V Amplifier System	MPVS 300/400	Millar Instruments, Houston, USA

Spectrophotometer	NanoDrop	Thermo Scientific PEQLAB, Erlangen, Germany
Photometer	SPECTRA max 340PC384	Molecular Devices, Biberach an der Riß, Germany
Tabletop centrifuge	Centrifuge 5415 C	Eppendorf, Wesseling-Berzdorf, Germany
Thermocycler	Mastercycler gradient	Eppendorf, Wesseling-Berzdorf, Germany
Thermomixer	Comfort	Eppendorf, Wesseling-Berzdorf, Germany
Ventilator	Mini-Vent	Harvard Apparatus, Massachusetts,USA
Vortexer	VF2	IKA-Labortechnik, Staufen, Germany

Table 3. Buffer, reagents and kits

Article	**Company**
1% ß-mercaptoethanol	Sigma-Aldrich Chemie GmbH, Taufkirchen, Germany
3-amino-9-ethylcarbazole (AEC)	Sigma-Aldrich Chemie GmbH, Taufkirchen, Germany
ABC Blocking Kit	Vector Labs, Burlingame, USA
ABC Kit Standard	Vector Labs, Burlingame, USA
Acetic acid	VWR International GmbH, Darmstadt, Germany
Acetone	VWR International GmbH, Darmstadt, Germany
Avidin-Biotin-Blocking-Kit	Vector Labs, Burlingame, USA

Bovine serum albumin (BSA)	Carl Roth, Karlsruhe, Germany
Calcium chloride	VWR International GmbH, Darmstadt, Germany
DeadEnd™ Colorimetric TUNEL System	Promega, Mannheim, Germany
Dianova (secondary antibody)	Dianova, Hamburg, Germany
Di-Sodium hydrogen phosphate dihydrate	VWR International GmbH, Darmstadt, Germany
Distilled water	Alleman Pharma GmbH, Rimbach, Germany
DNAse I	Qiagen, Hilden; Germany
EDTA	VWR International GmbH, Darmstadt, Germany
EnVision K4003	Dako, Hamburg, Germany
Ethanol	Sigma-Aldrich Chemie GmbH, Taufkirchen, Germany
Fetal Bovine Serum (FBS)	Biochrom, Berlin, Germany
Fixation/Permeabilization kit	BD Biosciences, New Jersey, USA
Formalin	Sigma-Aldrich Chemie GmbH, Taufkirchen, Germany
GLYCO-Tek Affinity Column Kit	Helena Laboratories, Texas, USA
Hemalum	VWR International GmbH, Darmstadt, Germany
High Capacity Archive Kit	Thermo Fisher Scientific, Waltham, Massachusetts, USA
High Capacity cDNA Reverse Transcription Kit	Applied Biosystems, Darmstadt, Germany
Hydrogen peroxide solution	Sigma-Aldrich Chemie GmbH, Taufkirchen, Germany

Isopropanol	Sigma-Aldrich Chemie GmbH, Taufkirchen, Germany
Kaiser's glycerol gelatin	Carl Roth, Karlsruhe, Germany
Magnesium chloride	VWR International GmbH, Darmstadt, Germany
N, N-dimethylformamide	Carl Roth, Karlsruhe, Germany
Potassium chloride	VWR International GmbH, Darmstadt, Germany
Potassium dihydrogen phosphate	VWR International GmbH, Darmstadt, Germany
RNase-free water	Thermo Fisher Scientific, Waltham, Massachusetts, USA
RNeasy Mini Kit	Qiagen, Hilden; Germany
Sodium acetate	VWR International GmbH, Darmstadt, Germany
Sodium chloride	VWR International GmbH, Darmstadt, Germany
Sodium hydrogen phosphate	VWR International GmbH, Darmstadt, Germany
Tissue Tek	Sakura, Zoeterwoude, Netherlands
Tris-Base	Sigma-Aldrich Chemie GmbH, Taufkirchen, Germany
Tris-HCl	VWR International GmbH, Darmstadt, Germany
TRIzol Reagent	Thermo Fisher Scientific, Waltham, Massachusetts, USA

Table 4. Real-time-PCR reagents

Reagents	**Company, ID**
Optical 384-well Reaction Plate	Applied Biosystems, Darmstadt, Germany
Optical Adhesive film	Applied Biosystems, Darmstadt, Germany
TaqMan®Gene Expression Master Mix (2×)	Thermo Fisher Scientific, Waltham, Massachusetts, USA
Universal PCR Master Mix	Applied Biosystems, Darmstadt, Germany

Table 5. Primers for Real-time-PCR

Murine primers	**Ordering number**	**Company, ID**
ASC	Mm00445747_g1	Applied Biosystems, Darmstadt, Germany
α-SMA	Mm00725412_s1	Applied Biosystems, Darmstadt, Germany
Caspase1	Mm00438023_m1	Applied Biosystems, Darmstadt, Germany
CDKN1b	Mm00438167_g1	Applied Biosystems, Darmstadt, Germany
Col1a1	Mm01302043_g1	Applied Biosystems, Darmstadt, Germany
Col3a1	Mm00802331_m1	Applied Biosystems, Darmstadt, Germany
GAPDH	Mm99999915_g1	Applied Biosystems, Darmstadt, Germany
IL-10	Mm00439616_m1	Applied Biosystems, Darmstadt, Germany
IL-1ß	Mm00434228_m1	Applied Biosystems, Darmstadt, Germany
Lox1	Mm00495386_m1	Applied Biosystems, Darmstadt, Germany
Loxl2	Mm00804740_m1	Applied Biosystems, Darmstadt, Germany
Nlrp3	Mm00840904_m1	Applied Biosystems, Darmstadt, Germany
TGF-ß	Mm00441724_m1	Applied Biosystems, Darmstadt, Germany
TNF-α	Mm00443258_m1	Applied Biosystems, Darmstadt, Germany

Table 6. Antibodies for the immunohistochemical studies of cardiac tissue

AB	**Company**
Anti-α-SMA	Abcam, Cambridge, UK
Anti-CD3	Santa-Cruz Biotechn, Heidelberg, Germany
Anti-CD4	BD Bioscience, Heidelberg, Germany
Anti-CD68	Abcam, Cambridge, Germany
Anti-CD8a	BioLegend, Koblenz, Germany
Anti-Collagen I (secondary antibody)	Merck Millipore, Darmstadt, Germany
Anti-Collagen III (secondary antibody)	Merck Millipore, Darmstadt, Germany

Table 7. Antibodies for flow cytometry

Antigen	**AB**	**Company**	**Cat.Nr.**	**Volume of AB**
Annexin V	Anti-Annexin V-V450	BD Bioscience	560506	5 µl
CD4	Anti-CD4 FITC	Miltenyi Biotec	130-094-164	5 µl
CD8	Anti-CD8a VioBlue	Miltenyi Biotec	130-102-431	2.5 µl
CD25	Anti-CD25 PE	Miltenyi Biotec	130-094-164	5 µl
CD68	Anti-CD68 VioBlue	Miltenyi Biotec	130-102-448	5 µl
FoxP3	Anti-APC	Miltenyi Biotec	130-094-164	10 µl
TGF-β	Anti-TGF-β APC	BioLegend	141406	2.5 µl

3.2. Methods

3.2.1. Study design

In this study, 8-week-old heterogeneous (db+/db) and homogeneous (db/db) BKS.Cg-m+/+Leprdb/BomTac mice from Taconic (Skensved, Denmark) were used and housed under standard housing conditions (12 hour (h) light/dark cycle, 50-70% humidity, 19-21 °C). Leptin receptor (Lepr) knockout (KO) mice, commonly known as db/db mice, are a suitable model for studying the pathogenesis of type 2 non-insulin-dependent DM. Only homogeneous mice are diabetic, whereas heterogeneous mice are non-diabetic. Once a week and before cell application, blood glucose (BG) was measured after 4h fasting. For cell treatment, db/db mice were randomly divided into 4 groups (**Table 8**).

Table 8. Groups of mice in the study.

Group	**Number**
db+/db	9
db/db	6
db/db -WT-MSC	8
db/db CD362$^-$ MSC	9
db/db CD362$^+$ MSC	9

WT-MSC (WT), CD362$^-$, and CD362$^+$ cells from the same donor were provided by Orbsen Therapeutics Ltd. One million cells of each celltype were i.v. injected in 200 µl PBS in 20-week-old db/db mice. The control animals received the corresponding volume of PBS. After 4 weeks, mice were anesthetized and cardiac function was measured by conductance catheter. Subsequently, blood was taken and the left ventricle (LV) was immediately snap frozen in liquid nitrogen for molecular and immunohistochemistry examinations. Additionally, spleens were collected for flow cytometry. The experiments followed the European guidelines for the Care and Use of

Laboratory Animals and approved by the local authority (Landesamt für Gesundheit und Soziales, G0254/13, Berlin, Germany).

3.2.2. Characterization of cardiac function by conductance catheter

3.2.2.1. Theoretical background of the conductance catheter technique

Conductance is the reciprocal of electrical resistance and depends on the volume of the LV. The conductance catheter, which comprises a pressure (P) sensor and four electrodes, generating a permanent electric field to measure the potential difference between the electrodes. During the cardiac cycle, the physiological changes of LV volume alter the resistance and thereby the conductance of the blood. The electric field generated by the conductance catheter represents the total conductance from blood and surrounding tissues, especially from the LV. Thus, the calculated volume is overestimated and known as parallel conductance or parallel resistance. It has to be converted to correct volumes by subtracting the volume caused by the parallel conductance [95]. In this study, volume was corrected by the injection of 5-10 µl of a 10% saline solution into the jugular vein.

3.2.2.2. Parameters for cardiac function

Table 9. Parameters for cardiac function.

Parameter (abbreviation)	**Parameter (full name)**	**Formula or description**	**Unit**
CO	Cardiac output	CO = HR × SV	µl /min
CI	Cardiac index	CI = CO / BW	µl /min /g
EF	Ejection fraction	EF = ((LVEDV − LVESV)/ LVEDV) × 100	%
LVP_{max}	Maximum LVP	Maximum pressure generated by the left ventricle during systole.	mmHg
dP/dt_{max}	Maximum LVP	Contractility of the LV, which	mmHg/s

	rise rate	describes the maximum speed of the P rise in the LV.	
dP/dt_{min}	Minimum LVP drop rate	The minimum rate of P change during the isovolemic LV relaxation.	mmHg/s
Tau	Time of the LVP decrease	Represents the exponential decay of the LVP during isovolemic relaxation	ms

3.2.2.3. Anesthesia

Mice were intraperitoneally (i.p.) injected with a mixture of buprenorphine (0.05 mg/kg) + urethane (0.8-1.2 g/kg), 10-30 minutes (min) before starting the measurement. The depth of the anesthesia was checked by the response to tail or paws pinch. The following protocol is adapted from the original publication of Pacher *et al* [95].

3.2.2.4. Intubation and ventilation

Mice were fixed in supine position on a surgical platform and their necks were put in hyperextension position. Using surgical tape, the front paws, the tail, as well as the snout was fixed. The tape across the tip of the snout pulls the head slightly back to create traction on the trachea. Following a midline neck incision, the skin was pulled away from the underlying muscles and cut off. Surrounding tissues and the paratracheal muscles were gently removed from the trachea by using forceps. Afterwards, a small hole was cut onto the surface and the tracheostomy cannula was inserted, which was immediately connected to the respirator **(Figure 4)**. Stroke volume and respiratory rate were estimated as 6.5 ml/kg body weight (BW) and 200 units/min.

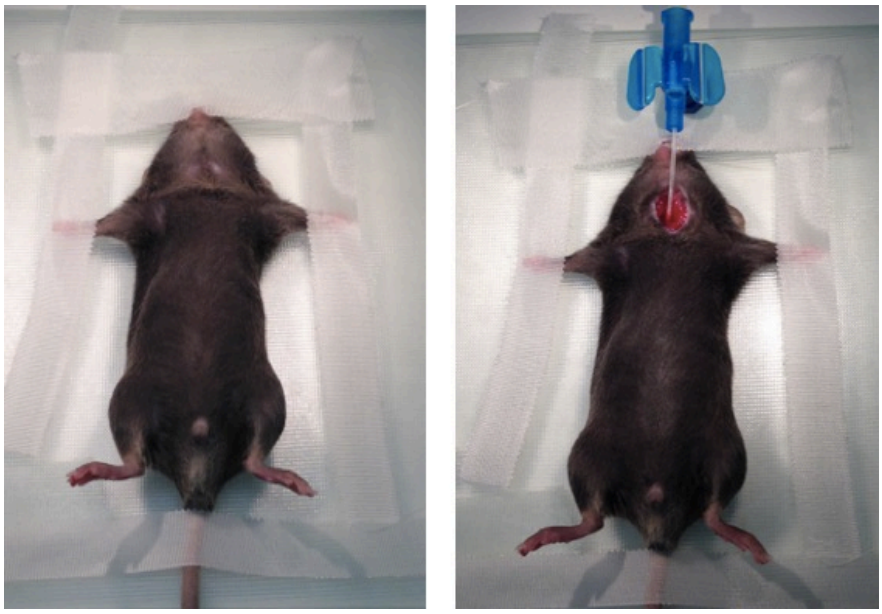

Figure 4. Intubation and ventilation of the mice for hemodynamic measurement.

3.2.2.5. Surgical procedures

The abdomen was opened with scissors in a transverse incision. To avoid excessive bleeding, the blood vessels were blocked with a cauter. Afterwards, an incision over the xiphoid process was made and the chest was opened. The edge of the diaphragm was cut to expose the apex of the heart. The pericardium was gently removed from the heart with forceps. A 25–30 gauge needle was used to punch circa 2-4 mm in the apex into the LV. After the needle was removed, the catheter tip was inserted into the LV until the proximal electrode on the catheter was in the LV **(Figure 5)**.

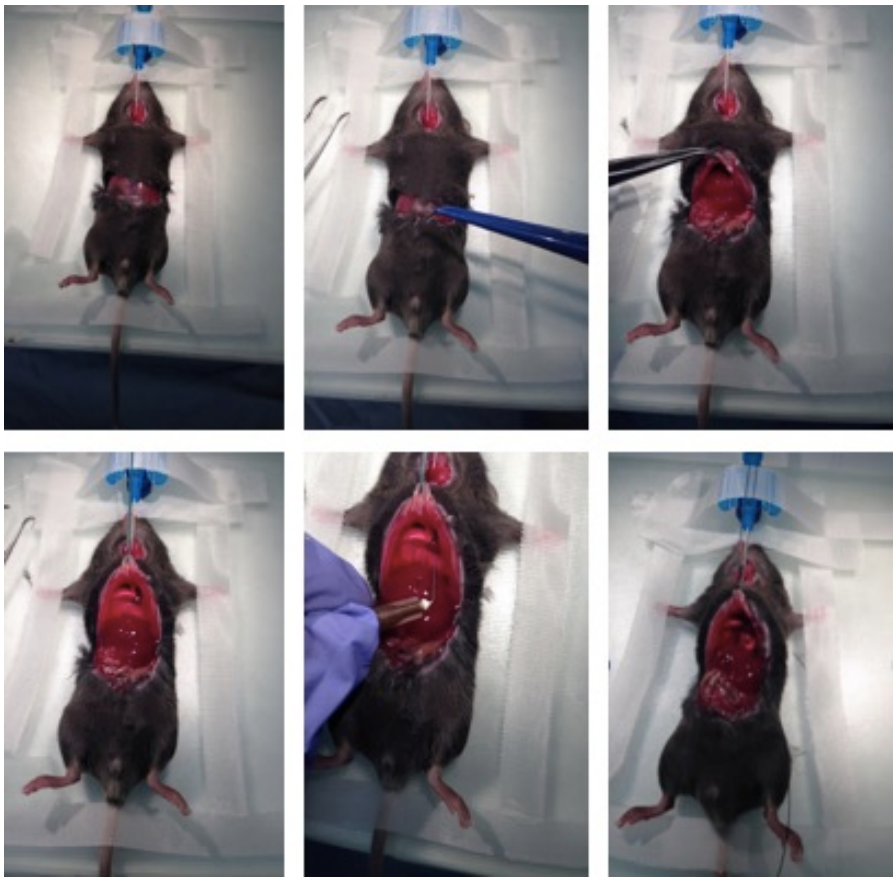

Figure 5. Surgical procedures of hemodynamic surgery.

3.2.2.6. Recording of pressure-volume loops by conductance catheter

In this study, the pressure-volume (PV) data of the LV were recorded in real time with the conductance catheter technique. With this method, it is possible to determine both volume-dependent and independent parameters describing the heart function. The catheter was connected to a PV-amplifier system and data were collected using the "IOX", 1.8.9 software (EMKA Technologies, Falls Church, USA). For analyzing, the program "Circlab 2004" (Paul Steendijk, GTX Medical Software, Belgium) was used.

For the recording, the position of the catheter was adjusted to obtain rectangular-shaped PV loops. The small animal respirator was shut off for 5 seconds (sec) to acquire data without lung motion artifacts. After stabilization of the signal, baseline PV loops at steady-state conditions were recorded 3 times. After recording the steady-state, 10% sodium chloride was injected into the jugular vein for volume

calibration. Analogous to the steady-state, the small animal respirator was shut off. Finally, the inferior vena cava was occluded for 1-2 sec and data were recorded as described above **(Figure 6)**. At the end of the experiment, the catheter was removed and mice were euthanized by cervical dislocation.

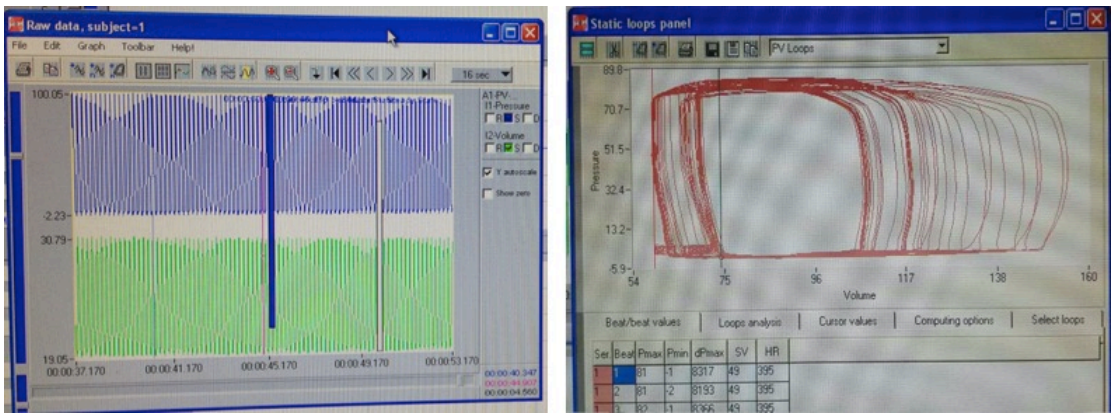

Figure 6. Recording of pressure-volume loops by conductance catheter.

3.2.3. Glycated hemoglobin kit

The Helena GLYCO-Tek kit (Helena Laboratories, Texas, USA) was used for the quantitation of a certain glycated hemoglobin fraction (HbA_{1c}) in whole blood samples. 50 µL of whole blood was placed in a tube and 400 µL GLYCO-Tek Hemolysate Reagent was added. To ensure complete hemolysis of the sample, the tube was vortexed. Afterwards, 100 µL of sample hemolysate was loaded onto the prepared GLYCO-Tek affinity columns, which were placed on the corresponding collection tubes. Next, the sample was allowed to set for 8 min, followed by washing each column with 0.5 ml GLYCO-Tek Developer A. Subsequently, additional 4 ml GLYCO-Tek Developer A was applied to the column with the large collection tube. The resulting eluate was adjusted to 15 ml with deionized water containing non-glycated hemoglobin (GHb). The column was then placed over the smaller collection tube and 3 ml GLYCO-Tek Developer B was added. The total eluent of the column contained GHb. Finally, both collection tubes were inverted 3 times and transferred to a cuvette. Immediately, absorbance of the GHb and non-GHb solution at 415 nm was measured.

The percentage of HbA_{1c} was calculated from the percentage of GHb by using the provided algorithm according to the manufacture's protocol.

3.2.4. Molecular methods

3.2.4.1. RNA extraction

RNA isolation was performed by using the TRIzol™ (Invitrogen, Heidelberg, Germany) method to isolate total RNA from tissue samples. For this purpose, frozen LV tissues were placed into a FACS tube containing 1 ml TRIzol™ reagent, and homogenized for 30 sec The homogenized samples were transferred to a 1.5 ml tube and 200 µl Chloroform was added. Samples were shaken for 15 sec and then incubated at room temperature (RT) for 2 min. After incubation, tubes were centrifuged with an acceleration of 10,000 rpm for 15 min at 4 °C. After centrifugation, the colorless upper phase containing the RNA, was carefully transferred into a new 1.5 ml tube. To precipitate the RNA, 500µl of 100% isopropanol was added to the sample and incubated at RT for 15 min, followed by centrifugation at 10,000 rpm for 10 min at 4 °C. To wash RNA pellets, 500 µl Ethanol (70%) was added and the samples were vortexed. After one more centrifugation for 10 min at 4 °C and with an acceleration of 7,500 rpm, the supernatant was removed and the remaining RNA pellets were dissolved in 100 µl RNase-free water. For purification, the NucleoSpin® RNA mini kit (Macherey-Nagel GmbH, Düren, Germany) was used according to the manufacturer's protocol. In detail, each sample was supplemented with 300 µl RA1 buffer and 300 µl ethanol (96%). Now, the lysates were loaded onto a NucleoSpin® RNA II column placed in a rack. After the next centrifugation at 12,000 rpm for 30 sec, columns were placed into a collection tube and 350 µl membrane desalting buffer was added. Additionally, a centrifugation at 12,000 rpm for 1 min was performed, followed by DNA digestion. For this purpose, 10 µl reconstituted rDNase was mixed with 90 µl reaction buffer and incubated for 15 min at RT. Subsequently, silica membranes were washed 3 times with 200 µl RA2, 600 µl RA3, and 250 µl RA3, respectively. Between washings, samples were

centrifuged for 30 sec at 12,000 rpm and the flow-through was discarded. Last centrifugation step was performed for 2 min and the column was placed into a 1.5 ml tube afterwards. To elute the RNA, 50 µl RNase-free water was used and centrifuged at 12,000 rpm for 1 min.

The concentration of RNA was measured at the absorbance of 260 nm by using a NanoDrop 1000 (Thermo Scientific, Erlangen, Germany).

3.2.4.2. Reverse Transcription

The High Capacity cDNA Reverse Transcription Kit from Applied Biosystems (Darmstadt, Germany) was used to perform reverse transcription, the generation of complementary DNA (cDNA) from RNA, from the isolated RNA. For this purpose, 1 µg RNA was filled up to a total volume of 11 µl with RNase-free water, and 2.8 µl random primers and dNTP´s were added. Random primers and template RNA were heated for 5 min at 70 °C in a thermocycler. Meanwhile, a master-mix was prepared by mixing the appropriate volumes of the following components: 2 µl buffer + 3.2 µl RNase-free water, and 1 µl reverse transcriptase. The heated tubes were directly put on ice and mixed with 6.2 µl of the mastermix. Reverse transcription was performed in a thermocycler according to the following program: 10 min at 25 °C, 2 h at 37 °C, followed by an additional 5 min at 85 °C and cooling to 4 °C. At the end of the reverse transcriptase, 30 µl RNase-free water was added to each sample to reach a final volume of 50 µl.

3.2.4.3. Real-time polymerase chain reaction

To evaluate the relative gene expression of different targets in the LV of the mice, a real-time polymerase chain reaction was performed using a mixture of 5 µl PCR master-mix, 0.5 µl gene reporter assay (both Life Technologies GmbH, Darmstadt, Germany), and 3.5 µl water.

The reporter assays include forward and reverse primers as well as the fluorescently 5' 6'FAM-labelled probe, with the 3' non-fluorescent Quencher NFQ-MGB). The volume of cDNA used is mentioned above **(Table 5)**. For the amplification of the sample, which is measured in duplicates, the 7900HT real-time system (Applied Biosystems, Darmstadt, Germany) with the subsequent program was used. First, addition at 50 °C for 2 min followed by an initial denaturation at 95 °C for 10 min. After the second denaturation at 95 °C for 15 sec, annealing and elongation at 60 °C for 1 min were performed. Depending on the target gene, the last two steps were repeated 40 or 45 times.

3.2.4.4. Housekeeping genes

We screened the Ct values of the housekeeping genes GAPDH and CDKN1b to determine which housekeeping gene could be used for normalization of the target gene data (**Figure 7**).

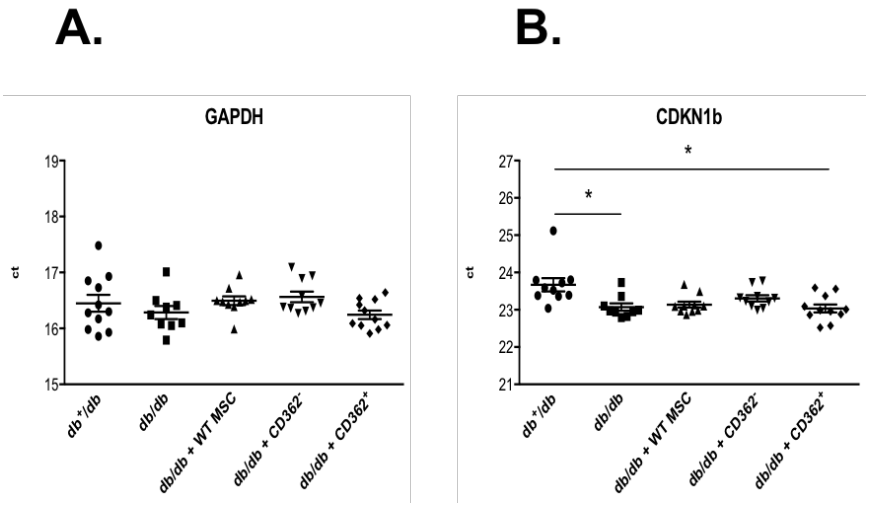

Figure 7. Evaluation of the Ct values of GAPDH and CDKN1b among the different experimental groups for housekeeping gene selection. Ct values of **A.** GAPDH and **B.** CDKN1b in db+/db, db/db, and db/db mice receiving WT-MSC, $CD362^-$ or $CD362^+$ cells. One-way ANOVA test. *$p<0.05$, with n=9 for db+/db, n=6 for db/db, n=8 for WT-MSC, n=9 for db/db $CD362^-$, and n=9 for db/db $CD362^+$.

There were no significant differences between the Ct values of GAPDH among the different groups, whereas the Ct values of CDKN1b were significantly different between db+/db and db/db, and db+/db and db/db $CD362^+$. Consequently, we used

GAPDH as housekeeping gene. Data were further normalized against GAPDH, which served as an endogenous control using the 2-ΔCt formula. To examine the n-fold change, mRNA levels were normalized to the db+/db group set as 1.

3.2.5. Immunohistochemistry

3.2.5.1. Generation of frozen sections

To obtain cryoslides from the LV, tissue samples were embedded in Tissue-Tek OCT (Sakura, Zoeterwoude, NL). Afterwards, they were cut into 5-µm-thick transverse sections using the cryostat (Microm, Minnesota, USA). Subsequently, the sections were immersed in ice-cold acetone for 10 min. After drying, the slides were immediately used for staining or stored at -20 °C.

3.2.5.2. Immunohistological staining

Immunohistochemistry (IHC) refers to the principle of specific antibody-antigen binding in a biological tissue [96]. In this study, two methods were used: the Avidin-biotin complex (ABC) method and the EnVision® method, depending on the biomarker investigated **(Table 10)**.

Table 10. Antibodies for immunohistochemistry: species, dilution, and method used.

1. AB	Species	Dilution	2.AB	Species	Dilution	Method
α-SMA	Rabbit	1:200	EnVision	Anti-Rabbit	—	EnVision
CD3	Goat	1:75	ABC-Kit	Anti-Goat	1:250	ABC
CD4	Rat	1:50	Dianova	Anti-Rat	1:250	ABC
CD8a	Rat	1:50	Dianova	Anti-Rat	1:250	ABC
CD68	Rabbit	1:600	Dianova	Anti-Rabbit	1:250	ABC
Col I	Rabbit	1:350	EnVision	Anti-Rabbit	—	EnVision
Col III	Rabbit	1:200	EnVision	Anti-Rabbit	—	EnVision

1. AB=primary antibody, 2. AB=secondary antibody.

3.2.5.3. EnVision® method

The EnVision® method was used to investigate cardiac collagen I, collagen III, and α-SMA expression. It is a two-step staining, combining the secondary antibodies with horseradish peroxidase (HRP) or alkaline phosphatase (AP) as detection system.

Procedure of the EnVision® method:

First, slides were washed once with 1x PBS for 5 min followed by adding 0.075% H_2O_2 for 7 min to block the endogenous peroxidase. Subsequently, slides were washed twice with 1xPBS, each time for 5 min on a shaker. Afterwards, 75-100 µl of the primary antibody (1.AB) was added to every section and slides were stored for 60 min in a moist vessel. Slides were washed twice again followed by addition of 75-100 µl of the secondary antibody (2.AB) and stored for 30 min in a moist vessel. As described above, additional washing was performed and slides were incubated for 12 min in the dark with substrate solution. Before hemalum staining, slides were washed again once with 1x PBS, and after 30 sec of staining 4-5 times with cold tap water.

3.2.5.4. Avidin-biotin complex method

The avidin-biotin complex (ABC) method is characterized by the extraordinary affinity of avidin for biotin, which allows specific binding between biotin-containing molecules and avidin. This method was used in this study to determine the presence of inflammatory cells such as CD3, CD4, CD8a and CD68.

Procedure of the ABC method:

As already described for the EnVision® method, slides were first washed and endogenous peroxidase was blocked. In contrast to the EnVision® method, 1x TBS was used instead of 1x PBS for all washing steps, but also for 5 min on a shaker.

Afterwards, 75-100 µl of a mixture containing 10% normal serum (depending on the species of the 2.AB), 1% BSA in 1x TBS, and 4 drops/ml Avidin was added to each section and stored for 30 min in a moist vessel. After adding 75-100µl antibody solution, which was supplemented with 1% BSA in 1x TBS, and 4 drops/ml Biotin,

the slides were kept for 60 min in the moist vessel. Subsequently, washing was performed twice and 75-100 µl of the 2.AB mixed with 1% BSA in 1x TBS was added for 60 min incubation. After washing twice with 1xTBS, and once with 1xTBS supplemented with 0.01% Tween, ABC-Solution was added (75-100 µl / section) and incubated for 30 min. Again, slides were washed 2 times followed by addition of the substrate solution for 12 min in the dark. Slides were washed twice and stained with hemalum. Finally, they were washed as described above.

3.2.6. Flow cytometry

To determine the immunomodulatory effects of MSCs application in diabetic db/db mice, flow cytometry was performed. For this purpose, the spleen of PBS- or cell-treated mice was collected and a single cell suspension was prepared. The collected spleens were positioned in a petri dish containing RMPI media. Afterwards, the spleens were mashed through a 70 µm cell strainer using the plunger of a 2.5 ml syringe. Subsequently, the cell strainer was flushed with 15 ml 1% FBS in 1xPBS. Afterwards, the solution was centrifuged for 5 min at 3500 rpm and RT. The supernatant was carefully aspirated and the remaining pellet was resuspended in 6 ml ACK lysis buffer. After 4 min incubation, lysis of the erythrocytes was stopped with 40 ml RPMI. Now, the cell suspension was passed through a 40 µm cell strainer and centrifuged at RT and 3500 rpm for 5 min. Subsequently, the supernatant was aspirated, and the cell pellet was resuspended in 2 ml FBS supplemented with 10% DMSO and stored at -80 °C for further analysis.

3.2.6.1. Investigation of splenic regulatory T cells

To analyze splenic regulatory T cells (Tregs), the mouse Tregs detection kit (Miltenyi Biotec) was used. Isolated splenocytes were defrozen. Afterwards, $1x10^6$ cells were resuspended in 85 µl binding buffer, which had previously been diluted 1/10 with water. The corresponding volume **(Table 7)** of CD4, CD25 and Annexin V V450 (BD

Bioscience, Heidelberg, Germany) AB was added to the solution and incubated for 20 min at 4℃ in the dark. Then, splenocytes were washed and centrifuged (always at 3000 rpm for 5 min at 4℃). After aspiration of the supernatant, cells were resuspended in 1 ml of cold, freshly prepared fixation/permeabilization solution and incubated 30 min at 4℃ in the dark. Following washing, and additional centrifugation, the cell pellet was resuspended in 80 µl of cold 1x permeabilization buffer for 15 min incubation. After that, cells were incubated for 30 min at 4 °C in the dark with a FoxP3 AB. For washing, cells were resuspended by adding 1 ml of cold 1x permeabilization buffer followed by additional centrifugation. To perform flow cytometry analysis, the cell pellet was resuspended in a suitable volume of PBS and measured on a MACSQuant Analyzer (Miltenyi Biotec). Further analysis was performed using the FlowJo software version 8.8.6. (Tree Star Inc., USA).

3.2.6.2. Investigation of splenic cytokine production

As described above, splenocytes were defrozen. Afterwards cells were plated at a density of $1x10^6$ cells/well in 96-well U-bottom plates (n=5 wells per condition) in Iscove medium (Sigma) containing 10% FBS and 1% P/S. To determine splenic cytokine production, cells were further stimulated with PMA/Ionomycin (BD Biosciences) at a final concentration of 50 ng/ml and 500 ng/ml in 6 ml Iscove medium. Finally, 4 µl of BD GolgiStop™ (BD Biosciences) was added for every 6 ml of the stimulation media with overnight incubation in the dark. On the next day, cells were collected, centrifuged and washed with PBS containing 1% FBS. First, cell surface staining of CD68 was performed followed by intracellular staining. For this purpose, cells where incubated with 300 µl fixation/permeabilization solution (Invitrogen) for 20min at 4 °C. To wash the cells, 1ml BD Perm/Wash™ buffer (Invitrogen) was added and samples were centrifuged. To stain for intracellular cytokines, 42.5 µl BD Perm/Wash™ buffer supplemented with TGF-β AB was added for 30 min at 4 °C in the dark. After additional washing, the cell pellet was resuspended in 200 µl PBS for flow cytometry analysis.

3.2.6.3. Investigation of splenocyte activation and proliferation

Splenocytes were defrozen and labeled with CFSE (CellTrace™ CFSE Cell Proliferation Kit; lifetechnologies). Subsequently, $1x10^6$ cells were resuspended with 10 µM CFSE in 1 ml PBS containing 0.1% BSA and incubated for 15 min at 37℃. Then, splenocytes were washed and centrifuged at 3000 rpm for 5 min. After discarding the supernatant, labeled cells were plated at a density of $1x10^6$ cells/well in 96 U-bottom well plates (n=5 wells per condition) in Iscove medium (Sigma) containing 10% FBS and 1% P/S. Subsequently, cells were stimulated with PMA/Ionomycin at a final concentration of 50 ng/ml and 500 ng/ml in 6 ml Iscove medium, with overnight incubation in the dark. On the following day, cell surface staining of CD4 and CD8 was performed. After additional washing, the cell pellet was resuspended in 200 µl PBS for flow cytometry analysis.

3.2.7. Heart section analysis by MALDI-Imaging mass spectrometry

MALDI-imaging mass spectrometry (IMS) was performed by Dr. Oliver Klein (corefacility proteomics, BCRT, Charité - Universitätsmedizin Berlin) according to an already established protocol [97].

In brief, paraformaldehyde (PFA)-fixed tissue samples of the LV were dehydrated by washing and embedded in paraffin. Afterwards, sections of 7 µm were prepared and transferred onto Indium-Tin-Oxide slides (Bruker Daltonik, Bremen, Germany). Samples were dewaxed and incubated with trypsin solution. According to the manufacturer's protocol, matrix solution was applied followed by MALDI-IMS. Data acquisition was performed on an Autoflex III MALDI-TOF/TOF with flexControl 3.0 and flexImaging 3.0 software (Bruker Daltonik) in a raster width of 80 µm. To determine regions of interest, tissue sections were stained after MALDI-IMS with hematoxylin and eosin (H/E). To identify proteins, the "bottom-up"-nano liquid chromatography (nLC) - MS/MS (nUPLC-MS/MS) approach was performed on an

adjacent tissue section. Comparison of MALDI-IMS and nUPLC−MS/MS data via a *Mus musculus* protein database downloaded from the UniProt database UniProt enables the identification of several peptides.

To assess statistical differences, data from each group were compared pairwise by using receiver operating characteristic (ROC, AUC < 0.4) analysis. P-values were calculated by the Wilcoxon rank-sum test and were set as significantly different at $p<0.05$.

3.2.8. Investigation of cardiac titin

The analysis of the phosphorylation state of cardiac titin and of protein kinase G activity was performed in cooperation with Dr. Nazha Hamdani (Department of Cardiovascular Physiology, Institute of Physiology, Ruhr University Bochum, Bochum, Germany).

3.2.8.1. All-titin phosphorylation by Pro-Q Diamond stain

Frozen tissues from LV mouse hearts were solubilized in 50 mM Tris sodium dodecyl sulfate (SDS) buffer (pH 6.8) supplemented with 8 µg/ml leupeptin (Peptin Institute, Japan) and phosphatase inhibitor cocktail (PIC [P2880], 10µl/ml; Sigma Aldrich). Afterwards, solubilized samples were heated, centrifuged, and separated on agarose-strengthened 1.8% sodium dodecyl sulfate-polyacrylamide gels. Following electrophoresis, gels were stained with Pro-Q Diamond phosphoprotein stain for 1h. According to the manufacturer's guidelines (Thermo Fisher Scientific), fixation, washing and de-staining were performed. Finally, gels were stained overnight with SYPRO Ruby (Thermo Fisher Scientific) to assess total protein content. Signals were visualized using the LAS-4000 Image Reader (460 nm/605 nm Ex/Em; 2 s illumination) and analyzed with Multi Gauge V3.2 and AIDA software.

3.2.8.2. Myocardial protein kinase G activity

LV tissue samples were homogenized to assess myocardial protein kinase G activity. For this purpose, tissue sections were treated with 25 mmol/l Tris (pH 7.4), 1 mmol/l EDTA, 2 mmol/l EGTA, 5 mmol/l dithiothreitol (DTT), 0.05% Triton X-100 and protease inhibitor cocktail (Sigma-Aldrich). Following centrifugation for 5 min, supernatants were incubated at 30 °C for 10min with a reaction mixture containing 40 mmol/l Tris-HCl (pH·7.4), 20 mmol/l magnesium acetate, 0.2 mmol/l [^{32}P] ATP (500-1000·c.p.m.·pmol^{-1}; GE Healthcare LifeScience, Little Chalfont, UK), 113·mg/ml heptapeptide (RKRSRAE), 3 mmol/l cGMP (Promega, Madison, Wisconsin, USA) and a highly specific inhibitor of cAMP-dependent protein kinase (5-24, Merck Millipore). Reaction was terminated by spotting 70 µl of the mix onto Whatman P-81 filters, which were then soaked with 75 mmol/l H_3PO_4 for 5 min. After washing three times with 75 mmol/l H_3PO_4 to remove any unbound [^{32}P] ATP, filters were rinsed with 100% ethanol and air dried before quantification. By using a universal scintillation cocktail, counts were taken in a Wallac 1409 Liquid Scintillation Counter. The activity of protein kinase G was expressed as pmol of ^{32}P, which was incorporated into the substrate (pmol/min/mg protein).

3.2.9. Statistical analysis

Statistical analysis was performed using GraphPad Prism 7.0 software (GraphPad Software, La Jolla, CA). Data are expressed as the mean ± SEM. The ordinary one-way ANOVA test was performed for data comparison. Differences were considered statistically significant at a value of $p<0.05$.

4. Results

4.1. Glucose

Blood glucose levels were 3.6-fold ($p<0.0001$), 4.6-fold ($p<0.0001$), and 4.7-fold ($p<0.0001$) higher in 9-, 20-, and 24-week-old db/db compared to db+/db mice, respectively. Stromal cell application in 20-week-old db/db mice did not affect blood glucose levels, nor HbA_{1c} levels in db/db mice. Blood glucose levels were 4.5-fold ($p<0.0001$), 4.5-fold ($p<0.0001$), and 4.9-fold ($p<0.0001$) higher in 24-week-old WT-MSC db/db, CD362$^-$ db/db, and CD362$^+$ db/db mice, i.e. 4 weeks post stromal cell injection, compared to db+/db mice, respectively **(Figure 8-9A)**. In parallel, HbA_{1c} levels were 1.7-fold ($p<0.05$) higher in db/db versus db+/db mice. These levels were not different in db/db mice receiving stromal cells, i.e. also in 24-week-old WT-MSC db/db, CD362$^-$ db/db, and CD362$^+$ db/db mice, i.e. 4 weeks post stromal cell injection, HbA_{1c} levels were 1.7-fold ($p<0.01$) higher than in db+/db mice. There were no differences among the different db/db groups **(Figure 9B)**.

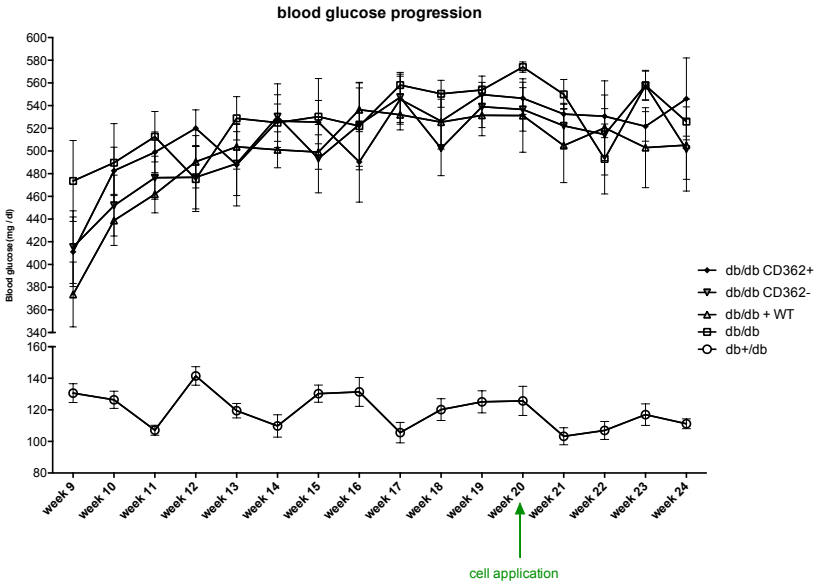

Figure 8. Blood glucose progression of db+/db mice and db/db mice intravenously injected with/without WT-MSC, CD362$^-$, or CD362$^+$. Intravenous stromal cell application occurred in 20-week-old db/db mice, as indicated with the green arrow. All values are expressed as the mean ± standard deviation (SD). One-way ANOVA test, with n=9 for db+/db, n=6 for db/db, n=8 for WT-MSC, n=9 for db/db CD362$^-$, and n=9 for db/db CD362$^+$.

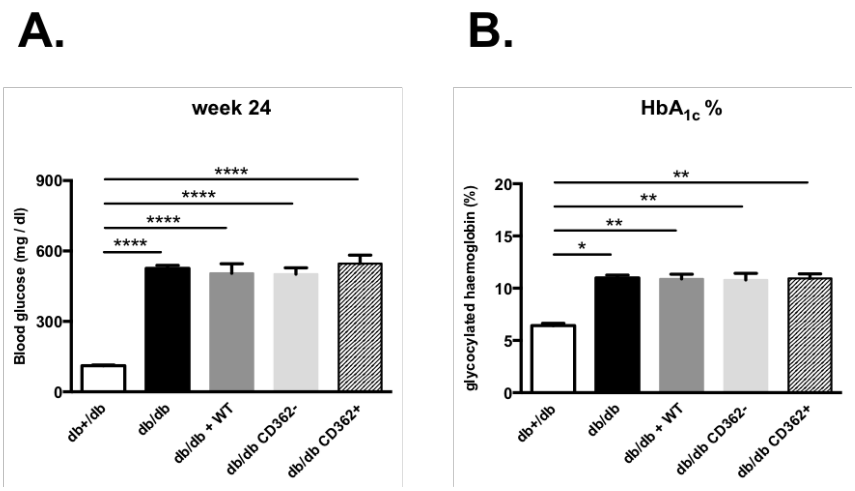

Figure 9. Impact of stromal cells on glucose and glycated hemoglobin levels in db/db mice 4 weeks after cell application. Bar graphs represent the mean ± SEM of **A.** blood glucose levels (mg/dl) and **B.** glycated hemoglobin (HbA1c) depicted as percentage in db+/db, db/db, and db/db mice receiving WT-MSC, $CD362^-$ or $CD362^+$ cells. One-way ANOVA test. *p<0.05, **p<0.01, ***p<0.001, with n=9 for db+/db, n=6 for db/db, n=8 for WT-MSC, n=9 for db/db $CD362^-$, and n=9 for db/db $CD362^+$.

4.2. Hemodynamic function

The cardiac ejection fraction (EF) is one of the key parameters to determine the global heart function. Within this study, no change in EF between db/db and db+/db mice was observed, whereas db/db $CD362^+$ mice showed a 1.1-fold ($p<0.05$) lower EF than db+/db mice. With respect to the other treatment groups, EF was not affected in comparison to db/db mice **(Figure 10A)**. In contrast to the EF, the cardiac index (CI), which describes the injected blood volume per minute in relation to the bodyweight (BW), was 1.4-fold ($p<0.05$) lower in db/db mice compared to db+/db mice. However, stromal cell application in db/db animals did not affect CI. Only $CD362^+$-treated db/db mice exhibited a 1.5-fold ($p<0.01$) lower CI than db+/db mice **(Figure 10B)**. Furthermore, the maximum LV pressure (LVP_{max}) did not differ between db/db and db+/db mice. With respect to stromal cell application, only db/db $CD362^+$ mice exhibited a 1.2-fold ($p<0.05$) lower LVP_{max} compared to db+/db mice. Additionally, LVP_{max} did not differ between PBS and cell-treated db/db mice **(Figure 10C)**.

To further characterize the systolic function, the maximum pressure (P) rise over time

was measured (dP/dt_{max}). A 1.3-fold ($p<0.01$) decrease in db/db mice compared to db+/db mice was observed. This effect was abolished in db/db mice injected with WT-MSC cells leading to a 1.2-fold ($p<0.05$) higher dP/dt_{max} versus db/db mice. Furthermore, $CD362^-$ and $CD362^+$ application led to a 1.2-fold ($p<0.05$) and 1.3-fold ($p<0.001$) lower dP/dt_{max} compared to db+/db mice, respectively **(Figure 10D)**.

As markers for the diastolic function, the isovolemic LV relaxation (dP/dt_{min}; **Figure 10E**) and Tau (**Figure 10F**) were investigated. DP/dt_{min}, was 1.3-fold ($p<0.05$) lower in db/db mice compared to db+/db mice, whereas i.v. application of WT-MSC and $CD362^-$ increased dP/dt_{min} 1.3-fold ($p<0.05$) and 1.3-fold ($p<0.05$), respectively, versus db/db mice. In addition, dP/dt_{min} was 1.4-fold ($p<0.01$) lower in db/db $CD362^+$ mice than db+/db mice (**Figure 10E**). With respect to the parameter Tau, db/db mice were characterized by a 1.2-fold ($p<0.05$) higher Tau compared to db+/db mice. Moreover, WT-MSC and db/db $CD362^-$ led to a 1.2-fold ($p<0.05$) and 1.1-fold ($p<0.05$) lower Tau versus db/db mice, respectively **(Figure 10F).**

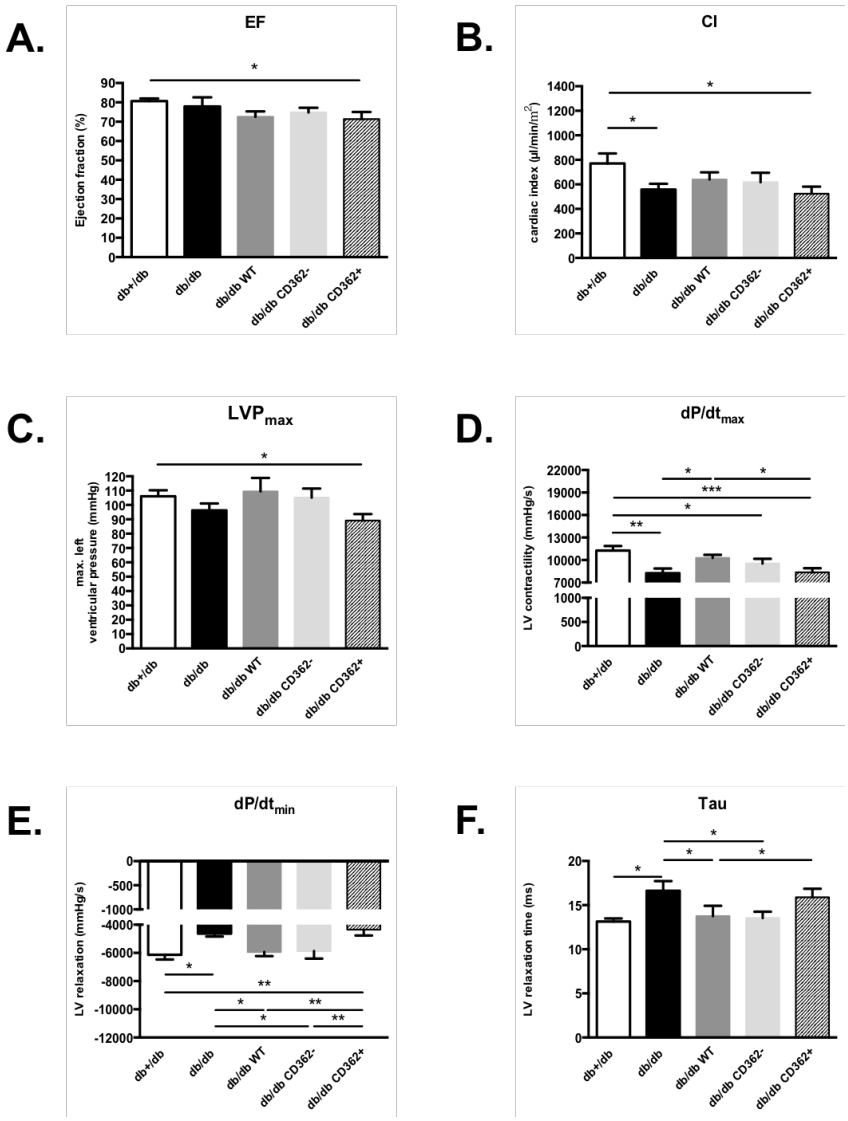

Figure 10. Impact of stromal cells on left ventricular function in db/db mice. Bar graphs represent the mean ± SEM of **A.** Ejection fraction (EF), **B.** Cardiac index (CI), **C.** maximum LV pressure (LVP_{max}), **D.** maximal LVP rise rate **(**dP/dt_{max}), **E.** maximal LVP drop rate (dP/dt_{min}), and **F.** Tau in db+/db, db/db, and db/db mice receiving WT-MSC, $CD362^-$ or $CD362^+$ cells. One-way ANOVA test. *p<0.05, **p<0.01, ***p<0.001, with n=9 for db+/db, n=6 for db/db, n=8 for WT-MSC, n=9 for db/db $CD362^-$, and n=9 for db/db $CD362^+$.

4.3. Myocardial fibrosis

4.3.1. Left ventricular collagen I and III mRNA expression

LV collagen 1a1 mRNA expression was 1.5-fold (p<0.05) higher in the db/db compared to the db+/db group, whereas only treatment with $CD362^-$ cells reduced the LV collagen 1a1 mRNA expression by 1.7-fold (p<0.01) versus db/db mice. LV collagen 1a1 was further 1.5-fold (p<0.05) lower in db/db mice $CD362^-$ compared to

db/db CD362^{+} mice **(Figure 11A)**. In contrast to collagen 1a1, there was no significant difference in LV collagen 3a1 mRNA expression between db/db and db+/db mice. Similar to collagen 1a1, LV collagen 3a1 was 1.5-fold ($p<0.05$) lower in db/db CD362^{-} versus db/db CD362^{+} mice **(Figure 11B)**.

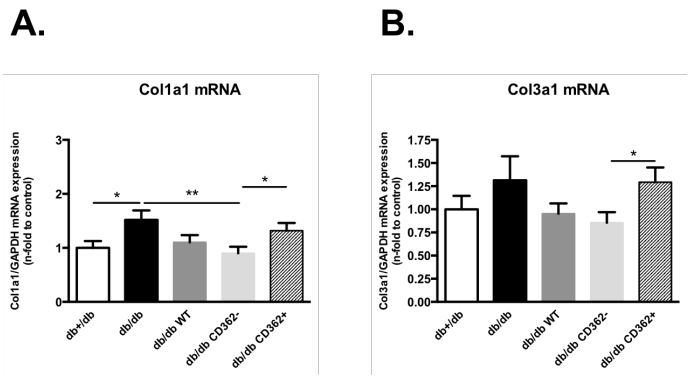

Figure 11. Impact of stromal cells on left ventricular collagen I and III mRNA expression in db/db mice. Bar graphs represent the mean ± SEM of LV **A.** col1a1 and **B.** col3a1 mRNA expression in db+/db, db/db, and db/db mice receiving WT-MSC, CD362^{-} or CD362^{+} cells. One-way ANOVA test. *$p<0.05$, **$p<0.01$, with n=9 for db+/db, n=6 for db/db, n=8 for WT-MSC, n=9 for db/db CD362^{-}, and n=9 for db/db CD362^{+}.

4.3.2. Left ventricular collagen I protein expression

LV collagen I was not significantly more expressed in db/db versus db+/db mice, but 1.3-fold ($p<0.05$), 1.6-fold ($p<0.05$), and 1.3-fold ($p<0.05$) higher in the LV of db/db WT-MSC, db/db CD362^{-}, and CD362^{+} mice compared to db+/db mice, respectively **(Figure 12B).**

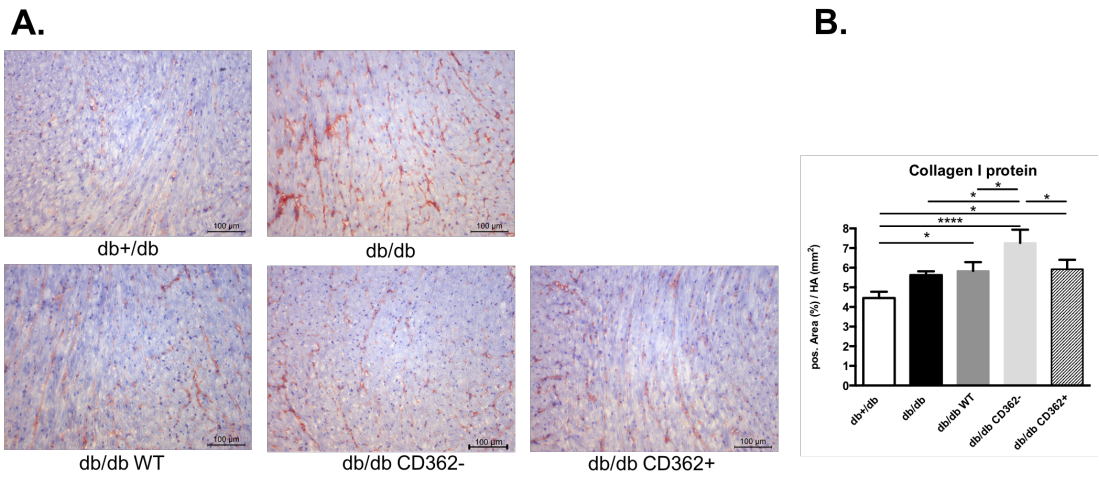

Figure 12. Impact of stromal cells on left ventricular collagen I expression in db/db mice. **A.** Representative collagen I+ LV sections of db+/db, db/db, WT-MSC, db/db CD362$^-$, and db/db CD362$^+$ mice, at 200x magnification. **B.** Bar graphs represent the mean ± SEM of LV collagen I protein expression per heart area (HA, mm^2) in db+/db, db/db, and db/db mice receiving WT-MSC, CD362$^-$ or CD362$^+$ cells. One-way ANOVA test. *p<0.05, ****p<0.0001, with n=9 for db+/db, n=6 for db/db, n=8 for WT-MSC, n=9 for db/db CD362$^-$, and n=9 for db/db CD362$^+$.

4.3.3. Left ventricular collagen III protein expression

Db/db mice did not establish higher LV collagen III protein levels compared to db+/db mice. I.v. application of stromal cells in db/db mice did not affect LV collagen III protein expression in db/db mice. However, in comparison to db+/db mice, collagen III protein expression was 1.3-fold ($p<0.05$) and 1.3-fold ($p<0.05$) lower in db/db WT-MSC and db/db CD362$^-$ mice, respectively **(Figure 13B)**.

The LV collagen I/III ratio was 1.6-fold ($p<0.01$) higher in db/db than in db+/db mice. I.v. stromal cell application did not reduce the collagen I/III ratio in db/db mice, leading to 1.7-fold ($p<0.001$), 2.0-fold ($p<0.0001$), and 1.5-fold ($p<0.05$) higher ratios in db/db WT-MSC, db/db CD362$^-$ and db/db CD362$^+$ mice compared to db+/db mice, respectively **(Figure 13B)**.

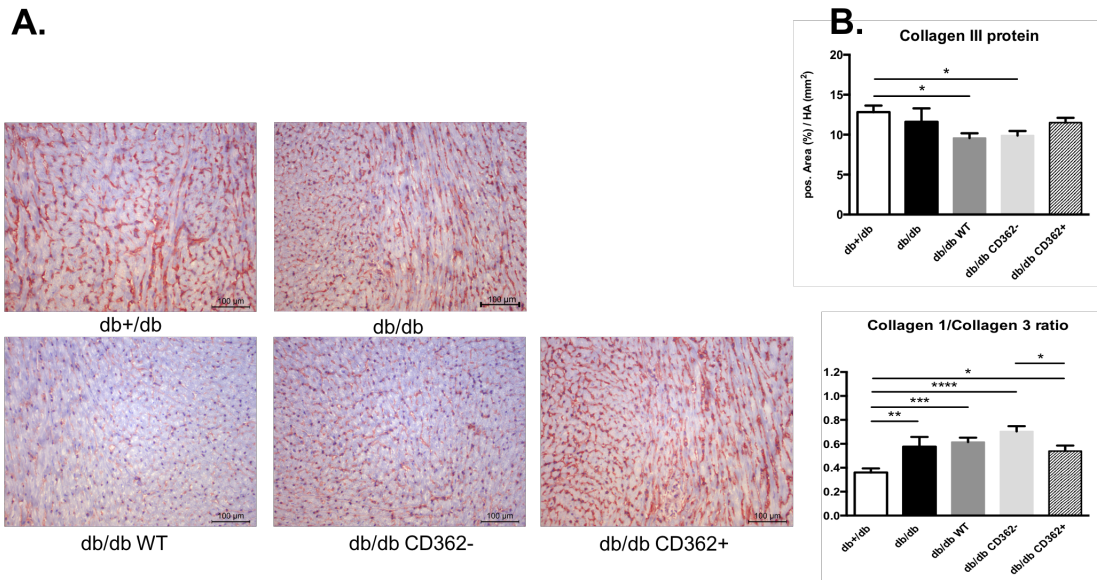

Figure 13. Impact of stromal cells on left ventricular collagen III expression and the collagen I to III ratio in db/db mice. A. Representative collagen III+ LV sections of db+/db, db/db, WT-MSC, db/db CD362$^-$, and db/db CD362$^+$ mice, at 200x magnification. **B.** Bar graphs represent the mean ± SEM of LV collagen III protein expression per heart area (HA, mm^2) (upper panel) and of the LV collagen I / III ratio (lower panel) in db+/db, db/db, and db/db mice receiving WT-MSC, CD362$^-$ or CD362$^+$ cells. One-way ANOVA test. *p<0.05, **p<0.01, ***p<0.001, ****p<0.0001, with n=9 for db+/db, n=6 for db/db, n=8 for WT-MSC, n=9 for db/db CD362$^-$, and n=9 for db/db CD362$^+$.

4.3.4. Left ventricular alpha-smooth muscle actin mRNA expression

LV mRNA expression of α-smooth muscle actin (α-SMA), a differentiation marker of myofibroblasts, was not statistically different between db/db and db+/db mice. Nor did i.v. stromal cell application affect the LV α-SMA mRNA in db/db mice. However, comparison of LV α-SMA mRNA expression in db/db CD362$^-$ versus db/db CD362$^+$ mice revealed a 1.4-fold ($p<0.05$) lower expression in db/db CD362$^-$ compared to db/db CD362$^+$ mice **(Figure 14)**.

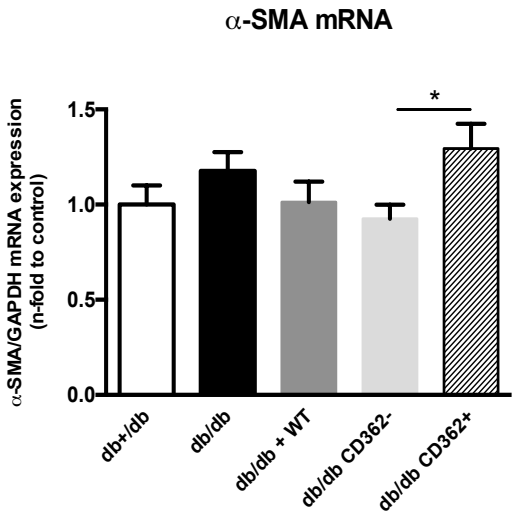

Figure 14. Impact of stromal cells on left ventricular alpha smooth muscle actin mRNA expression in db/db mice. Bar graphs represent the mean ± SEM of LV α-SMA mRNA expression in db+/db, db/db, and db/db mice receiving WT-MSC, CD362$^-$ or CD362$^+$ cells. One-way ANOVA test. *p<0.05, with n=9 for db+/db, n=6 for db/db, n=8 for WT-MSC, n=9 for db/db CD362$^-$, and n=9 for db/db CD362$^+$.

4.3.5. Left ventricular alpha-smooth muscle actin protein expression

LV α-SMA protein expression was not significantly different between the different experimental groups **(Figure 15)**.

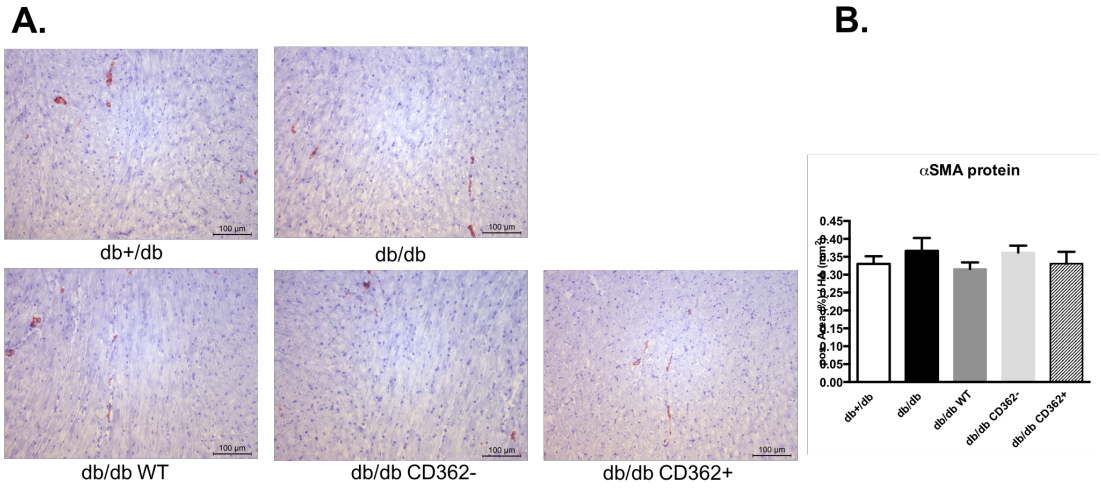

Figure 15. Impact of stromal cells on left ventricular alpha smooth muscle actin expression in db/db mice. A. Representative α-SMA+ LV sections of db+/db, db/db, WT-MSC, db/db CD362$^-$, and db/db CD362$^+$ mice, at 200x magnification. **B.** Bar graphs represent the mean ± SEM of LV α-SMA expression per heart area (HA, mm^2) in db+/db, db/db, and db/db mice receiving WT-MSC, CD362$^-$ or CD362$^+$ cells. One-way ANOVA test,

with n=9 for db+/db, n=6 for db/db, n=8 for WT-MSC, n=9 for db/db CD362^{-}, and n=9 for db/db CD362^{+}.

4.3.6. Left ventricular Lox1 and Loxl2 mRNA expression

LV Lox1 mRNA expression was 2.5-fold ($p<0.01$) higher in db/db than in db+/db mice. Stromal cell application did not lower the DM-associated induction in LV Lox1 mRNA expression, leading to 2.2-fold ($p<0.01$), 2.7-fold ($p<0.0001$), and 2.6-fold ($p<0.001$) higher LV Lox1 mRNA expression levels in db/db WT-MSC, db/db CD362^{-}, and db/db CD362^{+} mice versus db+/db mice, respectively **(Figure 16A)**. LV Loxl2 mRNA expression was only tendentially higher in db/db mice versus db+/db mice, whereas WT-MSC db/db and CD362^{+} db/db mice displayed 1.7-fold ($p<0.05$) and 1.7-fold ($p<0.05$) higher LV Loxl2 mRNA expression levels compared to db+/db mice, respectively **(Figure 16B)**.

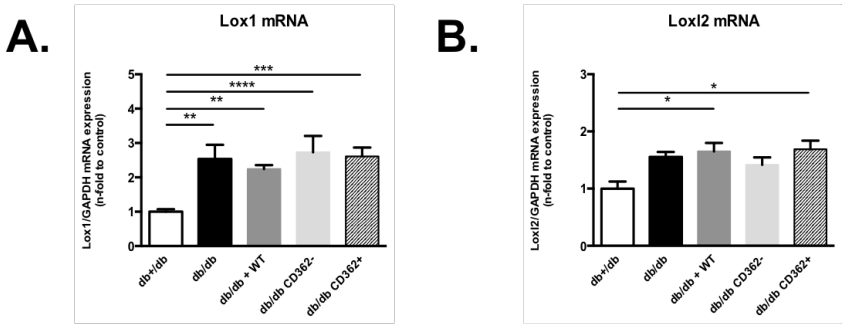

Figure 16. Impact of stromal cells on the left ventricular Lox1 and Loxl2 mRNA expression in db/db mice. Bar graphs represent the mean ± SEM of LV **A.** Lox1 and **B.** Loxl2, mRNA expression in db+/db, db/db, and db/db mice receiving WT-MSC, CD362^{-} or CD362^{+} cells. One-way ANOVA test. *$p<0.05$, **$p<0.01$, ***$p<0.001$, ****$p<0.0001$, with n=9 for db+/db, n=6 for db/db, n=8 for WT-MSC, n=9 for db/db CD362^{-}, and n=9 for db/db CD362^{+}.

4.4. Inflammation

4.4.1. Left ventricular presence of CD3^{+} cells

CD3^{+} cell presence was 1.6-fold ($p<0.01$) higher in the LV of db/db versus db+/db mice. Db/db mice receiving WT-MSC, CD362^{-}, or CD362^{+} cells exhibited 1.5-fold ($p<0.05$), 1.8-fold ($p<0.01$), and 1.7-fold ($p<0.01$) lower CD3^{+} cells in the LV,

respectively, compared to db/db mice **(Figure 17).**

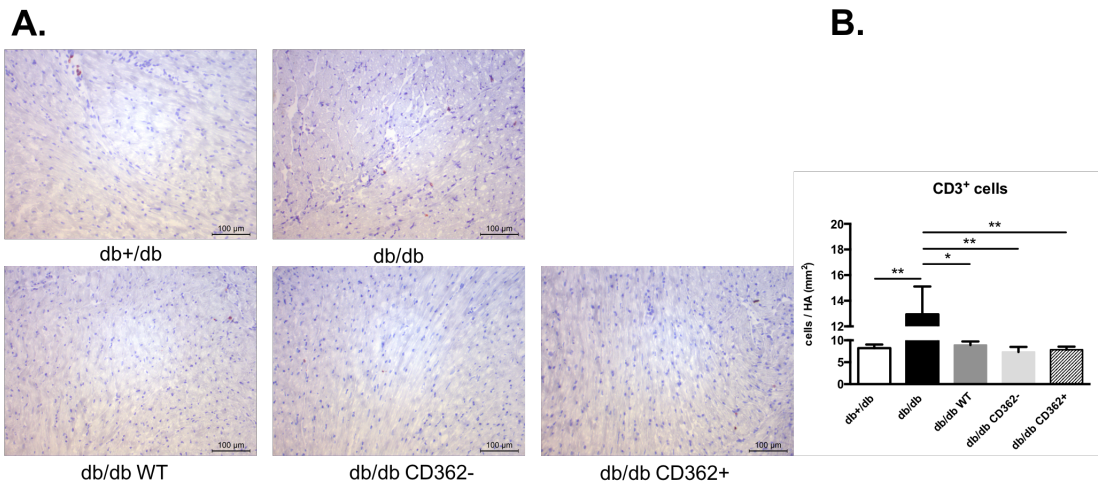

Figure 17. Impact of stromal cells on left ventricular CD3$^+$ cell presence in db/db mice. A. Representative CD3$^+$ LV sections of db+/db, db/db, WT-MSC, db/db CD362$^-$, and db/db CD362$^+$ mice, at 200x magnification. **B.** Bar graphs represent the mean ± SEM of LV CD3$^+$ cells present per heart area (HA, mm^2) in db+/db, db/db, and db/db mice receiving WT-MSC, CD362$^-$ or CD362$^+$ cells. One-way ANOVA test. *p<0.05, **p<0.01, with n=9 for db+/db, n=6 for db/db, n=8 for WT-MSC, n=9 for db/db CD362$^-$, and n=9 for db/db CD362$^+$.

4.4.2. Left ventricular presence of CD4$^+$ cells

The db/db group showed an up-regulated trend of CD4$^+$ cells in the LV compared to the db+/db group. Furthermore, stromal cell administration did not affect the LV CD4$^+$ cell presence in db/db mice **(Figure 18)**.

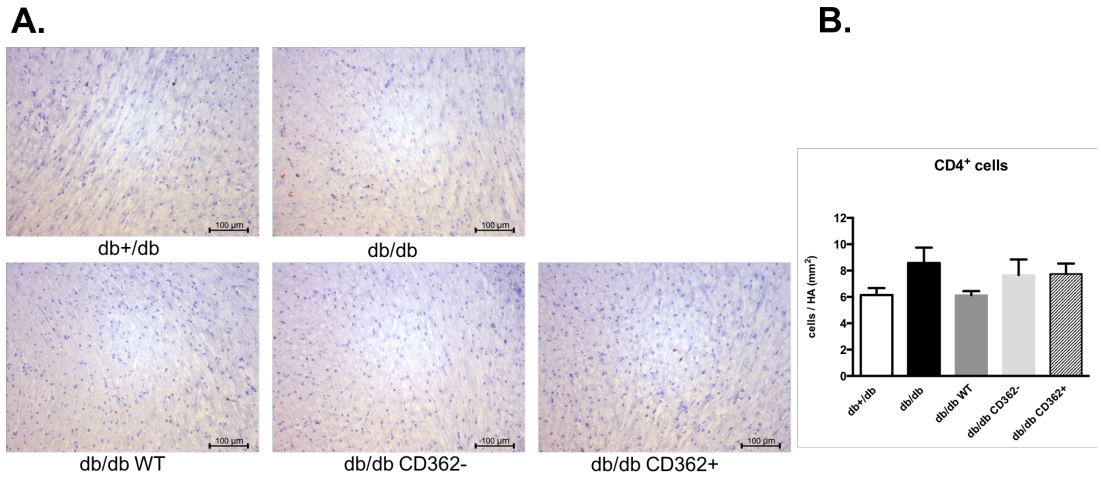

Figure 18. Impact of stromal cells on left ventricular CD4 cell presence in db/db mice. A. Representative CD4$^+$ LV sections of db+/db, db/db, WT-MSCs, db/db CD362$^-$, and db/db CD362$^+$ mice, at 200x magnification. **B.** Bar graphs represent the mean ± SEM of LV CD4$^+$

cells present per heart area (HA, mm^2) in db+/db, db/db, and db/db mice receiving WT-MSC, $CD362^-$ or $CD362^+$ cells. One-way ANOVA test, with n=9 for db+/db, n=6 for db/db, n=8 for WT-MSC, n=9 for db/db $CD362^-$, and n=9 for db/db $CD362^+$.

4.4.3. Left ventricular presence of $CD8a^+$ cells

Db/db mice exhibited 1.4-fold ($p<0.01$) higher presence of $CD8a^+$ cells in the LV compared to db+/db mice. Stromal cell application did not affect the presence of $CD8a^+$ cells in the LV of db/db mice **(Figure 19)**.

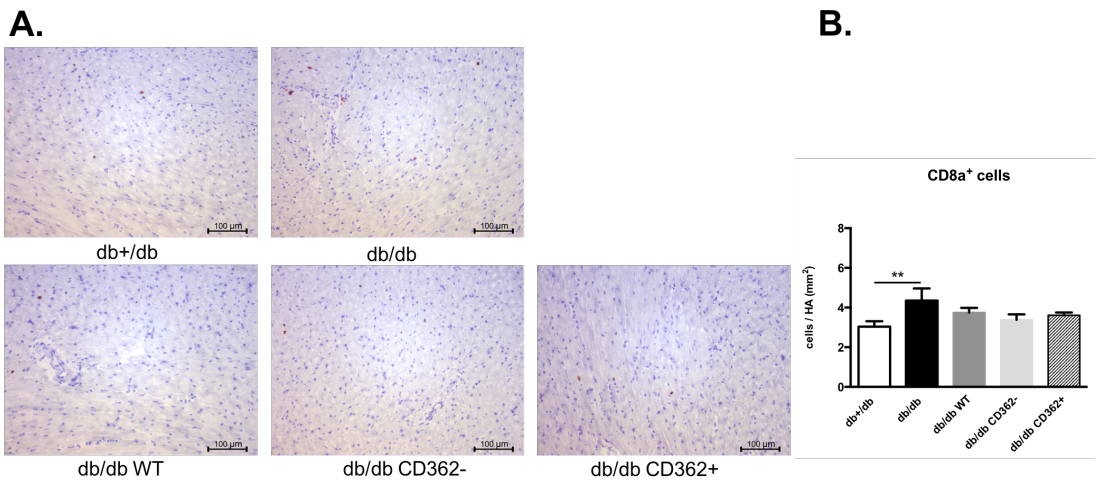

Figure 19. Impact of stromal cells on left ventricular CD8a cell presence in db/db mice. **A.** Representative $CD8a^+$ LV sections of db+/db, db/db, WT-MSC, db/db $CD362^-$, and db/db $CD362^+$ mice, at 200x magnification. **B.** Bar graphs represent the mean ± SEM of LV $CD8a^+$ cells present per heart area (HA, mm^2) in db+/db, db/db, and db/db mice receiving WT-MSC, $CD362^-$ or $CD362^+$ cells. One-way ANOVA test. **$p<0.01$, with n=9 for db+/db, n=6 for db/db, n=8 for WT-MSC, n=9 for db/db $CD362^-$, and n=9 for db/db $CD362^+$.

4.4.4. Left ventricular presence of $CD68^+$ cells

The presence of $CD68^+$ cells was tendentially increased in the LV of db/db versus db+/db mice. I.v. application of WT-MSC, $CD362^-$ or $CD362^+$ cells in db/db mice reduced the LV presence of $CD68^+$ cells by 1.6-fold ($p<0.05$), 1.8-fold ($p<0.01$), and 1.6-fold ($p<0.05$), respectively, compared to db/db mice **(Figure 20).**

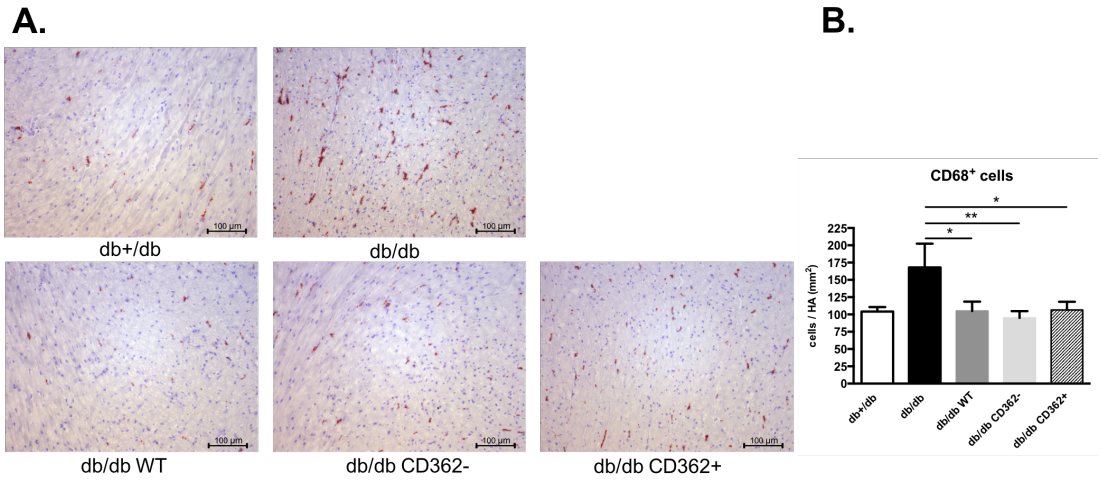

Figure 20. Impact of stromal cells on left ventricular CD68 cell presence in db/db mice. **A.** Representative $CD68^+$ LV sections of db+/db, db/db, WT-MSC, db/db $CD362^-$, and db/db $CD362^+$ mice, at 200x magnification. **B.** Bar graphs represent the mean ± SEM of LV $CD68^+$ cells present per heart area (HA, mm^2) in db+/db, db/db, and db/db mice receiving WT-MSC, $CD362^-$ or $CD362^+$ cells. One-way ANOVA test. *p<0.05, **p<0.01, with n=9 for db+/db, n=6 for db/db, n=8 for WT-MSC, n=9 for db/db $CD362^-$, and n=9 for db/db $CD362^+$.

4.4.5. Left ventricular cytokines mRNA expression

LV TNF-α mRNA expression was not increased in db/db mice versus db+/db mice. I.v. application of WT-MSC and $CD362^-$ in db/db mice resulted in 1.6-fold (p<0.05) and 1.5-fold (p<0.05) lower LV TNF-α mRNA expression levels compared to db+/db mice, but these levels were not significantly different from db/db mice. In addition, LV TNF-α mRNA expression in db/db $CD362^+$ mice was not different from that in db/db mice **(Figure 21A)**. LV TGF-β mRNA expression was tendentially higher in db/db versus db+/db mice. Stromal cell treatment did not affect LV TGF-ß mRNA in db/db mice, whereas i.v. injection of WT-MSC in db/db mice induced the LV TGF-ß mRNA by 1.3-fold (p<0.05) compared to db+/db mice. The TGF-ß mRNA expression levels in the LV of db/db WT-MSC mice were also 1.3-fold (p<0.05) higher than in db/db $CD362^-$ mice **(Figure 21B)**. Also with respect to LV IL-10 mRNA expression, no significant differences were found between the experimental groups **(Figure 21C)**.

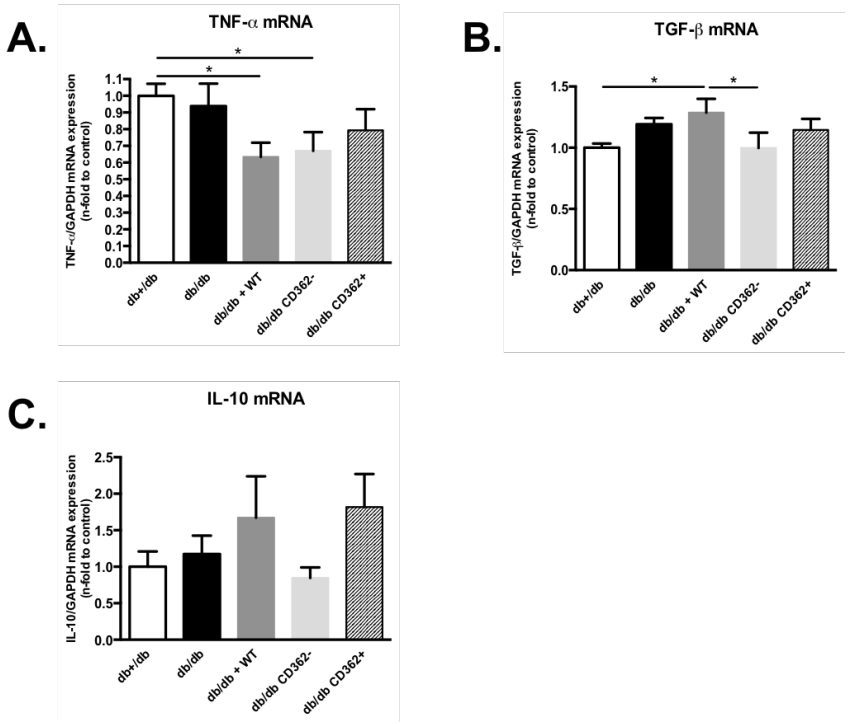

Figure 21. Impact of stromal cells on the left ventricular cytokine mRNA expression in db/db mice. Bar graphs represent the mean ± SEM of LV **A.** TNF-α, **B.** TGF-ß, and **C.** IL-10 mRNA expression in db+/db, db/db, and db/db mice receiving WT-MSC, $CD362^-$ or $CD362^+$ cells. One-way ANOVA test. *p<0.05, with n=9 for db+/db, n=6 for db/db, n=8 for WT-MSC, n=9 for db/db $CD362^-$, and n=9 for db/db $CD362^+$.

4.4.6. Left ventricular mRNA expression of components of the Nlrp3 inflammasome

Db/db mice exhibited 2.7-fold (p<0.01) higher LV Nlrp3 mRNA expression levels compared to db+/db mice. Both the injection of WT-MSC and of $CD362^-$ cells reduced LV Nlrp3 expression by 2.3-fold (p<0.05) and 2.4-fold (p<0.01), respectively. The 1.9-fold decrease in LV Nlrp3 expression in db/db $CD362^+$ versus db/db mice did not reach statistical significance (p=0.089) **(Figure 22A)**. In parallel to the LV Nlrp3 mRNA expression, LV ASC mRNA expression was 1.7-fold (p<0.01) higher in db/db mice compared to db+/db mice. This effect was abrogated in db/db mice injected with WT-MSC or $CD362^-$ cells, leading to a 1.4-fold (p<0.05) and 1.5-fold (p<0.05) lower ASC mRNA expression levels compared to db/db mice, respectively, and levels not different from db+/db controls **(Figure 22B)**. Concomitant with the LV expression

levels of the Nlrp3 inflammasome components Nlrp3 and ASC, LV caspase 1 mRNA expression was 1.7-fold ($p<0.01$) higher in db/db compared to db+/db mice, whereas its expression was 1.6-fold ($p<0.05$) lower in db/db CD362$^-$ compared to db/db mice. There was no significant difference in the LV caspase 1 mRNA expression of WT-MSC db/db and CD362$^+$ db/db mice compared to db/db mice **(Figure 22C)**. Interestingly, LV IL-1β mRNA expression was 1.9-fold ($p<0.05$) lower in db/db versus db+/db mice and 1.7-fold ($p<0.05$) lower in db/db WT-MSC compared to db+/db mice **(Figure 22D)**.

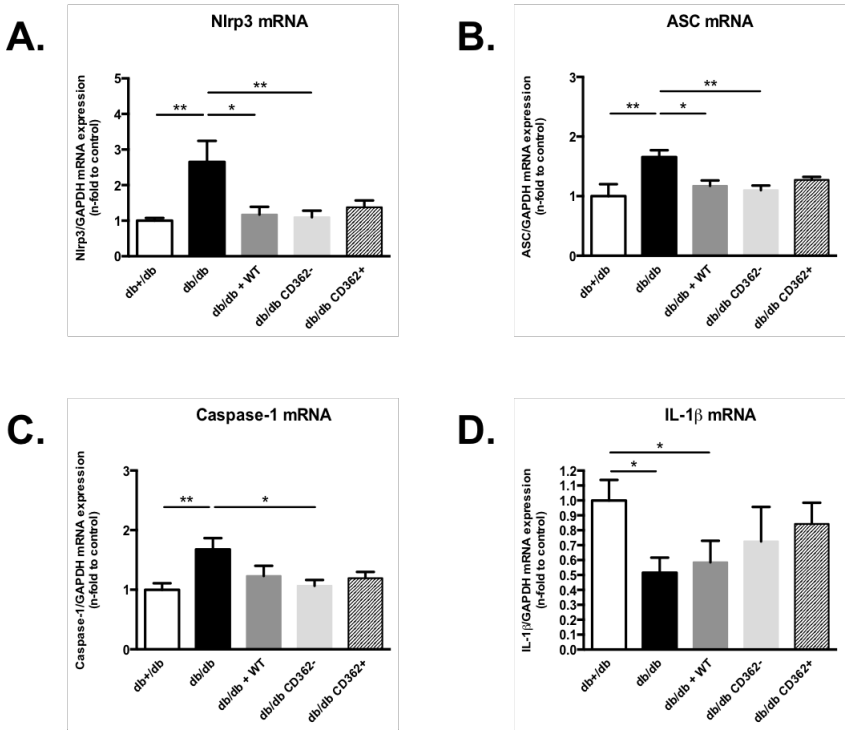

Figure 22. Impact of stromal cells on the left ventricular mRNA expression of components of the Nlrp3 inflammasome in db/db mice. Bar graphs represent the mean ± SEM of LV **A.** Nlrp3, **B.** ASC, **C.** caspase-1, and **D.** IL-1β mRNA expression in db+/db, db/db, and db/db mice receiving WT-MSC, CD362$^-$ or CD362$^+$ cells. One-way ANOVA test. *$p<0.05$, **$p<0.01$, with n=9 for db+/db, n=6 for db/db, n=8 for WT-MSC, n=9 for db/db CD362$^-$, and n=9 for db/db CD362$^+$.

4.5. Immune regulation in splenocytes

To assess the impact of the different stromal cells on the systemic immune status in db/db mice, flow cytometry on splenocytes isolated from the different experimental

groups was determined. The percentage of $CD68^{+}TGF\text{-}\beta^{+}$ cells was not significantly different in the splenocytes of db/db mice versus db+/db mice. Interestingly, the percentage of TGF-ß expressing CD68 cells was 2.1-fold ($p<0.0001$) lower and 2.0-fold ($p<0.0001$) higher in db/db $CD362^{-}$ and db/db $CD362^{+}$ compared to db+/db mice, respectively **(Figure 23A)**. With respect to MNCs activation, db/db mice displayed a 1.2-fold ($p<0.01$) higher MNCs activation/proliferation compared to db+/db mice. WT-MSC db/db mice exhibited a 1.1-fold ($p<0.05$) lower splenic MNCs activation than db/db mice, whereas the MNCs activity in db/db $CD362^{-}$ and db/db $CD362^{+}$ was not significantly different from db/db mice **(Figure 23B)**. The percentage of Tregs in the spleen was not significantly different between db/db and db+/db mice. I.v. application of $CD362^{+}$ cells raised the percentage of Tregs leading to 1.3-fold ($p<0.0001$), 1.3-fold ($p<0.001$), 1.3-fold ($p<0.001$) 1.4-fold ($p<0.0001$) higher percentage of Tregs compared to db+/db, db/db, WT-MSC db/db, and $CD362^{-}$ db/db mice, respectively **(Figure 23C)**. In contrast to the unchanged percentage in Tregs between db/db and db+/db mice, the percentage of apoptotic Tregs was 1.6-fold ($p<0.0001$) higher in db/db compared to db+/db mice. Stromal cell application in db/db mice decreased the percentage of apoptotic Tregs versus db/db mice resulting in a 1.7-fold ($p<0.0001$), 1.8-fold ($p<0.0001$), and 1.4-fold ($p<0.0001$) lower percentage of apoptotic Tregs in db/db WT-MSC, db/db $CD362^{-}$, and db/db $CD362^{+}$ than in db/db mice, respectively **(Figure 23D)**.

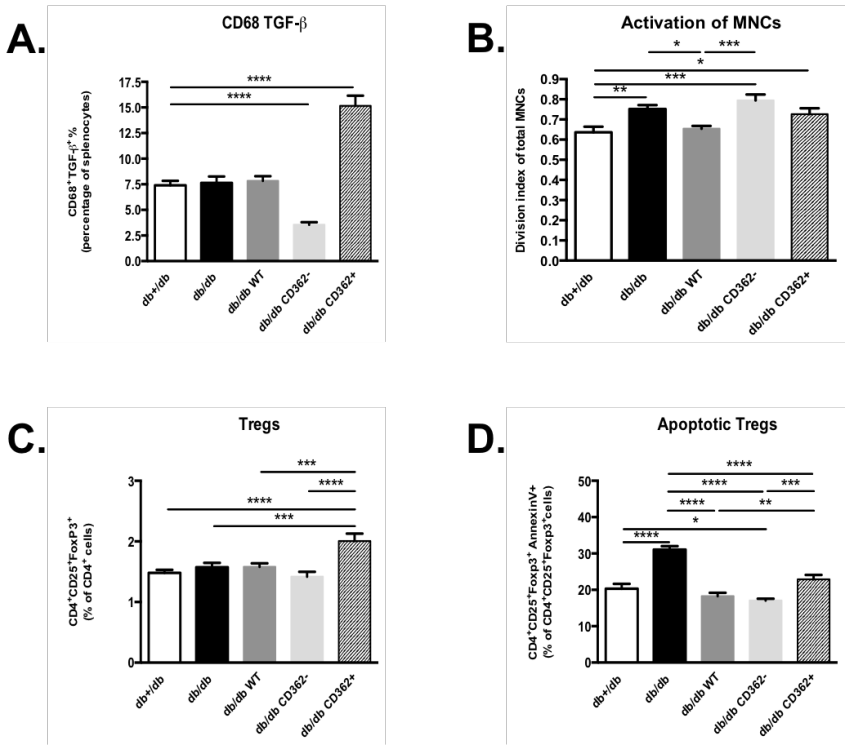

Figure 23. Impact of stromal cells on the immune status of splenocytes isolated from db/db mice. Bar graphs represent the mean ± SEM of **A.** TGF-ß-expressing CD68 cells, **B.** the division index of total MNCs, **C.** Tregs represented as CD4CD25FoxP3$^+$ cells depicted as the percentage of CD4 cells, and **D.** apoptotic Tregs represented as Annexin V+ CD4CD25FoxP3$^+$ cells depicted as the percentage of CD4CD25FoxP3$^+$ cells from db+/db, db/db, and db/db mice receiving WT-MSC, CD362$^-$, or CD362$^+$ cells. One-way ANOVA test. *p<0.05, **p<0.01, ***p<0.001, ****p<0.0001, with n=9 for db+/db, n=6 for db/db, n=8 for WT-MSC, n=9 for db/db CD362$^-$, and n=9 for db/db CD362$^+$.

4.6. Assessment of the pro-fibrotic potential of splenocytes

To assess the impact of i.v. stromal cell application on the pro-fibrotic potential of splenocytes in db/db mice, splenocytes of the different experimental groups were co-cultured on fibroblasts and their impact on collagen deposition of fibroblasts was determined. Collagen deposition was 1.2-fold ($p<0.05$) higher upon co-culture of fibroblasts with splenocytes derived from db/db mice compared to splenocytes from db+/db mice, indicating a higher pro-fibrotic potential of db/db splenocytes versus db+/db splenocytes. Only splenocytes isolated from db/db mice injected with CD362$^+$ cells induced a 1.3-fold ($p<0.01$) lower collagen deposition in fibroblasts compared to db/db splenocytes. Splenocytes from db/db WT-MSC and db/db CD362$^-$ did not lead

to a lower collagen production in fibroblasts upon co-culture compared to splenocytes from db/db mice **(Figure 24B)**.

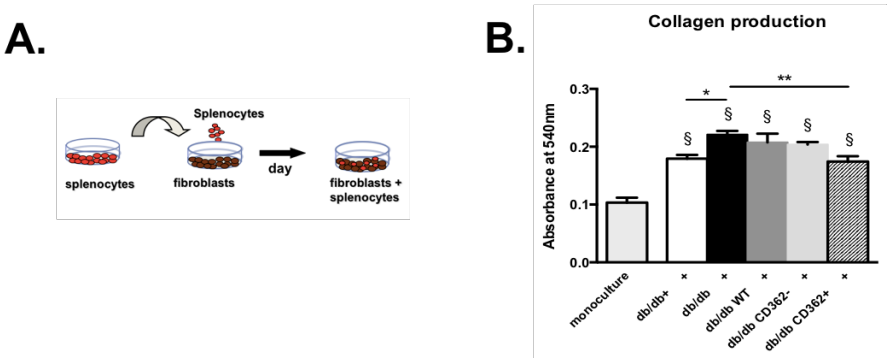

Figure 24. Impact of stromal cells on the pro-fibrotic capacity of splenocytes isolated from db/db mice. A. Experimental design illustrating that splenocytes isolated from the different experimental groups were co-cultured on murine fibroblasts for 1 day. Next, splenocytes were removed and collagen deposition of murine fibroblasts was determined via Sirius Red staining. **B.** Bar graphs represent the mean ± SEM of the absorbance at 540 nm, depicting the collagen deposition of monocultured murine fibroblasts or fibroblasts co-cultured with splenocytes isolated from db+/db, db/db, and db/db mice receiving WT-MSC, $CD362^-$, or $CD362^+$ cells. One-way ANOVA test. *$p<0.05$, **$p<0.01$, with n=9 for db+/db, n=6 for db/db, n=8 for WT-MSC, n=9 for db/db $CD362^-$, and n=9 for db/db $CD362^+$.

4.7. Imaging mass spectrometry and titin regulation

To further understand our findings, a hypothesis-free proteome analysis was performed via imaging mass spectrometry **(Figure 25)**. Principal component analysis of LVs from db+/db, db/db, and db/db mice i.v. injected with WT-MSC, $CD362^+$, or $CD362^-$ cells clearly distinguished different protein patterns between the groups.

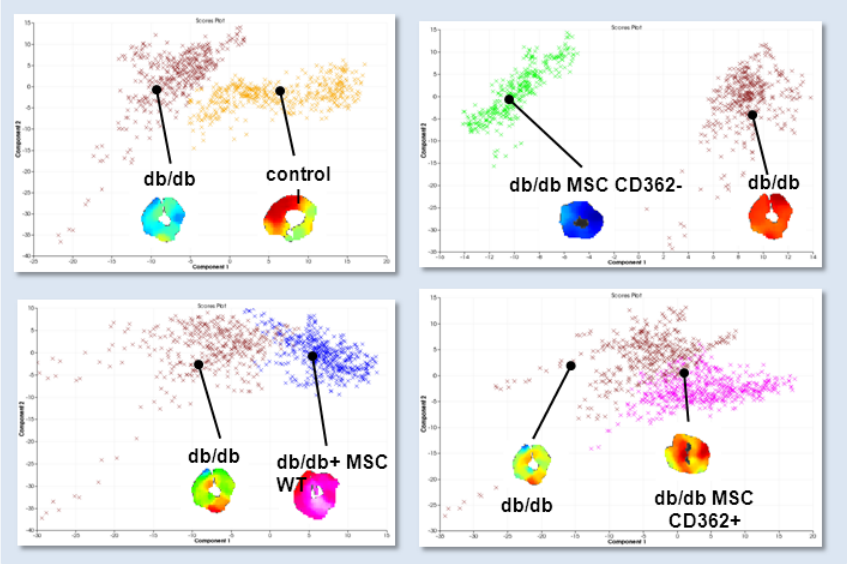

Figure 25. Cluster analysis of principal component analysis of left ventricles from db+/db (control), db/db, and db/db mice i.v. injected with WT-MSC, CD362^{+}, or CD362^{-} cells.

Further analysis indicated a lower expression of the sarcomere protein titin N2B isoform in db/db versus db+/db mice, which could be overcome by i.v. application of all investigated stromal cells **(Figure 26)**.

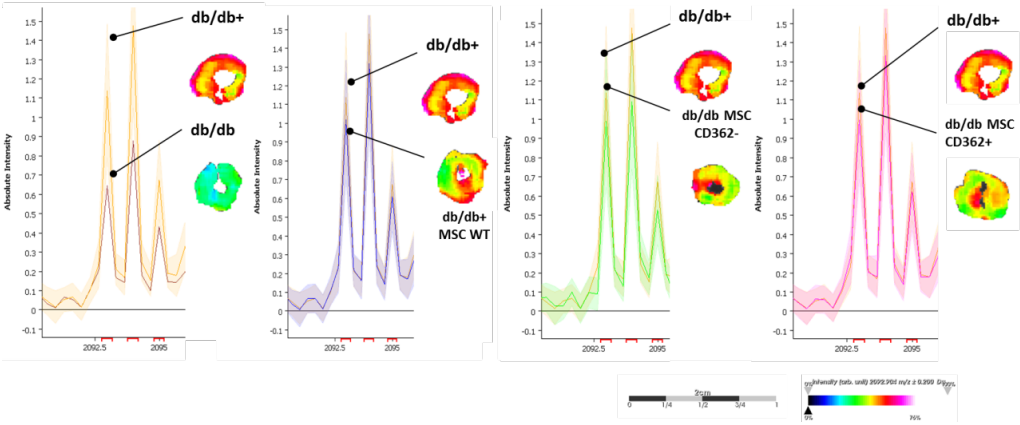

Figure 26. Imaging mass spectrometry analysis. Spatial distribution of characteristic m/z values of Titin N2B in left ventricles of db+/db, db/db, and db/db mice i.v. injected with WT-MSC, CD362^{-} and CD362^{+} cells. Average peak intensity and distribution of 2092.5 Da in left ventricles from db+/db (control), db/db, and db/db mice i.v. injected with WT-MSC, CD362^{+} and CD362^{-} cells. The m/z-values 2095.5 Da show a significantly higher intensity (AUC>0.75 p<0.01) in db+/db (control) compared to db/db, and db/db mice i.v. injected with WT-MSC, CD362^{+}, or CD362^{-} cells. Still, the m/z-values 2095.5 Da show significantly lower intensity in db/db in comparison to db/db mice i.v. injected with WT-MSC, CD362^{+} and CD362^{-} cells (AUC< 0.25 p<0.01).

In addition, the phosphorylation state of N2B titin was 1.8-fold ($p<0.01$) lower in db/db versus db+/db mice. Interestingly, the decreased phosphorylation state of N2B was 1.6-fold ($p<0.05$) and 1.5-fold ($p<0.05$) upregulated in the db/db mice receiving WT-MSC and $CD362^-$ cells, respectively, whereas i.v. application of $CD362^+$ cells had no effect on the phosphorylation of titin N2B compared to the db/db mice **(Figure 27A)**. In agreement with the phosphorylation of N2B, protein kinase G activity was 1.5-fold ($p<0.05$) lower in db/db versus db+/db mice and was 1.5-fold ($p<0.05$) and 1.5-fold ($p<0.05$) higher in db/db WT-MSC and db/db $CD362^-$ mice, respectively. Also here, there was no significant difference in the protein kinase G activity between the db/db and the db/db $CD362^+$ group **(Figure 27B)**.

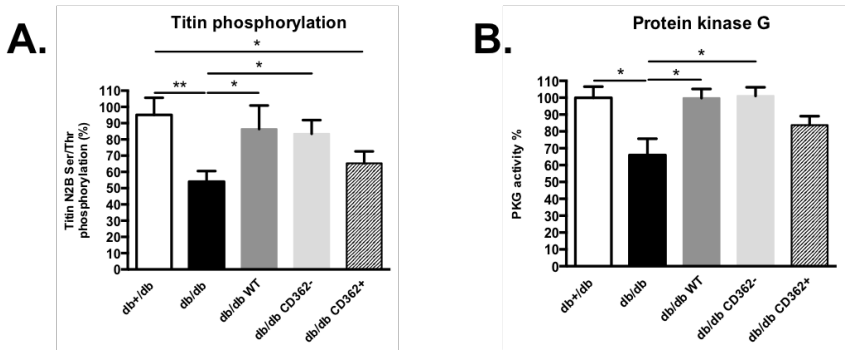

Figure 27. Impact of stromal cells on the titin 2B phosphorylation state and on the protein kinase G activity in the left ventricle of db/db mice. Bar graphs represent the mean ± SEM of the LV **A.** Titin N2B ser/Thr phosphorylation state depicted as the percentage of phosphorylation towards total protein and **B.** protein kinase G activity in db/db mice. One-way ANOVA test. *$p<0.05$, **$p<0.01$, n=7/8 group.

5. Discussion

The present study was focused on evaluating the impact of i.v. applied WT-MSC, $CD362^+$ and $CD362^-$-selected MSCs in diabetic db/db mice. In brief, only application of WT-MSC and $CD362^-$ cells improved LV function, as indicated by increased contractility and reduced cardiac stiffness compared to db/db mice (**Figure 10**). Further investigations showed that only WT-MSC and $CD362^-$ cells reduced the LV expression of the components of the Nlrp3 inflammasome (**Figure 22**). Additionally, a decreased number of splenic apoptotic Tregs was observed among all cell-treated db/db groups compared to db/db mice (**Figure 23**), whereas a reduction in the pro-fibrotic capacity of splenocytes could only be found in the splenocytes of db/db $CD362^+$ mice (**Figure 24**). Proteome analysis via imaging mass spectrometry showed that the sarcomere protein titin was downregulated in db/db mice, which could be overcome after stromal cell application in db/db mice (**Figure 26**). In agreement with cardiac function, subsequent analysis of all titin phosphorylation showed a drop within the db/db group, which could only be restored by application of WT-MSC and $CD362^-$ cells (**Figure 27**).

5.1. WT-MSC, $CD362^+$, and $CD362^-$ cells did not improve blood glucose levels

Elevated blood glucose levels are one of the main characteristics of DM. Previous studies in humans [98][99][100] and mice [65][66][101] have shown a therapeutic effect in glycemic control after MSCs treatment. This phenomenon was explained by the regenerative properties of MSCs, including their capacity to differentiate into insulin-producing cells [65], and their ability to repair pancreatic ß cells in a paracrine manner, including an increase in islet capillary density and reduction in ß-cell apoptosis [67][102]. In contrast to the abovementioned findings, we (and other partners of the REDDSTAR consortium) could not observe changes after cell application neither in blood glucose levels nor in the HbA_{1C} value compared to db/db mice (**Figure 8 and 9**). This discrepancy can be explained by the fact that we used an

allogeneic MSCs approach i.e. human WT-MSC and CD362$^-$ and CD362$^+$ cells were injected in immunocompetent mice. However, Lee *et al.* [65] used human MSCs, but in severe combined immunodeficient (SCID) mice, whereas Ezquer *et al.* [66] used murine MSCs injected in diabetic mice. Finally, Hao *et al.* [101] observed a decrease in blood glucose levels following human MSCs application in experimental type 2 diabetes rats, but here MSCs were administrated at different timepoints.

5.2. WT-MSC and CD362$^-$ cells ameliorate left ventricular function

Numerous *in vivo* studies have shown that MSCs application improves cardiac function [103][104][105], involving their ability to migrate towards the injured region [106] following i.v. injection [60]. In the present study, we investigated the heart function via conductance catheter. In line with the cardioprotective properties of MSCs, WT-MSC and CD362$^-$ cells improved LV function, as shown by the increase in dP/dt_{max}, and reduction of dP/dt_{min} and Tau **(Figure 10)**.

Impaired cardiac contractility is commonly associated with excessive cardiac fibrosis [107]. In our study, there was no induction of cardiac fibrosis in the db/db versus db+/db mice as indicated by no increased LV collagen I **(Figure 12)** and collagen III **(Figure 13)** protein expression in db/db mice versus db+/db mice. Activated fibroblasts, also called myofibroblasts, are the main producers of collagen during heart failure [108]. LV α-SMA protein expression, the marker of myofibroblasts, was not elevated in any experimental diabetic group. However, the ratio of collagen I (stiff form) towards collagen III (compliant form) [109] was increased in db/db versus non-diabetic mice. This change in collagen ratio might be connected to the reduced LV function of db/db versus db+/db mice. However, in contrast to cardiac function, none of the different stromal cells reduced the collagen I / III ratio, indicating that this altered ratio is probably not the major cause underlying cardiac dysfunction in these db/db mice. In fact, it has recently been demonstrated that dysregulation of the sarcomere protein titin alone (**paragraph 5.5.**), in the absence of cardiac fibrosis, may influence cardiac function in a rat model of the metabolic syndrome [110].

Furthermore, impaired endothelial function [111] and vascular rarefaction [112] may underlie impaired diastolic relaxation. Numerous studies have demonstrated MSC-mediated cardiac repair via promoting angiogenesis followed by an ameliorated cardiac function [113][114], whereas the impact of MSCs on titin regulation has not been demonstrated so far. In this study, we explored the impact of stromal cell application on titin regulation in db/db mice (**paragraph 5.5.**), but the evaluation of the impact of stromal cell application on cardiac capillary density and arteriole density requires still further investigation. It is interesting to note that De Rossi *et al.* [115] demonstrated that released syndecan 2 (CD362) has anti-angiogenic effects in a xenograft tumor model. The authors detected a reduced endothelial cell migration based on CD148 interaction, paralleled by inactivation of β1 integrin and finally decreased tumor size. Additionally, induced apoptosis was observed in osteosarcoma cells overexpressing CD362 [116]. Both findings could be helpful to understand the poor cardiac function after application of $CD362^+$ cells.

5.3. WT-MSC, $CD362^+$, and $CD362^-$ cells influence cardiac immune cell presence and modulate splenic immune cell activation

After investigating cardiac function and fibrosis, we next analyzed myocardial inflammation and immune cell presence as well as splenic immune cell modulation. Inflammatory mediators – among others TNF-α [117], TGF-β [118], and IL-1β [119] can induce heart failure through several mechanisms, including promotion of cardiac fibrosis [117][120][119], cardiac monocyte infiltration [121], and/or the ability to exert a direct negative inotrope effect. In our study, no relevant changes of cardiac TNF-α, TGF-β, and IL-10 mRNA expression were observed between diabetic db/db and db+/db control mice (**Figure 21**), whereas LV IL-1ß mRNA was reduced in db/db versus db+/db mice (**see paragraph 5.4**, **Figure 22**). Nevertheless, we detected enhanced cardiac presence of $CD3^+$ (**Figure 17**) and of $CD8a^+$ cells (**Figure 19**) in db/db mice compared to controls, whereas stromal cell application decreased cardiac $CD3^+$ cells in db/db mice. However, no significant differences in cardiac $CD8a^+$ cells

were found after stromal cell application in db/db mice versus PBS-treated db/db mice. I.v. application of WT-MSC, $CD362^-$, and $CD362^+$ cells in db/db mice decreased the cardiac presence of $CD68^+$ cells in db/db mice (**Figure 20**). These findings are in line with the well-established immunomodulatory properties of MSCs. MSCs have been shown to inhibit T cell proliferation [122][123] and to reduce cardiac MNCs activation [124] and cardiac pro-inflammatory $Ly6C^{high}$ and $Ly6C^{middle}$ monocytes presence [125].

Besides the heart, we evaluated the impact of i.v. application of WT-MSC, $CD362^-$ and $CD362^+$ cells on systemic immunomodulation. For this purpose, we examined the influence of stromal cell application on the percentage of TGF-ß-expressing $CD68^+$ cells, Tregs, apoptotic Tregs, and MNCs activation in the spleen, as well as the pro-fibrotic potential of splenocytes in db/db mice. The spleen was chosen, given the relevance of the cardiosplenic axis, i.e. the homing of immune cells from the spleen towards the heart and their subsequent involvement in cardiac remodeling in heart failure [126]. In accordance with observations in ob/ob mice [127], splenic MNCs activity was induced in diabetic db/db versus db+/db mice (**Figure 23**). This activity was lower in db/db mice, which received WT-MSC, but not in db/db mice injected with $CD362^-$ nor $CD362^+$ cells. The quantity of Tregs, known for their anti-fibrotic and anti-inflammatory properties [128][129][130], was not lower in db/db versus control mice, whereas their quality was impaired in the diabetic db/db compared to control mice as indicated by an induction in apoptotic Tregs. The percentage of apoptotic Tregs in db/db mice could be decreased by all stromal cells, whereas only $CD362^+$ cells raised the percentage of Tregs in db/db mice. These findings are supported by the ability of MSCs to increase Tregs [56]. Interestingly, only i.v. injection of $CD362^+$ cells reduced the pro-fibrotic potential of splenocytes in db/db mice (**Figure 24**). This can partly be explained by the observation that only $CD362^+$ cells induced the percentage of splenic Tregs, known for their anti-fibrotic properties [129] in db/db mice. On the other hand, also only $CD362^+$ db/db mice displayed an increase in splenic CD68 cells expressing the pro-fibrotic factor TGF-ß, indicating that the final lower pro-fibrotic potential of

splenocytes from CD362^{+} db/db mice is due to a delicate change in pro- versus anti-fibrotic mediators.

5.4. WT-MSC and CD362^{-} cells reduce the expression of components of the Nlrp3 inflammasome

The innate immune system recognizes danger-associated molecular patterns (DAMP) via pattern recognition receptors resulting, among others, in the activation of the inflammasome-3 [131][132]. The Nlrp3 inflammasome has effects in auto-inflammatory diseases and is associated with metabolic dysfunction [133]. It promotes obesity-induced autoinflammation and insulin resistance [134]. Danger signals induced by DM such as fatty acids [135], uric acid [136], endoplasmic reticulum stress [137], and reactive oxygen species [138] activate the Nlrp3 inflammasome. Subsequently, pro-inflammatory cytokines, which are inflammasome-dependent, induce insulin resistance and cause death of β-cells in the pancreas [139]. In the heart, the number of inflammasomes per field is higher in patients presenting with severe heart failure (NYHA III–IV) versus those with mild or no heart failure [140], indicating the relevance of the Nlrp3 inflammasome in heart failure.

With respect to our findings, LV Nlrp3, ASC, and caspase-1 mRNA expression was significantly induced in db/db mice compared to the control group. I.v. application of WT-MSC and CD362^{-} cells decreased LV Nlrp3, and ASC gene expression, while CD362^{+} cells had no effect. Moreover, only CD362^{-} cells were able to reduce LV caspase-1 mRNA expression in db/db mice. Our findings with WT-MSC are supported by previous studies demonstrating that the anti-inflammatory effects of MSCs include the downregulation of the inflammasome [141][142]. However, the present study is the first to demonstrate the impact of MSCs on the Nlrp3 inflammasome under diabetic conditions. Interestingly, our findings show lower LV IL-1ß mRNA expression in db/db versus control db+/db mice, which might be the result of a negative feedback mechanism in the presence of higher LV IL-1ß protein levels (**Figure 22**). Further studies are necessary to investigate whether WT-MSC and

CD362$^-$ cells reduce the NF-κB-dependent expression of Nlrp3, downstream the pattern recognition receptors NOD2 and TLR, which are also induced under DM [127] [143], and/or whether they also reduce the activity of the Nlrp3 inflammasome via the anti-oxidative properties of MSCs as shown by Oh *et al.* [144]. In this context, it will be necessary to evaluate caspase 1 activity and IL-1ß protein expression as endpoint of inflammasome activity following cleavage of pro-IL-1ß via caspase 1 [144].

5.5. WT-MSC and CD362$^-$ cells increase cardiac titin phosphorylation

Imaging mass spectrometry is a novel technique to determine region-dependent protein expression levels on tissue sections [97]. In the present study, imaging mass spectrometry revealed a significantly lower N2B isoform expression in db/db mice compared to db+/db mice (**Figure 26**), an effect which could be overcome by the application of WT-MSC, CD362$^-$ and CD362$^+$ cells. Titin is the largest sarcomere protein and exists in two isoforms: N2B and N2BA. Besides collagen, also titin influences cardiac function. A shift in isoform expression or titin hypophosphorylation results in the development of cardiac dysfunction [110][145][146]. Therefore, our imaging mass spectrometry findings are not conclusive and further evaluation on protein level is required to confirm the changes in N2B expression in relation to the N2BA isoform to show a possible relation to the observed cardiac dysfunction. However, we could demonstrate that the phosphorylation of the N2B isoform was downregulated in db/db mice and interestingly, that in line with cardiac function it could only be restored in db/db mice, which received WT-MSC or CD362$^-$ cells (**Figure 27**). DM is associated with oxidative stress and with particular changes in guanylyl cyclase intracellular pathways leading to a reduction in cyclic guanosine monophosphate (cGMP) levels [147] and subsequent low protein kinase G activity, leading to titin hypophosphorylation, which is associated with cardiomyocyte stiffness [20] [148]. Activation of protein kinase G via cGMP signaling can lower diastolic tone and increase LV extensibility [149] [150]. As shown in **Figure 27**, protein kinase G activity was downregulated in db/db

mice. Concomitant with the titin phosphorylation state, only the application of WT-MSC and $CD362^-$ cells normalized protein kinase G activity to control levels. In summary, the data indicate that the normalized titin phosphorylation and protein kinase G activity in db/db mice which received WT-MSC or $CD362^-$ cells underlie, be it in part, the improved cardiac function in those mice compared to untreated db/db mice and db/db mice which received $CD362^+$ cells.

5.6. Perspectives

This is the first study evaluating the impact of $CD362^+$-selected MSCs on cardiac function in mice. Consequently, there are no other studies available to reflect and understand the effect of $CD362^+$ cells in the db/db setting. At the present stage, this study is only descriptive and does not give any possible in-depth mechanism explaining the negative outcome of the $CD362^+$ cells following i.v. application in db/db mice. In order to gain a better understanding of the $CD362^+$ cells and their working mechanism, further knowledge of syndecans and particularly CD362 is required. Syndecans are single transmembrane domain proteins. These core proteins carry three to five heparan sulfate and chondroitin sulfate chains, and one of their main functions is the interaction with, and modulation of, a large variety of ligands [151]: they can carry and interact with fibroblast growth factors, vascular endothelial growth factor and also with TGF-β and TNF-α. These pleiotropic cytokines can lead to a disturbance of systolic and diastolic function by several mechanisms. In our experiment, only WT-MSC and $CD362^-$ db/db mice exhibited lower LV TNF-α mRNA expression versus db/db mice, whereas $CD362^+$ db/db mice did not (**Figure 21A**). In addition, the percentage of splenic CD68 cells expressing TGF-ß was higher in $CD362^+$ db/db mice versus db/db, WT-MSC db/db and $CD362^-$ db/db mice (**Figure 23A**). This suggests that interactions of $CD362^+$ with TGF-ß and TNF-α [151] may contribute to these observations. *In vitro* studies with $CD362^+$ cells co-cultured with immune cells, cardiac fibroblasts and cardiomyocytes are required to understand the impact of $CD362^+$ cells on cytokine expression, immune cell modulation, collagen production in cardiac fibroblasts, and titin regulation in cardiomyocytes, respectively.

Furthermore, the engraftment of WT-MSC, $CD362^-$, and $CD362^+$ cells in the heart, lung, spleen, liver, pancreas, and kidney following i.v. application in db/db mice should still be evaluated to verify that differences in their impact on cardiac function might be due to differences in engraftment. Last but not least, the impact of the different stromal cells on cardiac capillary and arteriole density in db/db mice should still be determined, given the relevance of an impaired angiogenesis and vascular rarefaction on diastolic dysfunction.

References

[1] J. A. Beckman, M. A. Creager, and P. Libby, “Diabetes and atherosclerosis: epidemiology, pathophysiology, and management.,” *JAMA*, vol. 287, no. 19, pp. 2570–81, May 2002.

[2] “WHO | The top 10 causes of death worldwide, January 2017,” *WHO*, 2017.

[3] V. L. Roger, A. S. Go, D. M. Lloyd-Jones, R. J. Adams, J. D. Berry, T. M. Brown, M. R. Carnethon, S. Dai, G. De Simone, E. S. Ford, C. S. Fox, H. J. Fullerton, C. Gillespie, K. J. Greenlund, S. M. Hailpern, J. A. Heit, P. Michael Ho, V. J. Howard, B. M. Kissela, S. J. Kittner, D. T. Lackland, J. H. Lichtman, L. D. Lisabeth, D. M. Makuc, G. M. Marcus, A. Marelli, D. B. Matchar, M. M. McDermott, J. B. Meigs, C. S. Moy, D. Mozaffarian, M. E. Mussolino, G. Nichol, N. P. Paynter, W. D. Rosamond, P. D. Sorlie, R. S. Stafford, T. N. Turan, M. B. Turner, N. D. Wong, and J. Wylie-Rosett, “Heart disease and stroke statistics-2011 update: A report from the American Heart Association,” *Circulation*, vol. 123, no. 4, 2011.

[4] S. Rubler, J. Dlugash, Y. Z. Yuceoglu, T. Kumral, A. W. Branwood, and A. Grishman, “New type of cardiomyopathy associated with diabetic glomerulosclerosis.,” *Am. J. Cardiol.*, vol. 30, no. 6, pp. 595–602, Nov. 1972.

[5] R. I. Hamby, S. Zoneraich, and L. Sherman, “Diabetic cardiomyopathy.,” *JAMA*, vol. 229, no. 13, pp. 1749–54, Sep. 1974.

[6] I. Falcão-Pires and A. F. Leite-Moreira, “Diabetic cardiomyopathy: Understanding the molecular and cellular basis to progress in diagnosis and treatment,” *Heart Fail. Rev.*, vol. 17, no. 3, pp. 325–344, 2012.

[7] Z. Y. Fang, J. B. Prins, and T. H. Marwick, “Diabetic Cardiomyopathy: Evidence, Mechanisms, and Therapeutic Implications,” *Endocr. Rev.*, vol. 25, no. 4, pp. 543–567, 2004.

[8] B. Maisch, P. Alter, and S. Pankuweit, “Diabetic cardiomyopathy - Fact or fiction?,” *Herz*, vol. 36, no. 2, pp. 102–115, 2011.

[9] W. B. Kannel, M. Hjortland, and W. P. Castelli, “Role of diabetes in congestive heart failure: the Framingham study.,” *Am. J. Cardiol.*, vol. 34, no. 1, pp. 29–34, Jul. 1974.

[10] D. M. Shindler, J. B. Kostis, S. Yusuf, M. A. Quinones, B. Pitt, D. Stewart, T. Pinkett, J. K. Ghali, and A. C. Wilson, “Diabetes mellitus, a predictor of morbidity and mortality in the Studies of Left Ventricular Dysfunction (SOLVD) trials and registry,” *Am. J. Cardiol.*, vol. 77, no. 11, pp. 1017–1020, 1996.

[11] S. Dandamudi, J. Slusser, D. W. Mahoney, M. M. Redfield, R. J. Rodeheffer, and H. H. Chen, “The prevalence of diabetic cardiomyopathy: A population-based study in Olmsted County, Minnesota,” *J. Card. Fail.*, vol. 20, no. 5, pp. 304–309, 2014.

[12] C. Mátyás, B. T. Németh, A. Oláh, M. Török, M. Ruppert, D. Kellermayer, B. A. Barta, G. Szabó, G. Kökény, E. M. Horváth, B. Bódi, Z. Papp, B. Merkely, and T. Radovits, “Prevention of the development of heart failure with preserved

ejection fraction by the phosphodiesterase-5A inhibitor vardenafil in rats with type 2 diabetes.," *Eur. J. Heart Fail.*, vol. 19, no. 3, pp. 326–336, Mar. 2017.

[13] S. Van Linthout, U. Seeland, A. Riad, O. Eckhardt, M. Hohl, N. Dhayat, U. Richter, J. W. Fischer, M. Böhm, M. Pauschinger, H.-P. Schultheiss, and C. Tschöpe, "Reduced MMP-2 activity contributes to cardiac fibrosis in experimental diabetic cardiomyopathy.," *Basic Res. Cardiol.*, vol. 103, no. 4, pp. 319–27, Jul. 2008.

[14] S. Van Linthout, F. Spillmann, A. Riad, C. Trimpert, J. Lievens, M. Meloni, F. Escher, E. Filenberg, O. Demir, J. Li, M. Shakibaei, I. Schimke, A. Staudt, S. B. Felix, H.-P. Schultheiss, B. De Geest, and C. Tschöpe, "Human apolipoprotein A-I gene transfer reduces the development of experimental diabetic cardiomyopathy.," *Circulation*, vol. 117, no. 12, pp. 1563–73, Mar. 2008.

[15] C. TSCHOPE, T. Walther, J. Königer, F. Spillmann, D. Westermann, F. Escher, M. Pauschinger, J. B. Pesquero, M. Bader, H.-P. Schultheiss, and M. Noutsias, "Prevention of cardiac fibrosis and left ventricular dysfunction in diabetic cardiomyopathy in rats by transgenic expression of the human tissue kallikrein gene," *FASEB J.*, vol. 18, no. 7, pp. 828–835, May 2004.

[16] A. Adameova and N. S. Dhalla, "Role of microangiopathy in diabetic cardiomyopathy," *Heart Fail. Rev.*, vol. 19, no. 1, pp. 25–33, Jan. 2014.

[17] S. Van Linthout, A. Riad, N. Dhayat, F. Spillmann, J. Du, S. Dhayat, D. Westermann, D. Hilfiker-Kleiner, M. Noutsias, U. Laufs, H.-P. Schultheiss, and C. Tschöpe, "Anti-inflammatory effects of atorvastatin improve left ventricular function in experimental diabetic cardiomyopathy.," *Diabetologia*, vol. 50, no. 9, pp. 1977–86, Sep. 2007.

[18] R. Vetter, U. Rehfeld, C. Reissfelder, W. Weiss, K.-D. Wagner, J. Günther, A. Hammes, C. Tschöpe, W. Dillmann, and M. Paul, "Transgenic overexpression of the sarcoplasmic reticulum Ca2+ATPase improves reticular Ca2+ handling in normal and diabetic rat hearts.," *FASEB J.*, vol. 16, no. 12, pp. 1657–9, Oct. 2002.

[19] C. Tschöpe, T. Walther, F. Escher, F. Spillmann, J. Du, C. Altmann, I. Schimke, M. Bader, C. F. Sanchez-Ferrer, H.-P. Schultheiss, and M. Noutsias, "Transgenic activation of the kallikrein-kinin system inhibits intramyocardial inflammation, endothelial dysfunction and oxidative stress in experimental diabetic cardiomyopathy.," *FASEB J.*, vol. 19, no. 14, pp. 2057–9, Dec. 2005.

[20] N. Hamdani, A.-S. Hervent, L. Vandekerckhove, V. Matheeussen, M. Demolder, L. Baerts, I. De Meester, W. A. Linke, W. J. Paulus, and G. W. De Keulenaer, "Left ventricular diastolic dysfunction and myocardial stiffness in diabetic mice is attenuated by inhibition of dipeptidyl peptidase 4.," *Cardiovasc. Res.*, vol. 104, no. 3, pp. 423–31, Dec. 2014.

[21] I. Falcão-Pires, N. Hamdani, A. Borbély, C. Gavina, C. G. Schalkwijk, J. van der Velden, L. van Heerebeek, G. J. M. Stienen, H. W. M. Niessen, A. F. Leite-Moreira, and W. J. Paulus, "Diabetes mellitus worsens diastolic left ventricular dysfunction in aortic stenosis through altered myocardial structure

and cardiomyocyte stiffness.," *Circulation*, vol. 124, no. 10, pp. 1151–9, Sep. 2011.

[22] B. Rodrigues, M. C. Cam, and J. H. McNeill, "Metabolic disturbances in diabetic cardiomyopathy.," *Mol. Cell. Biochem.*, vol. 180, no. 1–2, pp. 53–7, Mar. 1998.

[23] S. a Hayat, B. Patel, R. S. Khattar, and R. a Malik, "Diabetic cardiomyopathy: mechanisms, diagnosis and treatment.," *Clin. Sci. (Lond).*, vol. 107, no. 6, pp. 539–557, 2004.

[24] I. G. Poornima, P. Parikh, and R. P. Shannon, "Diabetic cardiomyopathy: The search for a unifying hypothesis," *Circ. Res.*, vol. 98, no. 5, pp. 596–605, 2006.

[25] F. Spillmann, S. Van Linthout, and C. Tschöpe, "Cardiac effects of HDL and its components on diabetic cardiomyopathy.," *Endocr. Metab. Immune Disord. Drug Targets*, vol. 12, no. 2, pp. 132–47, Jun. 2012.

[26] M. Brownlee, T. Nishikawa, D. Edelstein, X. L. Du, S. Yamagishi, T. Matsumura, Y. Kaneda, M. A. Yorek, D. Beebe, P. J. Oates, H.-P. Hammes, and I. Giardino, "Normalizing mitochondrial superoxide production blocks three pathways of hyperglycaemic damage.," *Nature*, vol. 404, no. 6779, pp. 787–790, Apr. 2000.

[27] R. Candido, J. M. Forbes, M. C. Thomas, V. Thallas, R. G. Dean, W. C. Burns, C. Tikellis, R. H. Ritchie, S. M. Twigg, M. E. Cooper, and L. M. Burrell, "A breaker of advanced glycation end products attenuates diabetes-induced myocardial structural changes.," *Circ. Res.*, vol. 92, no. 7, pp. 785–92, Apr. 2003.

[28] J. R. McMullen, T. Shioi, W.-Y. Huang, L. Zhang, O. Tarnavski, E. Bisping, M. Schinke, S. Kong, M. C. Sherwood, J. Brown, L. Riggi, P. M. Kang, and S. Izumo, "The insulin-like growth factor 1 receptor induces physiological heart growth via the phosphoinositide 3-kinase(p110alpha) pathway.," *J. Biol. Chem.*, vol. 279, no. 6, pp. 4782–93, Feb. 2004.

[29] F. Spillmann, C. Trimpert, J. Peng, L. G. Eckerle, A. Staudt, K. Warstat, S. B. Felix, B. Pieske, C. Tschöpe, and S. Van Linthout, "High-density lipoproteins reduce palmitate-induced cardiomyocyte apoptosis in an AMPK-dependent manner.," *Biochem. Biophys. Res. Commun.*, vol. 466, no. 2, pp. 272–7, Oct. 2015.

[30] D. X. Zhang, R. M. Fryer, A. K. Hsu, A. P. Zou, G. J. Gross, W. B. Campbell, and P. L. Li, "Production and metabolism of ceramide in normal and ischemic-reperfused myocardium of rats.," *Basic Res. Cardiol.*, vol. 96, no. 3, pp. 267–74.

[31] K. R. Bidasee, Y. Zhang, C. H. Shao, M. Wang, K. P. Patel, U. D. Dincer, and H. R. Besch, "Diabetes increases formation of advanced glycation end products on Sarco(endo)plasmic reticulum Ca2+-ATPase.," *Diabetes*, vol. 53, no. 2, pp. 463–73, Feb. 2004.

[32] K. M. Choi, Y. Zhong, B. D. Hoit, I. L. Grupp, H. Hahn, K. W. Dilly, S. Guatimosim, W. J. Lederer, and M. A. Matlib, "Defective intracellular Ca(2+)

signaling contributes to cardiomyopathy in Type 1 diabetic rats.," *Am. J. Physiol. Heart Circ. Physiol.*, vol. 283, no. 4, pp. H1398-408, Oct. 2002.

[33] M. Asif, J. Egan, S. Vasan, G. N. Jyothirmayi, M. R. Masurekar, S. Lopez, C. Williams, R. L. Torres, D. Wagle, P. Ulrich, A. Cerami, M. Brines, and T. J. Regan, "An advanced glycation endproduct cross-link breaker can reverse age-related increases in myocardial stiffness.," *Proc. Natl. Acad. Sci. U. S. A.*, vol. 97, no. 6, pp. 2809–13, Mar. 2000.

[34] V. A. Lacombe, K. W. Hinchcliff, and S. T. Devor, "Effects of exercise and glucose administration on content of insulin-sensitive glucose transporter in equine skeletal muscle.," *Am. J. Vet. Res.*, vol. 64, no. 12, pp. 1500–6, Dec. 2003.

[35] T. Szkudelski, "The mechanism of alloxan and streptozotocin action in B cells of the rat pancreas," *Physiol. Res.*, vol. 50, no. 6, pp. 537–546, 2001.

[36] S. Yoshida, H. Tanaka, H. Oshima, T. Yamazaki, Y. Yonetoku, T. Ohishi, T. Matsui, and M. Shibasaki, "AS1907417, a novel GPR119 agonist, as an insulinotropic and β-cell preservative agent for the treatment of type 2 diabetes.," *Biochem. Biophys. Res. Commun.*, vol. 400, no. 4, pp. 745–51, Oct. 2010.

[37] J. S. Park, S. D. Rhee, N. S. Kang, W. H. Jung, H. Y. Kim, J. H. Kim, S. K. Kang, H. G. Cheon, J. H. Ahn, and K. Y. Kim, "Anti-diabetic and anti-adipogenic effects of a novel selective 11??-hydroxysteroid dehydrogenase type 1 inhibitor, 2-(3-benzoyl)-4-hydroxy-1,1-dioxo-2H-1,2-benzothiazine-2-yl-1-phenylethanone (KR-66344)," *Biochem. Pharmacol.*, vol. 81, no. 8, pp. 1028–1035, 2011.

[38] V. a Gault, B. D. Kerr, P. Harriott, and P. R. Flatt, "Administration of an acylated GLP-1 and GIP preparation provides added beneficial glucose-lowering and insulinotropic actions over single incretins in mice with Type 2 diabetes and obesity.," *Clin. Sci. (Lond).*, vol. 121, no. 3, pp. 107–17, 2011.

[39] A. Uccelli, L. Moretta, and V. Pistoia, "Mesenchymal stem cells in health and disease," *Nat Rev Immunol*, vol. 8, no. 9, pp. 726–736, 2008.

[40] M. Ohishi and E. Schipani, "Bone marrow mesenchymal stem cells," *J. Cell. Biochem.*, vol. 109, no. 2, pp. 277–282, 2010.

[41] M. Dominici, K. Le Blanc, I. Mueller, I. Slaper-Cortenbach, F. Marini, D. Krause, R. Deans, A. Keating, D. Prockop, and E. Horwitz, "Minimal criteria for defining multipotent mesenchymal stromal cells. The International Society for Cellular Therapy position statement.," *Cytotherapy*, vol. 8, no. 4, pp. 315–7, 2006.

[42] A. J. Friedenstein, R. K. Chailakhyan, and U. V Gerasimov, "Bone marrow osteogenic stem cells: in vitro cultivation and transplantation in diffusion chambers.," *Cell Tissue Kinet.*, vol. 20, no. 3, pp. 263–72, May 1987.

[43] G. I. Shulman, "On diabetes : insulin resistance Cellular mechanisms of insulin resistance," vol. 106, no. 2, pp. 171–176, 2000.

[44] M. F. Pittenger, A. M. Mackay, S. Beck, R. K. Jaiswal, R. Douglas, J. D. Mosca, M. a. Moorman, D. W. Simonetti, S. Craig, and D. Marshak, "Multilineage

Potential of Adult Human Mesenchymal Stem Cells," *Science (80-.).*, vol. 284, no. April, pp. 143–147, 1999.

[45] A. R. Chugh, E. K. Zuba-Surma, and B. Dawn, "Bone marrow-derived mesenchymal stems cells and cardiac repair.," *Minerva Cardioangiol.*, vol. 57, no. 2, pp. 185–202, Apr. 2009.

[46] P. Chhabra and K. L. Brayman, "The use of stem cells in kidney disease.," *Curr. Opin. Organ Transplant.*, vol. 14, no. 1, pp. 72–78, 2009.

[47] A. A. Rzhaninova, S. N. Gornostaeva, and D. V Goldshtein, "Isolation and phenotypical characterization of mesenchymal stem cells from human fetal thymus.," *Bull. Exp. Biol. Med.*, vol. 139, no. 1, pp. 134–40, Jan. 2005.

[48] Y. Hu, L. Liao, Q. Wang, L. Ma, G. Ma, X. Jiang, and R. C. Zhao, "Isolation and identification of mesenchymal stem cells from human fetal pancreas," *J. Lab. Clin. Med.*, vol. 141, no. 5, pp. 342–349, 2003.

[49] R. Moreno, I. Martínez-González, M. Rosal, A. Farwati, E. Gratacós, and J. M. Aran, "Characterization of mesenchymal stem cells isolated from the rabbit fetal liver.," *Stem Cells Dev.*, vol. 19, no. 10, pp. 1579–88, 2010.

[50] Z. Miao, J. Jin, L. Chen, J. Zhu, W. Huang, J. Zhao, H. Qian, and X. Zhang, "Isolation of mesenchymal stem cells from human placenta: Comparison with human bone marrow mesenchymal stem cells," *Cell Biol. Int.*, vol. 30, no. 9, pp. 681–687, 2006.

[51] W. R. Prather, A. Toren, M. Meiron, R. Ofir, C. Tschope, and E. M. Horwitz, "The role of placental-derived adherent stromal cell (PLX-PAD) in the treatment of critical limb ischemia.," *Cytotherapy*, vol. 11, no. 4, pp. 427–34, Jan. 2009.

[52] C. E. Gargett, K. E. Schwab, R. M. Zillwood, H. P. T. Nguyen, and D. Wu, "Isolation and culture of epithelial progenitors and mesenchymal stem cells from human endometrium.," *Biol. Reprod.*, vol. 80, no. 6, pp. 1136–45, 2009.

[53] T. G. Koch, T. Heerkens, P. D. Thomsen, and D. H. Betts, "Isolation of mesenchymal stem cells from equine umbilical cord blood.," *BMC Biotechnol.*, vol. 7, no. 1, p. 26, 2007.

[54] P. De Coppi, M. Pozzobon, M. Piccoli, M. V. Gazzola, L. Boldrin, E. Slanzi, R. Destro, L. Zanesco, G. F. Zanon, and P. Gamba, "Isolation of mesenchymal stem cells from human vermiform appendix.," *J. Surg. Res.*, vol. 135, no. 1, pp. 85–91, Sep. 2006.

[55] S. Aggarwal and M. F. Pittenger, "Human mesenchymal stem cells modulate allogeneic immune cell responses.," *Blood*, vol. 105, no. 4, pp. 1815–22, Feb. 2005.

[56] K. Savvatis, S. van Linthout, K. Miteva, K. Pappritz, D. Westermann, J. C. Schefold, G. Fusch, A. Weithäuser, U. Rauch, P.-M. Becher, K. Klingel, J. Ringe, A. Kurtz, H.-P. Schultheiss, and C. Tschöpe, "Mesenchymal stromal cells but not cardiac fibroblasts exert beneficial systemic immunomodulatory effects in experimental myocarditis.," *PLoS One*, vol. 7, no. 7, p. e41047, Jul. 2012.

[57] S. Van Linthout, C. Stamm, H.-P. Schultheiss, and C. Tschöpe, “Mesenchymal stem cells and inflammatory cardiomyopathy: cardiac homing and beyond.,” *Cardiol. Res. Pract.*, vol. 2011, p. 757154, Mar. 2011.

[58] J. M. Hare, J. H. Traverse, T. D. Henry, N. Dib, R. K. Strumpf, S. P. Schulman, G. Gerstenblith, A. N. DeMaria, A. E. Denktas, R. S. Gammon, J. B. Hermiller, M. A. Reisman, G. L. Schaer, and W. Sherman, “A randomized, double-blind, placebo-controlled, dose-escalation study of intravenous adult human mesenchymal stem cells (prochymal) after acute myocardial infarction.,” *J. Am. Coll. Cardiol.*, vol. 54, no. 24, pp. 2277–86, Dec. 2009.

[59] H. C. Quevedo, K. E. Hatzistergos, B. N. Oskouei, G. S. Feigenbaum, J. E. Rodriguez, D. Valdes, P. M. Pattany, J. P. Zambrano, Q. Hu, I. McNiece, A. W. Heldman, and J. M. Hare, “Allogeneic mesenchymal stem cells restore cardiac function in chronic ischemic cardiomyopathy via trilineage differentiating capacity.,” *Proc. Natl. Acad. Sci. U. S. A.*, vol. 106, no. 33, pp. 14022–7, Aug. 2009.

[60] R. H. Lee, A. A. Pulin, M. J. Seo, D. J. Kota, J. Ylostalo, B. L. Larson, L. Semprun-Prieto, P. Delafontaine, and D. J. Prockop, “Intravenous hMSCs improve myocardial infarction in mice because cells embolized in lung are activated to secrete the anti-inflammatory protein TSG-6.,” *Cell Stem Cell*, vol. 5, no. 1, pp. 54–63, Jul. 2009.

[61] S. Van Linthout, K. Savvatis, K. Miteva, J. Peng, J. Ringe, K. Warstat, C. Schmidt-Lucke, M. Sittinger, H.-P. Schultheiss, and C. Tschöpe, “Mesenchymal stem cells improve murine acute coxsackievirus B3-induced myocarditis.,” *Eur. Heart J.*, vol. 32, no. 17, pp. 2168–78, Sep. 2011.

[62] S. Ohnishi, H. Sumiyoshi, S. Kitamura, and N. Nagaya, “Mesenchymal stem cells attenuate cardiac fibroblast proliferation and collagen synthesis through paracrine actions.,” *FEBS Lett.*, vol. 581, no. 21, pp. 3961–6, Aug. 2007.

[63] T. Kinnaird, E. Stabile, M. S. Burnett, M. Shou, C. W. Lee, S. Barr, S. Fuchs, and S. E. Epstein, “Local delivery of marrow-derived stromal cells augments collateral perfusion through paracrine mechanisms.,” *Circulation*, vol. 109, no. 12, pp. 1543–9, Mar. 2004.

[64] N. Wang, C. Chen, D. Yang, Q. Liao, H. Luo, X. Wang, F. Zhou, X. Yang, J. Yang, C. Zeng, and W. E. Wang, “Mesenchymal stem cells-derived extracellular vesicles, via miR-210, improve infarcted cardiac function by promotion of angiogenesis.,” *Biochim. Biophys. Acta*, Feb. 2017.

[65] R. H. Lee, M. J. Seo, R. L. Reger, J. L. Spees, A. A. Pulin, S. D. Olson, and D. J. Prockop, “Multipotent stromal cells from human marrow home to and promote repair of pancreatic islets and renal glomeruli in diabetic NOD/scid mice.,” *Proc. Natl. Acad. Sci. U. S. A.*, vol. 103, no. 46, pp. 17438–43, Nov. 2006.

[66] F. E. Ezquer, M. E. Ezquer, D. B. Parrau, D. Carpio, A. J. Yañez, and P. A. Conget, “Systemic administration of multipotent mesenchymal stromal cells reverts hyperglycemia and prevents nephropathy in type 1 diabetic mice.,” *Biol. Blood Marrow Transplant.*, vol. 14, no. 6, pp. 631–40, Jun. 2008.

[67] S. Van Linthout, F. Spillmann, H.-P. Schultheiss, and C. Tschöpe, “Effects of mesenchymal stromal cells on diabetic cardiomyopathy.,” *Curr. Pharm. Des.*, vol. 17, no. 30, pp. 3341–7, Oct. 2011.

[68] K. Otsu, S. Das, S. D. Houser, S. K. Quadri, S. Bhattacharya, and J. Bhattacharya, “Concentration-dependent inhibition of angiogenesis by mesenchymal stem cells.,” *Blood*, vol. 113, no. 18, pp. 4197–205, Apr. 2009.

[69] M. Di Nicola, C. Carlo-Stella, M. Magni, M. Milanesi, P. D. Longoni, P. Matteucci, S. Grisanti, and A. M. Gianni, “Human bone marrow stromal cells suppress T-lymphocyte proliferation induced by cellular or nonspecific mitogenic stimuli.,” *Blood*, vol. 99, no. 10, pp. 3838–43, May 2002.

[70] S. Ghannam, J. Pène, G. Moquet-Torcy, G. Torcy-Moquet, C. Jorgensen, and H. Yssel, “Mesenchymal stem cells inhibit human Th17 cell differentiation and function and induce a T regulatory cell phenotype.,” *J. Immunol.*, vol. 185, no. 1, pp. 302–12, Jul. 2010.

[71] G. Xu, Y. Zhang, L. Zhang, G. Ren, and Y. Shi, “The role of IL-6 in inhibition of lymphocyte apoptosis by mesenchymal stem cells,” *Biochem. Biophys. Res. Commun.*, vol. 361, no. 3, pp. 745–750, Sep. 2007.

[72] A. I. Caplan, “Review: mesenchymal stem cells: cell-based reconstructive therapy in orthopedics.,” *Tissue Eng.*, vol. 11, no. 7–8, pp. 1198–211.

[73] J. Hollinger and M. E. K. Wong, “The integrated processes of hard tissue regeneration with special emphasis on fracture healing,” *Oral Surgery, Oral Med. Oral Pathol. Oral Radiol. Endodontology*, vol. 82, no. 6, pp. 594–606, 1996.

[74] E. M. Horwitz, “Marrow mesenchymal cell transplantation for genetic disorders of bone.,” *Cytotherapy*, vol. 3, no. 5, pp. 399–401, 2001.

[75] E. M. Horwitz, T. J. Hofmann, J. E. Garlits, D. Campioni, and M. Dominici, “On the development of cell therapy for genetic disorders.,” *Cytotherapy*, vol. 4, no. 6, pp. 511–2, 2002.

[76] S. Wecht and M. Rojas, “Mesenchymal stem cells in the treatment of chronic lung disease.,” *Respirology*, Sep. 2016.

[77] D. Haldar, N. C. Henderson, G. Hirschfield, and P. N. Newsome, “Mesenchymal stromal cells and liver fibrosis: a complicated relationship.,” *FASEB J.*, Sep. 2016.

[78] L. R. Gao, Y. Chen, N. K. Zhang, X. L. Yang, H. L. Liu, Z. G. Wang, X. Y. Yan, Y. Wang, Z. M. Zhu, T. C. Li, L. H. Wang, H. Y. Chen, Y. D. Chen, C. L. Huang, P. Qu, C. Yao, B. Wang, G. H. Chen, Z. M. Wang, Z. Y. Xu, J. Bai, D. Lu, Y. H. Shen, F. Guo, M. Y. Liu, Y. Yang, Y. C. Ding, Y. Yang, H. T. Tian, Q. A. Ding, L. N. Li, X. C. Yang, and X. Hu, “Intracoronary infusion of Wharton’s jelly-derived mesenchymal stem cells in acute myocardial infarction: double-blind, randomized controlled trial.,” *BMC Med.*, vol. 13, no. 1, p. 162, Jul. 2015.

[79] A. W. Heldman, D. L. DiFede, J. E. Fishman, J. P. Zambrano, B. H. Trachtenberg, V. Karantalis, M. Mushtaq, A. R. Williams, V. Y. Suncion, I. K. McNiece, E. Ghersin, V. Soto, G. Lopera, R. Miki, H. Willens, R. Hendel, R.

Mitrani, P. Pattany, G. Feigenbaum, B. Oskouei, J. Byrnes, M. H. Lowery, J. Sierra, M. V Pujol, C. Delgado, P. J. Gonzalez, J. E. Rodriguez, L. L. Bagno, D. Rouy, P. Altman, C. W. P. Foo, J. da Silva, E. Anderson, R. Schwarz, A. Mendizabal, and J. M. Hare, "Transendocardial mesenchymal stem cells and mononuclear bone marrow cells for ischemic cardiomyopathy: the TAC-HFT randomized trial.," *JAMA*, vol. 311, no. 1, pp. 62–73, Jan. 2014.

[80] T. Squillaro, G. Peluso, and U. Galderisi, "Clinical Trials With Mesenchymal Stem Cells: An Update.," *Cell Transplant.*, vol. 25, no. 5, pp. 829–48, Apr. 2016.

[81] S. Chen, W. Fang, J. Qian, F. Ye, Y. Liu, S. Shan, J. Zhang, S. Lin, L. Liao, and R. C. H. Zhao, "Improvement of cardiac function after transplantation of autologous bone marrow mesenchymal stem cells in patients with acute myocardial infarction.," *Chin. Med. J. (Engl).*, vol. 117, no. 10, pp. 1443–8, Oct. 2004.

[82] J. H. Houtgraaf, W. K. den Dekker, B. M. van Dalen, T. Springeling, R. de Jong, R. J. van Geuns, M. L. Geleijnse, F. Fernandez-Aviles, F. Zijlsta, P. W. Serruys, and H. J. Duckers, "First experience in humans using adipose tissue-derived regenerative cells in the treatment of patients with ST-segment elevation myocardial infarction.," *J. Am. Coll. Cardiol.*, vol. 59, no. 5, pp. 539–40, Jan. 2012.

[83] A. W. Heldman, D. L. DiFede, J. E. Fishman, J. P. Zambrano, B. H. Trachtenberg, V. Karantalis, M. Mushtaq, A. R. Williams, V. Y. Suncion, I. K. McNiece, E. Ghersin, V. Soto, G. Lopera, R. Miki, H. Willens, R. Hendel, R. Mitrani, P. Pattany, G. Feigenbaum, B. Oskouei, J. Byrnes, M. H. Lowery, J. Sierra, M. V. Pujol, C. Delgado, P. J. Gonzalez, J. E. Rodriguez, L. L. Bagno, D. Rouy, P. Altman, C. W. P. Foo, J. da Silva, E. Anderson, R. Schwarz, A. Mendizabal, and J. M. Hare, "Transendocardial Mesenchymal Stem Cells and Mononuclear Bone Marrow Cells for Ischemic Cardiomyopathy," *JAMA*, vol. 311, no. 1, p. 62, Jan. 2014.

[84] J. M. Hare, J. E. Fishman, G. Gerstenblith, D. L. DiFede Velazquez, J. P. Zambrano, V. Y. Suncion, M. Tracy, E. Ghersin, P. V Johnston, J. A. Brinker, E. Breton, J. Davis-Sproul, I. H. Schulman, J. Byrnes, A. M. Mendizabal, M. H. Lowery, D. Rouy, P. Altman, C. Wong Po Foo, P. Ruiz, A. Amador, J. Da Silva, I. K. McNiece, A. W. Heldman, R. George, and A. Lardo, "Comparison of allogeneic vs autologous bone marrow–derived mesenchymal stem cells delivered by transendocardial injection in patients with ischemic cardiomyopathy: the POSEIDON randomized trial.," *JAMA*, vol. 308, no. 22, pp. 2369–79, Dec. 2012.

[85] J. M. Hare, J. H. Traverse, T. D. Henry, N. Dib, R. K. Strumpf, S. P. Schulman, G. Gerstenblith, A. N. DeMaria, A. E. Denktas, R. S. Gammon, J. B. Hermiller, M. A. Reisman, G. L. Schaer, and W. Sherman, "A Randomized, Double-Blind, Placebo-Controlled, Dose-Escalation Study of Intravenous Adult Human Mesenchymal Stem Cells (Prochymal) After Acute Myocardial Infarction," *J. Am. Coll. Cardiol.*, vol. 54, no. 24, pp. 2277–2286, Dec. 2009.

[86] J. Butler, S. E. Epstein, S. J. Greene, A. A. Quyyumi, S. Sikora, R. J. Kim, A. S. Anderson, J. E. Wilcox, N. I. Tankovich, M. J. Lipinski, Y.-A. Ko, K. B. Margulies, R. T. Cole, H. A. Skopicki, and M. Gheorghiade, "Intravenous Allogeneic Mesenchymal Stem Cells for Nonischemic Cardiomyopathy: Safety and Efficacy Results of a Phase II-A Randomized Trial.," *Circ. Res.*, vol. 120, no. 2, pp. 332–340, Jan. 2017.

[87] S. Sarrazin, W. C. Lamanna, and J. D. Esko, "Heparan Sulfate Proteoglycans," *Cold Spring Harb. Perspect. Biol.*, vol. 3, no. 7, pp. a004952–a004952, Jul. 2011.

[88] M. W. M. Schellings, D. Vanhoutte, G. C. van Almen, M. Swinnen, J. J. G. Leenders, N. Kubben, R. E. W. van Leeuwen, L. Hofstra, S. Heymans, and Y. M. Pinto, "Syndecan-1 amplifies angiotensin II-induced cardiac fibrosis.," *Hypertens. (Dallas, Tex. 1979)*, vol. 55, no. 2, pp. 249–56, Feb. 2010.

[89] J. Lei, S. N. Xue, W. Wu, S. X. Zhou, Y. L. Zhang, G. Y. Yuan, and J. F. Wang, "Increased level of soluble syndecan-1 in serum correlates with myocardial expression in a rat model of myocardial infarction.," *Mol. Cell. Biochem.*, vol. 359, no. 1–2, pp. 177–82, Jan. 2012.

[90] J. Tromp, A. van der Pol, IJ. T. Klip, R. A. de Boer, T. Jaarsma, W. H. van Gilst, A. A. Voors, D. J. van Veldhuisen, and P. van der Meer, "Fibrosis marker syndecan-1 and outcome in patients with heart failure with reduced and preserved ejection fraction.," *Circ. Heart Fail.*, vol. 7, no. 3, pp. 457–62, May 2014.

[91] Y. Matsui, M. Ikesue, K. Danzaki, J. Morimoto, M. Sato, S. Tanaka, T. Kojima, H. Tsutsui, and T. Uede, "Syndecan-4 Prevents Cardiac Rupture and Dysfunction After Myocardial Infarction," *Circ. Res.*, vol. 108, no. 11, pp. 1328–1339, May 2011.

[92] H. Park, Y. Kim, Y. Lim, I. Han, and E.-S. Oh, "Syndecan-2 mediates adhesion and proliferation of colon carcinoma cells.," *J. Biol. Chem.*, vol. 277, no. 33, pp. 29730–6, Aug. 2002.

[93] S. Méndez-Ferrer, T. V Michurina, F. Ferraro, A. R. Mazloom, B. D. Macarthur, S. A. Lira, D. T. Scadden, A. Ma'ayan, G. N. Enikolopov, and P. S. Frenette, "Mesenchymal and haematopoietic stem cells form a unique bone marrow niche.," *Nature*, vol. 466, no. 7308, pp. 829–34, Aug. 2010.

[94] S. J. Turley, A. L. Fletcher, and K. G. Elpek, "The stromal and haematopoietic antigen-presenting cells that reside in secondary lymphoid organs.," *Nat. Rev. Immunol.*, vol. 10, no. 12, pp. 813–25, Dec. 2010.

[95] P. Pacher, T. Nagayama, P. Mukhopadhyay, S. Bátkai, and D. A. Kass, "Measurement of cardiac function using pressure-volume conductance catheter technique in mice and rats.," *Nat. Protoc.*, vol. 3, no. 9, pp. 1422–34, Aug. 2008.

[96] J. A. Ramos-Vara and M. A. Miller, "When Tissue Antigens and Antibodies Get Along," *Vet. Pathol.*, vol. 51, no. 1, pp. 42–87, Jan. 2014.

[97] O. Klein, K. Strohschein, G. Nebrich, J. Oetjen, D. Trede, H. Thiele, T. Alexandrov, P. Giavalisco, G. N. Duda, P. von Roth, S. Geissler, J. Klose, and T. Winkler, "MALDI imaging mass spectrometry: discrimination of

pathophysiological regions in traumatized skeletal muscle by characteristic peptide signatures.," *Proteomics*, vol. 14, no. 20, pp. 2249–60, Oct. 2014.

[98] E. J. Estrada, F. Valacchi, E. Nicora, S. Brieva, C. Esteve, L. Echevarria, T. Froud, K. Bernetti, S. M. Cayetano, O. Velazquez, R. Alejandro, and C. Ricordi, "Combined treatment of intrapancreatic autologous bone marrow stem cells and hyperbaric oxygen in type 2 diabetes mellitus.," *Cell Transplant.*, vol. 17, no. 12, pp. 1295–304, 2008.

[99] A. Bhansali, V. Upreti, N. Khandelwal, N. Marwaha, V. Gupta, N. Sachdeva, R. R. Sharma, K. Saluja, P. Dutta, R. Walia, R. Minz, S. Bhadada, S. Das, and S. Ramakrishnan, "Efficacy of autologous bone marrow-derived stem cell transplantation in patients with type 2 diabetes mellitus.," *Stem Cells Dev.*, vol. 18, no. 10, pp. 1407–16, Dec. 2009.

[100] A. Bhansali, P. Asokumar, R. Walia, S. Bhansali, V. Gupta, A. Jain, N. Sachdeva, R. R. Sharma, N. Marwaha, and N. Khandelwal, "Efficacy and safety of autologous bone marrow-derived stem cell transplantation in patients with type 2 diabetes mellitus: a randomized placebo-controlled study.," *Cell Transplant.*, vol. 23, no. 9, pp. 1075–85, Sep. 2014.

[101] H. Hao, J. Liu, J. Shen, Y. Zhao, H. Liu, Q. Hou, C. Tong, D. Ti, L. Dong, Y. Cheng, Y. Mu, J. Liu, X. Fu, and W. Han, "Multiple intravenous infusions of bone marrow mesenchymal stem cells reverse hyperglycemia in experimental type 2 diabetes rats.," *Biochem. Biophys. Res. Commun.*, vol. 436, no. 3, pp. 418–23, Jul. 2013.

[102] X. Gao, L. Song, K. Shen, H. Wang, M. Qian, W. Niu, and X. Qin, "Bone marrow mesenchymal stem cells promote the repair of islets from diabetic mice through paracrine actions.," *Mol. Cell. Endocrinol.*, vol. 388, no. 1–2, pp. 41–50, May 2014.

[103] K. Savvatis, S. van Linthout, K. Miteva, K. Pappritz, D. Westermann, J. C. Schefold, G. Fusch, A. Weithäuser, U. Rauch, P.-M. Becher, K. Klingel, J. Ringe, A. Kurtz, H.-P. Schultheiss, and C. Tschöpe, "Mesenchymal Stromal Cells but Not Cardiac Fibroblasts Exert Beneficial Systemic Immunomodulatory Effects in Experimental Myocarditis," *PLoS One*, vol. 7, no. 7, p. e41047, Jul. 2012.

[104] C.-B. Liu, H. Huang, P. Sun, S.-Z. Ma, A.-H. Liu, J. Xue, J.-H. Fu, Y.-Q. Liang, B. Liu, D.-Y. Wu, S.-H. Lü, and X.-Z. Zhang, "Human Umbilical Cord-Derived Mesenchymal Stromal Cells Improve Left Ventricular Function, Perfusion, and Remodeling in a Porcine Model of Chronic Myocardial Ischemia.," *Stem Cells Transl. Med.*, vol. 5, no. 8, pp. 1004–13, Aug. 2016.

[105] M. T. Abdel Aziz, M. F. El-Asmar, M. Haidara, H. M. Atta, N. K. Roshdy, L. A. Rashed, D. Sabry, M. A. Youssef, A. T. Abdel Aziz, and M. Moustafa, "Effect of bone marrow-derived mesenchymal stem cells on cardiovascular complications in diabetic rats.," *Med. Sci. Monit.*, vol. 14, no. 11, p. BR249-55, Nov. 2008.

[106] C. Schmidt-Lucke, F. Escher, S. Van Linthout, U. Kühl, K. Miteva, J. Ringe, T. Zobel, H.-P. Schultheiss, and C. Tschöpe, "Cardiac migration of endogenous

mesenchymal stromal cells in patients with inflammatory cardiomyopathy.," *Mediators Inflamm.*, vol. 2015, p. 308185, 2015.

[107] L. Li, Y. Zhang, Y. Li, B. Yu, Y. Xu, S. Zhao, and Z. Guan, "Mesenchymal stem cell transplantation attenuates cardiac fibrosis associated with isoproterenol-induced global heart failure.," *Transpl. Int.*, vol. 21, no. 12, pp. 1181–9, Dec. 2008.

[108] D. Westermann, D. Lindner, M. Kasner, C. Zietsch, K. Savvatis, F. Escher, J. von Schlippenbach, C. Skurk, P. Steendijk, A. Riad, W. Poller, H.-P. Schultheiss, and C. Tschöpe, "Cardiac inflammation contributes to changes in the extracellular matrix in patients with heart failure and normal ejection fraction.," *Circ. Heart Fail.*, vol. 4, no. 1, pp. 44–52, Jan. 2011.

[109] A. J. Hance and R. G. Crystal, "Rigid control of synthesis of collagen types I and III by cells in culture.," *Nature*, vol. 268, no. 5616, pp. 152–4, Jul. 1977.

[110] N. Hamdani, C. Franssen, A. Lourenço, I. Falcão-Pires, D. Fontoura, S. Leite, L. Plettig, B. López, C. A. Ottenheijm, P. M. Becher, A. González, C. Tschöpe, J. Díez, W. A. Linke, A. F. Leite-Moreira, and W. J. Paulus, "Myocardial titin hypophosphorylation importantly contributes to heart failure with preserved ejection fraction in a rat metabolic risk model.," *Circ. Heart Fail.*, vol. 6, no. 6, pp. 1239–49, Nov. 2013.

[111] C. Tschöpe, C.-T. Bock, M. Kasner, M. Noutsias, D. Westermann, P.-L. Schwimmbeck, M. Pauschinger, W.-C. Poller, U. Kühl, R. Kandolf, and H.-P. Schultheiss, "High prevalence of cardiac parvovirus B19 infection in patients with isolated left ventricular diastolic dysfunction.," *Circulation*, vol. 111, no. 7, pp. 879–86, Feb. 2005.

[112] S. F. Mohammed, S. Hussain, S. A. Mirzoyev, W. D. Edwards, J. J. Maleszewski, and M. M. Redfield, "Coronary Microvascular Rarefaction and Myocardial Fibrosis in Heart Failure With Preserved Ejection Fraction," *Circulation*, vol. 131, no. 6, pp. 550–559, Feb. 2015.

[113] H. I. Ammar, G. L. Sequiera, M. B. Nashed, R. I. Ammar, H. M. Gabr, H. E. Elsayed, N. Sareen, E. A.-E. Rub, M. B. Zickri, and S. Dhingra, "Comparison of adipose tissue- and bone marrow- derived mesenchymal stem cells for alleviating doxorubicin-induced cardiac dysfunction in diabetic rats," *Stem Cell Res. Ther.*, vol. 6, no. 1, p. 148, Dec. 2015.

[114] L. Liang, Z. Li, T. Ma, Z. Han, W. Du, J. Geng, H. Jia, M. Zhao, J. Wang, B. Zhang, J. Feng, L. Zhao, A. Rupin, Y. Wang, and Z. C. Han, "Transplantation of Human Placenta-Derived Mesenchymal Stem Cells Alleviates Critical Limb Ischemia in Diabetic Nude Rats.," *Cell Transplant.*, vol. 26, no. 1, pp. 45–61, Jan. 2017.

[115] G. De Rossi, A. R. Evans, E. Kay, A. Woodfin, T. R. McKay, S. Nourshargh, and J. R. Whiteford, "Shed syndecan-2 inhibits angiogenesis.," *J. Cell Sci.*, vol. 127, no. Pt 21, pp. 4788–99, Nov. 2014.

[116] D. Modrowski, A. Orosco, J. Thévenard, O. Fromigué, and P. J. Marie, "Syndecan-2 overexpression induces osteosarcoma cell apoptosis: Implication

of syndecan-2 cytoplasmic domain and JNK signaling.," *Bone*, vol. 37, no. 2, pp. 180–9, Aug. 2005.

[117] M. Sun, M. Chen, F. Dawood, U. Zurawska, J. Y. Li, T. Parker, Z. Kassiri, L. A. Kirshenbaum, M. Arnold, R. Khokha, and P. P. Liu, "Tumor Necrosis Factor-? Mediates Cardiac Remodeling and Ventricular Dysfunction After Pressure Overload State," *Circulation*, vol. 115, no. 11, pp. 1398–1407, Mar. 2007.

[118] W. Yan, P. Wang, C. X. Zhao, J. Tang, X. Xiao, and D. W. Wang, "Decorin gene delivery inhibits cardiac fibrosis in spontaneously hypertensive rats by modulation of transforming growth factor-beta/Smad and p38 mitogen-activated protein kinase signaling pathways.," *Hum. Gene Ther.*, vol. 20, no. 10, pp. 1190–200, Oct. 2009.

[119] P. Blyszczuk, G. Kania, T. Dieterle, R. R. Marty, A. Valaperti, C. Berthonneche, T. Pedrazzini, C. T. Berger, S. Dirnhofer, C. M. Matter, J. M. Penninger, T. F. Luscher, and U. Eriksson, "Myeloid Differentiation Factor-88/Interleukin-1 Signaling Controls Cardiac Fibrosis and Heart Failure Progression in Inflammatory Dilated Cardiomyopathy," *Circ. Res.*, vol. 105, no. 9, pp. 912–920, Oct. 2009.

[120] F. Kuwahara, H. Kai, K. Tokuda, M. Kai, A. Takeshita, K. Egashira, and T. Imaizumi, "Transforming growth factor-beta function blocking prevents myocardial fibrosis and diastolic dysfunction in pressure-overloaded rats.," *Circulation*, vol. 106, no. 1, pp. 130–5, Jul. 2002.

[121] C. Humeres, R. Vivar, P. Boza, C. Muñoz, S. Bolivar, R. Anfossi, J. M. Osorio, F. Olivares-Silva, L. García, and G. Díaz-Araya, "Cardiac fibroblast cytokine profiles induced by proinflammatory or profibrotic stimuli promote monocyte recruitment and modulate macrophage M1/M2 balance in vitro," *J. Mol. Cell. Cardiol.*, vol. 101, pp. 69–80, Dec. 2016.

[122] E. Zappia, S. Casazza, E. Pedemonte, F. Benvenuto, I. Bonanni, E. Gerdoni, D. Giunti, A. Ceravolo, F. Cazzanti, F. Frassoni, G. Mancardi, and A. Uccelli, "Mesenchymal stem cells ameliorate experimental autoimmune encephalomyelitis inducing T-cell anergy," *Blood*, vol. 106, no. 5, pp. 1755–1761, Sep. 2005.

[123] S. Glennie, I. Soeiro, P. J. Dyson, E. W.-F. Lam, and F. Dazzi, "Bone marrow mesenchymal stem cells induce division arrest anergy of activated T cells.," *Blood*, vol. 105, no. 7, pp. 2821–7, Apr. 2005.

[124] S. Van Linthout, K. Savvatis, K. Miteva, J. Peng, J. Ringe, K. Warstat, C. Schmidt-Lucke, M. Sittinger, H.-P. Schultheiss, and C. Tschöpe, "Mesenchymal stem cells improve murine acute coxsackievirus B3-induced myocarditis," *Eur. Heart J.*, vol. 32, no. 17, pp. 2168–2178, Sep. 2011.

[125] K. Miteva, K. Pappritz, M. El-Shafeey, F. Dong, J. Ringe, C. Tsch?pe, and S. Van Linthout, "Mesenchymal Stromal Cells Modulate Monocytes Trafficking in Coxsackievirus B3-Induced Myocarditis," *Stem Cells Transl. Med.*, vol. 6, no. 4, pp. 1249–1261, Apr. 2017.

[126] M. A. Ismahil, T. Hamid, S. S. Bansal, B. Patel, J. R. Kingery, and S. D. Prabhu, "Remodeling of the Mononuclear Phagocyte Network Underlies Chronic

Inflammation and Disease Progression in Heart Failure: Critical Importance of the Cardiosplenic Axis," *Circ. Res.*, vol. 114, no. 2, pp. 266–282, Jan. 2014.

[127] F. Spillmann, B. De Geest, I. Muthuramu, R. Amin, K. Miteva, B. Pieske, C. Tschöpe, and S. Van Linthout, "Apolipoprotein A-I gene transfer exerts immunomodulatory effects and reduces vascular inflammation and fibrosis in ob/ob mice.," *J. Inflamm. (Lond).*, vol. 13, no. 1, p. 25, Dec. 2016.

[128] H. Kvakan, M. Kleinewietfeld, F. Qadri, J.-K. Park, R. Fischer, I. Schwarz, H.-P. Rahn, R. Plehm, M. Wellner, S. Elitok, P. Gratze, R. Dechend, F. C. Luft, and D. N. Muller, "Regulatory T Cells Ameliorate Angiotensin II-Induced Cardiac Damage," *Circulation*, vol. 119, no. 22, pp. 2904–2912, Jun. 2009.

[129] Y. Cao, W. Xu, and S. Xiong, "Adoptive transfer of regulatory T cells protects against Coxsackievirus B3-induced cardiac fibrosis.," *PLoS One*, vol. 8, no. 9, p. e74955, Sep. 2013.

[130] Y. Shi, M. Fukuoka, G. Li, Y. Liu, M. Chen, M. Konviser, X. Chen, M. A. Opavsky, and P. P. Liu, "Regulatory T Cells Protect Mice Against Coxsackievirus-Induced Myocarditis Through the Transforming Growth Factor ?-Coxsackie-Adenovirus Receptor Pathway," *Circulation*, vol. 121, no. 24, pp. 2624–2634, Jun. 2010.

[131] Z. Sepehri, Z. Kiani, A. A. Nasiri, and F. Kohan, "Toll-like receptor 2 and type 2 diabetes," *Cell. Mol. Biol. Lett.*, vol. 21, no. 1, p. 2, Dec. 2016.

[132] G. Srikrishna and H. H. Freeze, "Endogenous damage-associated molecular pattern molecules at the crossroads of inflammation and cancer.," *Neoplasia*, vol. 11, no. 7, pp. 615–28, Jul. 2009.

[133] C. N. Lumeng and A. R. Saltiel, "Inflammatory links between obesity and metabolic disease.," *J. Clin. Invest.*, vol. 121, no. 6, pp. 2111–7, Jun. 2011.

[134] B. Vandanmagsar, Y.-H. Youm, A. Ravussin, J. E. Galgani, K. Stadler, R. L. Mynatt, E. Ravussin, J. M. Stephens, and V. D. Dixit, "The NLRP3 inflammasome instigates obesity-induced inflammation and insulin resistance.," *Nat. Med.*, vol. 17, no. 2, pp. 179–88, Feb. 2011.

[135] H. Wen, D. Gris, Y. Lei, S. Jha, L. Zhang, M. T.-H. Huang, W. J. Brickey, and J. P.-Y. Ting, "Fatty acid-induced NLRP3-ASC inflammasome activation interferes with insulin signaling.," *Nat. Immunol.*, vol. 12, no. 5, pp. 408–15, May 2011.

[136] D. I. Jalal, D. M. Maahs, P. Hovind, and T. Nakagawa, "Uric Acid as a Mediator of Diabetic Nephropathy," *Semin. Nephrol.*, vol. 31, no. 5, pp. 459–465, Sep. 2011.

[137] A. Lerner, J.-P. Upton, P. V. K. Praveen, R. Ghosh, Y. Nakagawa, A. Igbaria, S. Shen, V. Nguyen, B. Backes, M. Heiman, N. Heintz, P. Greengard, S. Hui, Q. Tang, A. Trusina, S. Oakes, and F. Papa, "IRE1? Induces Thioredoxin-Interacting Protein to Activate the NLRP3 Inflammasome and Promote Programmed Cell Death under Irremediable ER Stress," *Cell Metab.*, vol. 16, no. 2, pp. 250–264, Aug. 2012.

[138] R. Zhou, A. S. Yazdi, P. Menu, and J. Tschopp, “A role for mitochondria in NLRP3 inflammasome activation,” *Nature*, vol. 469, no. 7329, pp. 221–225, Jan. 2011.
[139] H.-M. Lee, J.-J. Kim, H. J. Kim, M. Shong, B. J. Ku, and E.-K. Jo, “Upregulated NLRP3 inflammasome activation in patients with type 2 diabetes.,” *Diabetes*, vol. 62, no. 1, pp. 194–204, Jan. 2013.
[140] S. Toldo, H. Kannan, R. Bussani, M. Anzini, C. Sonnino, G. Sinagra, M. Merlo, E. Mezzaroma, F. De-Giorgio, F. Silvestri, B. W. Van Tassell, A. Baldi, and A. Abbate, “Formation of the inflammasome in acute myocarditis,” *Int. J. Cardiol.*, vol. 171, no. 3, pp. e119–e121, Feb. 2014.
[141] Q. Zhu, X.-X. Li, W. Wang, J. Hu, P.-L. Li, S. Conley, and N. Li, “Mesenchymal stem cell transplantation inhibited high salt-induced activation of the NLRP3 inflammasome in the renal medulla in Dahl S rats.,” *Am. J. Physiol. Renal Physiol.*, vol. 310, no. 7, pp. F621–F627, Apr. 2016.
[142] J. Y. Oh, J. H. Ko, H. J. Lee, J. M. Yu, H. Choi, M. K. Kim, W. R. Wee, and D. J. Prockop, “Mesenchymal Stem/Stromal Cells Inhibit the NLRP3 Inflammasome by Decreasing Mitochondrial Reactive Oxygen Species,” *Stem Cells*, vol. 32, no. 6, pp. 1553–1563, Jun. 2014.
[143] B. Dong, D. Qi, L. Yang, Y. Huang, X. Xiao, N. Tai, L. Wen, and F. S. Wong, “TLR4 regulates cardiac lipid accumulation and diabetic heart disease in the nonobese diabetic mouse model of type 1 diabetes,” *AJP Hear. Circ. Physiol.*, vol. 303, no. 6, pp. H732–H742, Sep. 2012.
[144] F. S. Sutterwala, S. Haasken, and S. L. Cassel, “Mechanism of NLRP3 inflammasome activation,” *Ann. N. Y. Acad. Sci.*, vol. 1319, no. 1, pp. 82–95, Jun. 2014.
[145] N. Hamdani and W. J. Paulus, “Myocardial titin and collagen in cardiac diastolic dysfunction: partners in crime.,” *Circulation*, vol. 128, no. 1, pp. 5–8, Jul. 2013.
[146] W. A. Linke and N. Hamdani, “Gigantic business: titin properties and function through thick and thin.,” *Circ. Res.*, vol. 114, no. 6, pp. 1052–68, Mar. 2014.
[147] L. van Heerebeek, N. Hamdani, I. Falcao-Pires, A. F. Leite-Moreira, M. P. V. Begieneman, J. G. F. Bronzwaer, J. van der Velden, G. J. M. Stienen, G. J. Laarman, A. Somsen, F. W. A. Verheugt, H. W. M. Niessen, and W. J. Paulus, “Low Myocardial Protein Kinase G Activity in Heart Failure With Preserved Ejection Fraction,” *Circulation*, vol. 126, no. 7, pp. 830–839, Aug. 2012.
[148] W. J. Paulus and C. Tschöpe, “A novel paradigm for heart failure with preserved ejection fraction: comorbidities drive myocardial dysfunction and remodeling through coronary microvascular endothelial inflammation.,” *J. Am. Coll. Cardiol.*, vol. 62, no. 4, pp. 263–71, Jul. 2013.
[149] M. Krüger, S. Kötter, A. Grützner, P. Lang, C. Andresen, M. M. Redfield, E. Butt, C. G. dos Remedios, and W. A. Linke, “Protein kinase G modulates human myocardial passive stiffness by phosphorylation of the titin springs.,” *Circ. Res.*, vol. 104, no. 1, pp. 87–94, Jan. 2009.
[150] A. F. Leite-Moreira, P. Castro-Chaves, P. Pimentel-Nunes, A. Lima-Carneiro, M. S. Guerra, J. B. Soares, and J. Ferreira-Martins, “Angiotensin II acutely

decreases myocardial stiffness: a novel AT1, PKC and Na+/H+ exchanger-mediated effect.," *Br. J. Pharmacol.*, vol. 147, no. 6, pp. 690–7, Mar. 2006.

[151] D. J. Carey, "Syndecans: multifunctional cell-surface co-receptors.," *Biochem. J.*, no. Pt 1, pp. 1–16, Oct. 1997.

Eidesstattliche Versicherung

„Ich, Fengquan Dong, versichere an Eides statt durch meine eigenhändige Unterschrift, dass ich die vorgelegte Dissertation mit dem Thema: Impact of $CD362^{+}$-selected mesenchymal stromal cells on left ventricular function in type 2 diabetic db/db mice selbstständig und ohne nicht offengelegte Hilfe Dritter verfasst und keine anderen als die angegebenen Quellen und Hilfsmittel genutzt habe.
Alle Stellen, die wörtlich oder dem Sinne nach auf Publikationen oder Vorträgen anderer Autoren beruhen, sind als solche in korrekter Zitierung (siehe „Uniform Requirements for Manuscripts (URM)“ des ICMJE -www.icmje.org) kenntlich gemacht. Die Abschnitte zu Methodik (insbesondere praktische Arbeiten, Laborbestimmungen, statistische Aufarbeitung) und Resultaten (insbesondere Abbildungen, Graphiken und Tabellen) entsprechen den URM (s.o) und werden von mir verantwortet.
Meine Anteile an etwaigen Publikationen zu dieser Dissertation entsprechen denen, die in der untenstehenden gemeinsamen Erklärung mit dem/der Betreuer/in, angegeben sind. Sämtliche Publikationen, die aus dieser Dissertation hervorgegangen sind und bei denen ich Autor bin, entsprechen den URM (s.o) und werden von mir verantwortet.

Die Bedeutung dieser eidesstattlichen Versicherung und die strafrechtlichen Folgen einer unwahren eidesstattlichen Versicherung (§156,161 des Strafgesetzbuches) sind mir bekannt und bewusst.“

Datum Unterschrift:

My curriculum vitae does not appear in the electronic version of my paper for reasons of data protection.

Anteilserklärung an etwaigen erfolgten Publikationen

Fengquan Dong hatte folgenden Anteil an den folgenden Publikationen:

Publikation 1: Miteva K, Pappritz K, El-Shafeey M, **Dong F**, Ringe J, Tschöpe C, Van Linthout S. Mesenchymal stromal cells modulate monocytes trafficking in Coxsackievirus B3-induced myocarditis. Stem Cells Translational Medicine，2017; 6:1249-1261.
Beitrag:

- injection of Coxsackievirus B3 for the induction of myocarditis
- cell application
- organ harvest

Publikation 2: Müller I, Pappritz K, Savvatis K, Puhl K, **Dong F**, El-Shafeey M, Hamdani N, Hamann I, Noutsias M, Infante-Duarte C, Linke WA, Van Linthout S, Tschöpe C. CX3CR1 knockout aggravates Coxsackievirus B3-induced myocarditis. PLoS One. 2017;12:e0182643.
Beitrag:

- hemodynamic analysis

Publikation 3: Miteva K, Pappritz K, Sosnowski M, El-Shafeey M, Müller I, **Dong F**, Savvatis K, Ringe J, Tschöpe C, Van Linthout S. Mesenchymal stomal cells inhibit NLRP3 inflammasome activation in a model of Coxsackievirus B3-induced inflammatory cardiomyopathy. Sci Rep. 2018;8:2820.
Beitrag:

- injection of Coxsackievirus B3 for the induction of myocarditis
- cell application
- organ harvest
- cutting of cryosections

Unterschrift, Datum und Stempel des betreuenden Hochschullehrers/der betreuenden Hochschullehrerin

Unterschrift des Doktoranden/der Doktorandin

ACKNOWLEDGEMENTS

I would like to express my sincere gratitude to my supervisor, Prof. Dr. Carsten Tschöpe for offering the opportunity and providing support to carry out this study, and for his continuous guidance, encouragement and care throughout the entire period of study.

I would also like to express my sincere gratitude to PD Dr. Sophie Van Linthout, who led me to the scientific research field, for her constructive and helpful directions throughout the entire period of study, and for her critical reading and revision.

I am very grateful to Annika Koschel, Dr. Kathleen Pappritz, Kerstin Puhl, PD Dr. Kostas Savvatis, Marzena Sosnowski, and Georg Zingler for their technical assistance.

I further want to thank Kathleen Pappritz for proofreading the thesis.

I want to thank my whole family for their love, encouragement, and support.

Finally, I would like to thank the China Scholarship Council (CSC), without their financial support this study would not have been possible.